Universidade do Minho
Escola de Engenharia

Ana Catarina Branco Lima

Magnetically responsive inks for printed electronics components and devices: integration into fully printed magnetic sensors

junho 2022

Ana Catarina Branco Lima **Magnetically responsive inks for printed electronics components and devices: integration into fully printed magnetic sensors**
UMinho | 2022

Universidade do Minho
Escola de Engenharia

Ana Catarina Branco Lima

Magnetically responsive inks for printed electronics components and devices: integration into fully printed magnetic sensors

Tese de Doutoramento
Doutoramento em Engenharia de Materiais

Trabalho realizado sob a orientação do
Professor Doutor Senentxu Lanceros-Méndez
Doutor Pedro Martins
Doutor Yury Kolen'ko

junho 2022

DIREITOS DE AUTOR E CONDIÇÕES DE UTILIZAÇÃO DO TRABALHO POR TERCEIROS

Acknowledgements

This is the moment when one of the biggest chapters of my life is complete, and I would first like to thank the Foundation for Science and Technology - FCT for having financially supported my research over these 4 years (grant SFRH/BD/132624/2017), to INL - International Nanotechnology Laboratory and University of Minho, as my host institutions that provided all the necessary conditions to develop this thesis.

To all my friends from Electroactive Smart Materials Group, I would like to thank for all the help, companionship, and good memories. In a special way, I wish to thank Nelson, Juliana, Bruna, Hugo and Sylvie for all the support and affection through these years. I also want to thank my colleagues from Nanochemistry Research Group for helping me whenever I needed, and for you I simply want to say, "Keep pushing!".

I'm grateful for the kind way that I was received in BC Materials - Basque Center for Materials, Applications and Nanostructures. Thanks to all that worked with me!

To Doctor Pedro Martins, my supervisor and my Friend. Thank you for all the moments you have encouraged me, always showing the positive side of every scenario. Thank you for all your help, wisdom and support. To Professor Senentxu, my co-supervisor, I want to thank for everything: for the opportunity to work in this amazing group through these years, for every wise word, for all the courage and confidence that gave me the strength to never give up, for trusting in me and in my projects and essentially, for your friendship and true inspiration. To Yury Kolen'ko, my co-supervisor, thanks for your availability, advices and for every M&M that maintained my sugar level stable for a better work!

To my fantastic family, specially my parents and brother, thank you for everything that you taught me, for all the love and affection, for being always by my side, no matter what.

Lastly, but most important, I wish to thank my husband, Daniel, for always walking by my side and for being my biggest support. To my beautiful daughter Leonor, thanks for being the light of my eyes, that inspires me every day to be a better person.

STATEMENT OF INTEGRITY

I hereby declare having conducted this academic work with integrity. I confirm that I have not used plagiarism or any form of undue use of information or falsification of results along the process leading to its elaboration.

I further declare that I have fully acknowledged the Code of Ethical Conduct of the University of Minho.

Tintas magneticamente responsivas para componentes e dispositivos eletrónicos impressos: integração em sensores magnéticos totalmente impressos

"Flexível", "extensível" e "dobrável" são alguns dos conceitos que podem alterar a nossa relação com o mundo que nos rodeia, num futuro muito próximo. Entre as técnicas que podem permitir estes desenvolvimentos, o destaque científico tem-se centrado em todas aquelas relacionadas com a impressão, uma vez que estas possibilitam a obtenção de dispositivos com um custo reduzido e com menor impacto ambiental, bom desempenho, permitindo também o seu processamento em grandes áreas e, ainda, o uso de substratos flexíveis. Desta forma, as técnicas de impressão estão a tornar-se num fator chave para a indústria, comércio e consumidores finais. Apesar das vantagens acima mencionadas, os sensores impressos disponíveis atualmente, apresentam várias limitações em comparação com os sensores convencionais, nomeadamente o baixo tempo de vida útil e de operação, a baixa sensibilidade, o baixo alcance e o elevado ruído. Além disso, com a necessária redução da pegada ecológica em todos os tipos de setores, é cada vez mais importante o desenvolvimento de tintas com alternativas aos solventes tóxicos utilizados, rumo a abordagens "ecologicamente mais sensatas". Neste contexto, o presente trabalho centra-se no desenvolvimento de materiais magneticamente responsivos para o desenvolvimento de sensores magnéticos impressos. Assim, um compósito magnetoelétrico (ME) flexível e transparente foi preparado com base em microfios magnetostritivos $Fe_{72.5}Si_{12.5}B_{15}$ e poli (fluoreto de vinilideno-trifluoroetileno), P(VDF-TrFE). A alta magnetostrição de $Fe_{72.5}Si_{12.5}B_{15}$ (35 ppm) permitiu uma elevada resposta de tensão ME (65 mV cm^{-1} Oe^{-1}) obtida no campo magnético longitudinal crítico igualando a anisotropia transversal (14500 Am^{-1}) na camada externa do microfio. Este é um caminho interessante para a eletrónica transparente. Além disso, um novo material ME flexível e totalmente impresso, foi desenvolvido com base em P(VDF-TrFE) e PVDF-CFO, exibindo um comportamento ferromagnético com magnetização de saturação de 16 emu g^{-1}, resposta piezoelétrica −26 pC N^{-1} e um coeficiente ME (α) de 164 mV cm^{-1} Oe^{-1} a uma frequência de ressonância longitudinal de 16,2 kHz. Este comportamento otimizado demonstra a compatibilidade do material desenvolvido para aplicações, incluindo sensores impressos, atuadores e armazenamento de energia. Após estes resultados promissores, o passo seguinte foi a redução do impacto ambiental nos materiais desenvolvidos. Foi demonstrado que nanocompósitos de P(VDF-TrFE) / $CoFe_2O_4$ podem ser preparados por fusão de solvente utilizando 3 solventes diferentes: dimetilsulfóxido (DMSO), N, N′-dimetilpropilenoureia (DMPU) e trietilfosfato (TEP). A sensibilidade dos nanocompósitos ME propostos, em condições específicas de H_{AC} (2188 μV T^{-1}), duplicou relativamente aos valores reportados na literatura para solventes não verdes (1280 μV T^{-1}), abrindo caminho para o desenvolvimento de sensores e atuadores mais ecológicos. Finalmente, foi também desenvolvido um sensor de proximidade magnética baseado em compósitos ME de PVDF/Metglas® e uma bobina impressa. O sensor de proximidade magnética proposto apresentou um α = 50,2 V cm^{-1} Oe^{-1}, uma resposta linear AC (R^2 = 0,997) e uma saída de tensão máxima de 362 mV, adequado para aplicações de deteção de proximidade em diversas áreas, tais como aerospacial e automóvel. Como conclusão, o presente trabalho demonstrou a compatibilidade do desenvolvimento de tintas inteligentes com resposta funcional otimizada para a fabricação de dispositivos magnéticos e ME por tecnologias de manufaturação aditiva.

Palavras-chave: eletrónica impressa; manufaturação aditiva; materiais magnetoativos; sensores magnéticos; tintas magnéticas.

Magnetically responsive inks for printed electronics components and devices: integration into fully printed magnetic sensors

"Flexible", "stretchable", "foldable" and "usable" are just some of the most common concepts that can change our relationship with other people and with the world around us. Among all the techniques that allowed those developments, the highlight goes to all those related to printing, since they make it possible to obtain devices with a reduced cost and reduced environmental impact, good performance, still allowing processing in large areas and flexible substrates, thus becoming a key factor for industry, commerce and consumers. Despite the advantages mentioned above, the available printed sensors nowadays, have several limitations in comparison with conventional sensors, namely the short useful and operating life, low sensitivity, low range, and high noise. Further, with the needed reduction of the ecological footprint in all types of sectors, it is increasingly important the development of inks with alternatives to conventionally used toxic solvents, heading towards "environmentally friendly" approaches. In this context, the present work focuses on the development of magnetically responsive materials for the development of printable magnetic sensors. Thus, a flexible and transparent magnetoelectric (ME) composite was prepared based on magnetostrictive $Fe_{72.5}Si_{12.5}B_{15}$ microwires and piezoelectric poly (vinylidene fluoride-trifluoroethylene) P(VDF–TrFE). The high magnetostriction of $Fe_{72.5}Si_{12.5}B_{15}$ (35 ppm) enabled superior ME voltage response (65 mV cm^{-1} Oe^{-1}) obtained at the critical longitudinal magnetic field equating the transverse anisotropy (14500 A m^{-1}) on the external shell of the microwire. This is an interesting path towards transparent electronics. Also, a novel screen-printed, and flexible ME material was developed based on P(VDF–TrFE) and PVDF–CFO. The all-printed ME composite exhibited a ferromagnetic behavior with 16 emu g^{-1} saturation magnetization, –26 pC N^{-1} piezoelectric response and a ME voltage coefficient (α) of 164 mV cm^{-1} Oe^{-1} at a longitudinal resonance frequency of 16.2 kHz. Such optimized behavior demonstrates the suitability of the developed material for applications including printed sensors, actuators, and energy harvesters. After such promising results, the next step was the reduction of the environmental impact of the developed high-performance materials. It was reported that P(VDF-TrFE)/ $CoFe_2O_4$ nanocomposite films can be prepared by solvent casting using Dimethyl sulfoxide (DMSO), N, N′-Dimethylpropyleneurea (DMPU) and Triethyl phosphate (TEP). The sensitivity of the proposed ME nanocomposites under specific H_{AC} conditions (2188 μV T^{-1}) almost doubled the highest values reported in the literature (1280 μV T^{-1}), opening the path for the development of environmentally friendlier sensors and actuators. Finally, a magnetic proximity sensor was developed based on ME PVDF/Metglas® composites and an excitation-printed coil. The proposed magnetic proximity sensor showed a maximum resonant α = 50.2 V cm^{-1} Oe^{-1}, an AC linear response (R^2 = 0.997) and a maximum voltage output of 362 mV, which suggests suitability for proximity-sensing applications in a variety of areas, such as aerospace and automotive. As a conclusion, the present work has demonstrated the suitability of developing smart inks with tailored functional response for the fabrication of magnetic and ME devices by additive manufacturing technologies.

Keywords: additive manufacturing; magnetic inks; magnetic sensors; magnetoactive materials, printed electronics.

Table of Contents

List of Symbols

B

B_{AC}	AC magnetic field
B_{DC}	DC magnetic field

D

d_{33}	Piezoelectric coefficient

F

f	Frequency

H

H_{AC}	Intensity of the AC magnetic field
H_{DC}	Intensity of the DC magnetic field
H_t	Transverse magnetoelastic anisotropy field

J

J_s	Magnetic polarization

K

K_t	Transverse magnetoelastic anisotropy energy density

L

L	Inductance

M

m_i	Polymer-CFO interphase
m_{IO}	Mass of pristine P(VDF-TrFE)
$m(x)_{IO}$	Mass of the composite containing a given wt.% of CFO nanoparticles

R

R	Electrical Resistance

T

T_c	Curie temperature
T_m	Melting temperature
t	Thickness
tg (δ)	Dielectric loss

W

wt. %	Weight percentage

Y

Y	Young's Modulus

X

X_c	Degree of crystallinity
X_L	Inductive reactance

Z

Z	Impedance

Greek

α_{ME}	ME voltage coefficient
α_{33}	Transversal ME voltage coefficient
α_{31}	Longitudinal ME voltage coefficient
ΔV	Output voltage
ΔH_f	Melting enthalpy
ΔH_{100}	Enthalpy of pure PVDF
λ_s	Magnetostriction coefficient
ε'	Dielectric permittivity
μ_0	Vacuum permeability
σ	Electrical conductivity

List of Acronyms

A

A	Area
ABS	Acrylonitrile butadiene styrene
AC	Alternating current
Ag NW	Silver nanowires
APME	All printed magnetoelectric

C

CAGR	Compound annual growth rate
CFO	$CoFe_2O_4$
CNT	Carbon nanotubes

D

DC	Direct current
DTG	Differential thermogravimetry
DMF	N, N-dimethylformamide
DMPU	N, N′-Dimethylpropyleneurea
DMSO	Dimethyl sulfoxide
DOD	Drop-on-demand
DSC	Differential scanning calorimetry
DTGA	Derivative Thermogravimetry

E

EB	Electron Beam
ET	Engineering Technology

F

FeSiB	Iron-silicon-boron

G

GMR	Giant magnetoresistance

I

IIoT	Industrial Internet of Things
IT	Information Technology
IoT	Internet of Things
IR	Infrared
ITO	Indium tin oxide

L

LbL	Layer-by-layer
LED	Light emitting diode

M

ME	Magnetoelectric
MOF	Metal organic frameworks
MS	Magnetostrictive
MIBK	Methyl isobutyl ketone
MWCNT	Multi-Walled Carbon Nanotubes
MWs	Microwires

N

NP	Nanoparticle
NMP	N-methyl-2-pyrrolidone

O

OT	Operational Technology

P

PEDOT/PSS	Poly (3,4-ethylenedioxythiophene)-poly(styrenesulfonate)
PDMS	Polydimethylsiloxane
P(VDF-TrFE)	Poly (vinylidene fluoride-trifluoroethylene)

PVDF	Poly (vinylidene fluoride)
PCB	Printed circuit board
PE	Printed electronics
PET	Polyethylene terephthalate
PMMA	Polymethyl methacrylate
PVP	Polyvinylpyrrolidone

R

RFID	Radio frequency identification

S

SEM	Scanning electron microscopy

T

TEP	Triethyl phosphate
TGA	Thermal gravimetric analysis
THF	Tetrahydrofuran
TMD	Temperature of maximum rate of weight loss

U

UV	Ultraviolet

V

VSM	Vibrating-sample magnetometer

X

XRD	X-ray diffraction

List of Figures

List of Tables

To my beautiful daughter, Leonor

"All of our dreams come true if we have the courage to pursue them."

– Walt Disney

CHAPTER I

INTRODUCTION

Chapter I - Introduction

The digital transformation of industries, infrastructures and cities has begun. Whether it's called Industrial Internet of Things (IIoT), Industry 4.0, or Digitalization, manufacturing and service companies have begun to use available technologies to adapt their business model to the new reality. Thus, this chapter introduces the main concepts related to magnetically responsive materials and their importance in the technology revolution.

This chapter also presents the main objectives, the methodology and the structure of this thesis.

This chapter is based on the following scientific publication:

A. C. Lima, N. Pereira, P. Martins, S. Lanceros-Méndez, Magnetic Materials for magnetoelectric coupling: an unexpected journey, Handbook of Magnetic Materials, Chapter 2, vol. 29, 57-110, 2020. DOI: https://doi.org/10.1016/bs.hmm.2020.09.002

N. Pereira**, A. C. Lima,** S. Lanceros-Méndez, and P. Martins, Magnetoelectrics: Three Centuries of Research Heading Towards the 4.0 Industrial Revolution, Materials, 13, 4033, 2020. DOI: https://doi.org/10.3390/ma13184033

K. J. Merazzo, **A. C. Lima**, M. Rincón-Iglesias, L. C. Fernandes, N. Pereira, S. Lanceros-Méndez, P. Martins Magnetoactive materials: a journey from finding north to an exciting, printed future, Materials Horizons, 2021. DOI: https://doi.org/10.1039/D1MH00641J

1.1 Main Concepts

1.1.1 IoT and 4.0 Industry

The world is experiencing constant revolutions that somehow shape the route and history of humanity itself. From the first industrial revolution (mechanization through water and steam power) to the mass production and assembly lines by means of electricity in the second, the fourth industrial revolution will continue what was started in the third revolution with the implementation of computers and automation and improve it with autonomous and smart systems driven by data and machine learning (Figure I-1) [1].

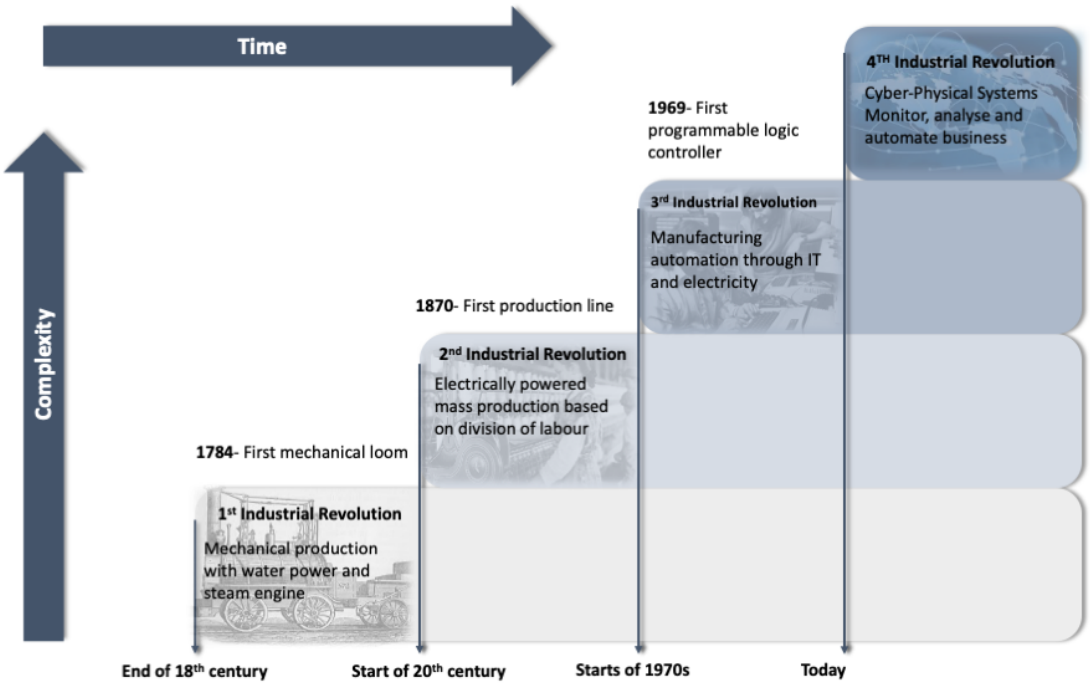

Figure I-1- *The 4th industrial revolutions leading to the smart factory of the future and cyber-physical production systems.*

At this moment, we are in the center of a transformation concerning the way we fabricate products thanks to the digitization of manufacturing. This transition is being named "Industry 4.0" or "Industrial IoT (IIoT)" [2].

The Internet of Things (IoT) is a revolutionary paradigm that is quickly gaining ground in the modern wireless telecommunications landscape. The concept is the widespread presence around us of a diversity of things or items - such as radio frequency identification (RFID) tags, sensors, actuators, cell phones, etc. - that through single addressing schemes can interact with each other and cooperate to reach common purposes [3]. The focal strength of the IoT idea is the high influence it will have on various

aspects of everyday life and the behavior of potential users - everything is connected and the information it is available in real-time [4].

Electronics has become an integral part of our daily lives with applications establishing a significant part of the infrastructures, communication installations, industry and all kinds of mobile devices and consumable electronics we are using [5]. Electronic materials shaped the way humans, as users, think, work, and communicate. The IoT are expected to increase the level of communication between individual electronics devices, which also requires the development of new materials for the electronics to meet the specifications of these interconnection systems such as, easy integration of electronics and connection ways in all kinds of devices (flat, flexible, stretchable), and, at the same time, maintaining low cost of fabrication and providing sustainable solutions [6, 7].

In the case of Industry 4.0, the industrial machines need to employ many easily implementable low-cost sensors (flexible, conformable, thin, lightweight, or stretchable). This also implies the use of new materials with advanced sensing properties, combined with the use of low-cost fabrication processes. All these current and future requirements and expectations can be met by combination of materials science and printing technologies together with processes of advanced manufacturing [8].

1.1.2 Printed Electronics

Printed Electronics, PE, can be stated as a manufacturing process of using functional inks to print onto a variety of substrates (foil, paper, glass, organic matter, fabrics and so on) [9-11], leading to the production of electronic devices [12]. Such printed electronics can be rolled, stretched, shaped to fit any form, no matter the size, making them employable in a wide range of products and applications [13].

In the context of a new technological revolution, based on the industry 4.0 and the IoT, despite the short useful and operating life, low sensitivity, low range, and high noise, PE possess a few key advantages over traditional, silicon-based electronics, namely low-cost manufacturing with high throughput, compatibility with flexible systems (large area electronics and hybrid system fabrication on flexible substrates) and relative ease of integration [14]. Thus, the number of studies on PE has increased in a very accentuated way, since the first reported PE until today, and as of first semester 2021, already 563 studies regarding the field have been published (Figure I-2a) [15].

Reports on the topic point out that the global PE market will rise from USD 6.24 billion in 2018 to USD 11.50 billion by 2023, with a CAGR rate of 13.0 %, during the forecast period, 2018-2023 (Figure I-2b) [16].

Printed circuitry has the potential to decrease, in a substantial way, costs and technical restrictions usually related with mass producing electronics [12, 14]. In addition, PE require fewer input materials and less energy to work with them [10].

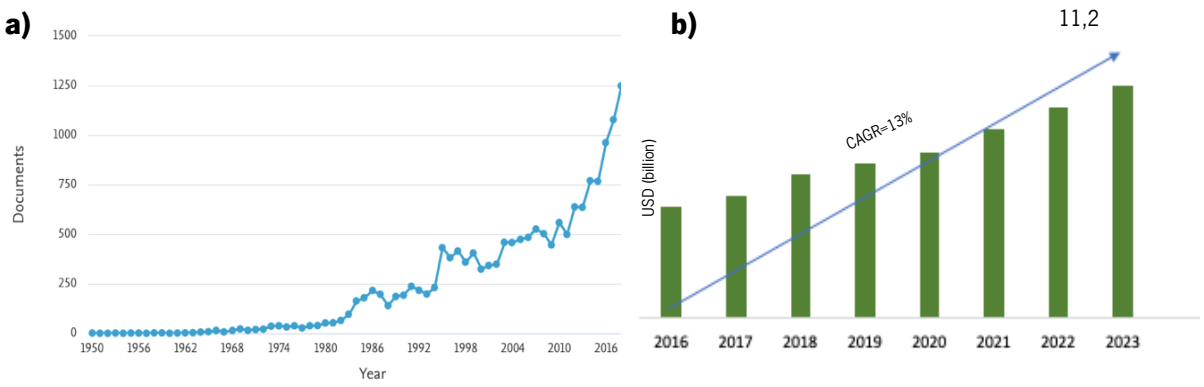

Figure I-2- a) *Research publications per year obtained for the term "Printed Electronics" on SCOPUS;* ***b)*** *PE Market Size 2016-2023 (USD Dollars), Based on MRFR Analysis [16].*

In a general way, PE turned reality flexible and transparent devices that adjust to our body, or to our clothes, for example. Nowadays, companies are working on using printed electronics for labelling banknotes, credit cards, legal documents, and other elements with exclusive printed signatures. Another industry benefiting from printed electronics advancements is photovoltaics. Printed electronics have the capacity to significantly change solar power projects, thanks to less expensive polymer electronics [17].

For the fabrication of electronic components, several printing techniques can be employed. A general classification can be made in terms of whether there is physical contact with the substrate or not. In the former methods, known as contact printing techniques, the ink is transferred directly onto the target substrate. They are suitable for the mass production of PE, although they require a high setup cost. Some of the most used contact printing techniques include screen-printing and flexographic-printing. Non-contact techniques, on the contrary, are those which eject the materials through a nozzle without any direct contact with the substrate. Inkjet-printing and spray-printing, among others, are included in this classification [18].

Screen-printing (Figure I-3a) is one of the most versatile contact techniques, since it allows to print high areas onto plastic, glass, silicon, or cellulosic substrates [19]. Screen-printing also permits the printing of high aspect ratio particles. However, a mesh made of elastic threads and a coating polymer is mandatory [20].

The ink is deposited over the mesh, a squeegee presses the mesh contacting the substrate and spreads the ink reproducing the designed pattern. The used inks need to be highly viscous and non-volatile to obtain a successful print, which does not crack in the curing process. Preferably, polymer solutions presenting shear-thinning behavior are used once they flow when the external force of the squeegee is applied but do not spread after the printing process [12]. The selected mesh (number of threads) will depend on the size of the fillers that are used and on the solvent of the ink (coating polymer). Wet thick films can be obtained with just one step. Screen-printing technique can also be used in additive manufacturing through printing layer-by-layer (LbL), even allowing the printing of different active materials in different layers [21-23].

This technology has the advantage of being fast at producing multiple copies with the same design. It is used to manufacture large areas of devices and electronics, showing cost-effectiveness and simple processing [24]. Another advantage is that it provides the option to print in different substrates, from fabric [25] to stainless steel substrates [26]. The main disadvantages are related with the low resolution and the lack of precise matching between multiple layers.

Flexographic-printing (Figure I-3b) is a fast-printing method based on spinning rollers. Multiple feed roller systems supply ink to a transfer roller and the print is made onto a flexible substrate. In flexography, the transfer roller is the one that contains the setoff pattern. This technique uses low viscosity inks since the speed is very high and the pressure on the flexible substrates is lower than screen-printing. The materials that can printed through this technique includes water-based inks, solvent-based inks, electron beam (EB) curing inks, ultraviolet (UV) cured inks, two-part chemically curing inks (typically built on polyurethane isocyanate reactions) [27].

As main advantages emerge the highly automated process, the cost efficiency and the high printing versatility, as main disadvantages appear the inability to produce complicated and extensive prints and the need quite complex equipment [18].

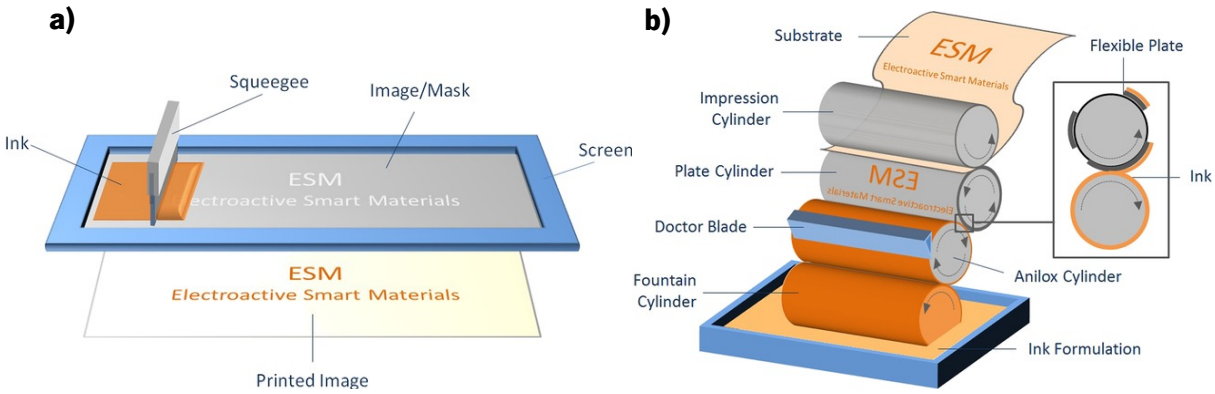

Figure I-3- *Schematic illustration of* ***a)*** *screen-printing and* ***b)*** *flexographic-printing [28].*

Spray-printing (Figure I-4a) is a non-contact printing technique popularly used on printing electronics. This method is based on aerodynamic process and the main component is an atomizer, typically ultrasonic or pneumatic. Firstly, the atomizer can create fine droplets of ink that are carried from the ink reservoir to the virtual impactor by a carrier gas (usually nitrogen gas). When fine droplets arrive to the virtual impactor, excess of carrier gas is removed increasing the droplets density. Subsequently, ink droplets are carried to the nozzle and finally discharged onto the substrate. A wide range of materials can be printed by spray-printing such as polymeric composites (dielectric, conductors), liquid metal solutions, biomaterials, or inorganic solutions [17,19].

According to ink properties, different substrates could be used. The main advantage of aerosol jet printing is the distance between print head and substrate, high enough to make possible print on substrates that are not flat or smooth. In addition, the resolution is higher than other non-contact printing technique such as inkjet-printing. Thus, electronic devices such as film transistor displays or solar cells, have been printed using aerosol jet/spray-printing [20].

Inkjet-printing (Figure I-4b-c) is the main non-contact printing technique. Two type of inkjet approaches are available- the continuous type (binary or multi-deflection) and drop-on-demand (DOD) type (thermal, piezoelectric, or electrostatic). During the printing process, small droplets of ink are ejected from the print-head nozzle to the substrate without contact between them and according to the computer pattern. The inkjet type changes the way the inkjet is ejected or how its deposition is controlled [21].

As same as other printing techniques, different substrates such as paper, polymers, metals, or ceramics could be employed. Different inks, water or alcohol-based, are useful for inkjet-printing but conductive ones are the main explored for electronic printing [11]. This technique uses low viscous ink, is relatively fast, reduces contamination and damages of components, as well as reduces material wastage. Therefore, transistors, resistors, capacitors, or antennas are some electronic components inkjet-printed [17].

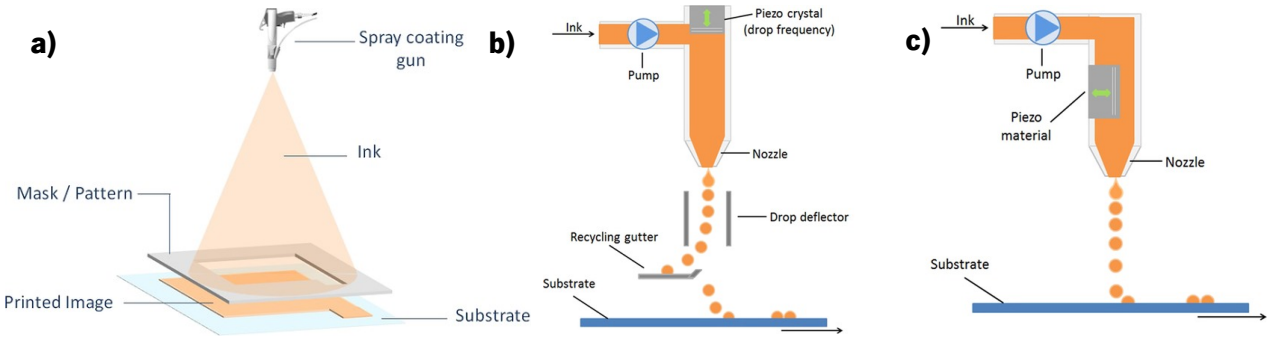

Figure I-4- *Schematic illustration of* ***a)*** *spray-printing and* ***b)*** *inkjet-printing continuous flow and* ***c)*** *DOD (piezoelectric) [28].*

1.1.3 Magnetically responsive materials

The capability of smart materials to respond in a controlled and reversible manner, by varying physical and/or chemical properties, to external stimuli, such as temperature, pressure, electric and magnetic fields, or light, make them a key element in such IoT and industry 4.0 scenarios (Figure I-5) [29-31].

Often, printable smart materials take advantage of nano- and micro-composite systems conjugating the mechanical and binding properties of polymers/ceramics and specific active functionalities of metallic and ceramic nano-/ micro-fillers, metal organic frameworks (MOF), ionic liquids or carbon-based materials [32]. The combined properties and functionalities of the different components lead to multifunctional materials with increased efficiency and integration capabilities [33, 34].

The smart material classification is often based on the nature of the external stimulus and the consequent response of the material [35-36]. Among the different responsive multifunctional materials (thermo-responsive, mechano-responsive, electro-responsive, chemo-responsive, photo-responsive, magneto-responsive, pH-responsive, and so on) [37], magneto-responsive materials are particularly interesting due to their non-contact activation, non-local modulation, and in some cases fast switching [38, 39].

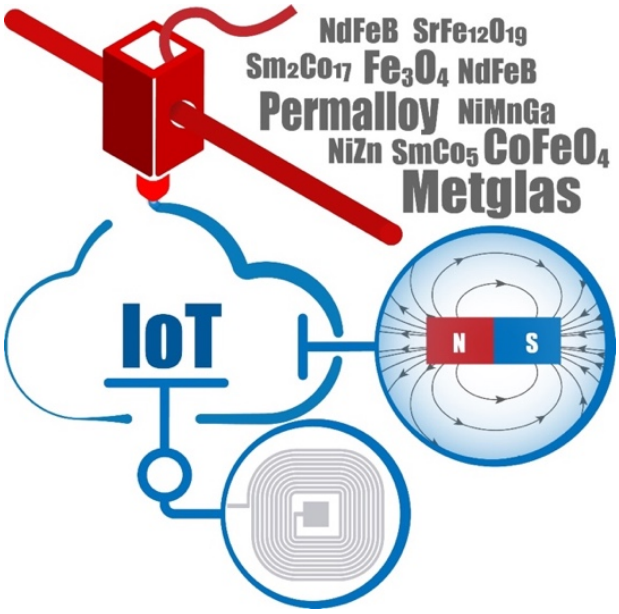

Figure I-5- *Printable magnetoactive smart materials within the IoT context***.**

Magnetoactive materials integration into the IoT environment is a hot topic since they will trigger the fabrication of antennas, bioelectronics, transformers, sensors, and actuators that are often produced by combining magnetic fillers and polymeric/ceramic matrices. In these systems, the effect of an external magnetic field over magnetic particles starts a physical change in the composite [34].

Due to their high application potential, magnetorheological elastomers, magnetoresistive, magnetocaloric, magnetostrictive and magnetoelectric (ME) composites are among the most studied/discussed magneto-active materials [40-45].

ME materials are a particularly interesting class of magnetoactive materials once they offer operative coupling between magnetic and electric orders of matter [46], being technologically appealing to the design of devices such as sensors, scaffolds, actuators and information storage [47].

The term "magnetoelectric" was introduced by Debye in 1926, after the first unsuccessful attempts to experimentally verify the ME effect. The first specific written mention of the ME effect (Figure I-6) occurred in 1958 in the classic book "Electrodynamics of Continuous Media" by Landau and Lifshitz [48] which affirmed, "*Let us point out two more phenomena, which, in principle, could exist. One is piezomagnetism. The other is a linear coupling between magnetic and electric fields in a media, which would cause, for example, a magnetization proportional to an electric field."* The authors continue, *"We will not discuss these phenomena in more detail because it seems that till present, presumably, they have not been observed in any substance*."

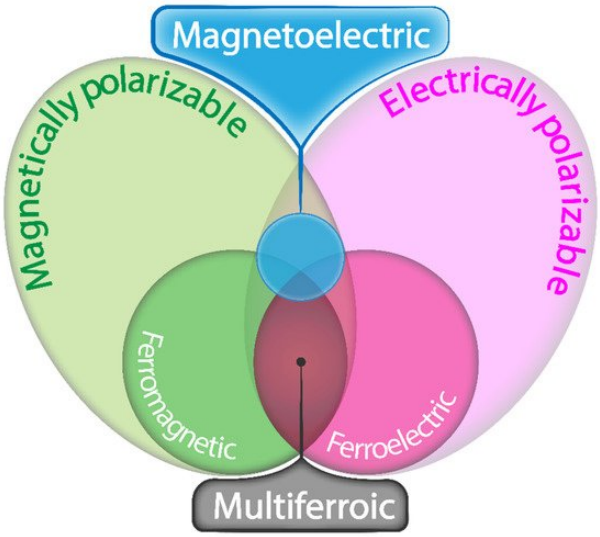

Figure I-6- *ME effect and its relationship with other physical phenomena.*

The magnetic and piezoelectric phases in ME composites can be divided based on their connectivity types in: (0-3) particulate composite; (2-2) laminate composite and (1-3) fiber/rod composite (Figure I-7a-c) [49].

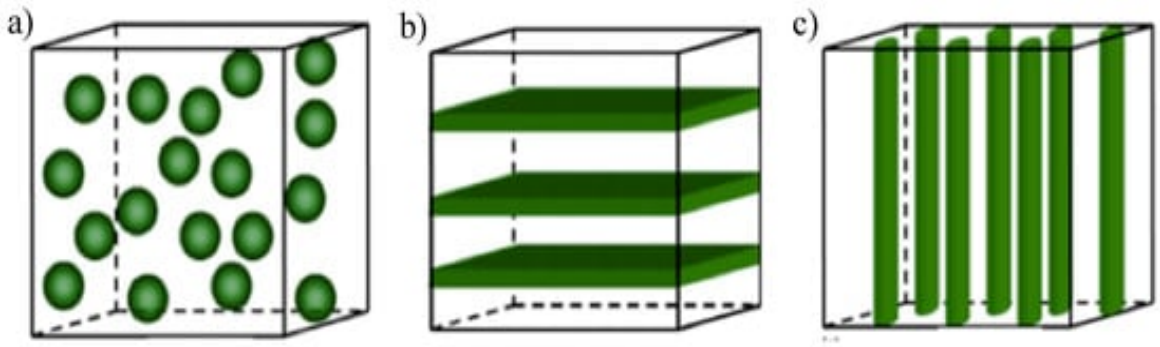

Figure I-7- *The schematic illustration of three bulk composites with different connectivity:* ***a)*** *(0-3) particulate composite;* ***b)*** *(2-2) laminate composite;* ***c) (1-3)*** *fiber/rod composite. Reproduced with permission from [49].*

In (0-3) particulate composites, a high concentration of magnetostrictive particles needs to be dispersed into the selected piezoelectric matrix. The properties of the composite can be easily tailored by selecting the constituent phases, the particle sizes, and processing parameters [50].

In (2-2) laminate composites, the piezoelectric and magnetostrictive phases are often joined by a coupling agent, leading to an elimination of the leakage current, resulting on a superior ME performance [51]. Such laminates can be arranged in different shapes and geometries, including discs, squares,

rectangles, and rings, with different dimensions. They can be arranged as unimorphs and bimorphs as well as bilayered and multilayered structures [52].

Regarding to the (1-3) fiber/rod composites, the magnetic phase can also lead to leakage currents during polarization [47], and very few attempts have been made to fabricate this type of bulk ME composites. To overcome this, (1-3) fiber/rod composites typically consist of three phases: PE bulk, magnetostrictive (MS) material and insulating polymers [53].

The polymer-based ME composites strategy offered a new approach for developing new applications with easy production at low temperatures and additive manufacturing capability (inkjet-printing and screen-printing, among others), tuned mechanical properties for flexible devices, large area applications, low-cost and biocompatible devices, suitable for the IoT and Industry 4.0 [54]. Such IoT devices demands on optimized performances, low power consumption and integrated applications can be achieved with ME materials.

The main experimental methods for measuring the ME coefficient are the static, quasi-static, dynamic and pulsed dynamic methods. For the dynamic method, the sample is subjected to the action of a superimposed AC field in a variable DC magnetic field, which generates at the ends of the material a voltage response (ME signal) which allows to obtain the ME voltage coefficient (α_{ME}) value indirectly through Equation I.1 [55].

$$\alpha_{ME} = \frac{\Delta V}{t.H_{AC}} \qquad \text{(Equation I.1)}$$

where ΔV is the generated voltage, t the thickness of the piezoelectric material and H_{AC} the intensity of the AC magnetic field. This method had a great reception since it reduces the problems of charge accumulation at the edge of the sample, and for such reason in the most used in the literature [55].

ME systems converting magnetic energy into electrical output (or vice-versa) can increase the productivity and efficiency of resources [56]. Additionally, information and communication technologies allow ME smart products with embedded sensors, actuators, processing units, connected via internet enabling functionalities for monitoring, control, real time optimization and autonomy [57, 58].

1.1.4 Green Chemistry

When we discuss the theme “pollution” and “waste”, electronics are not the first thing that comes to mind, nevertheless electronic waste, or the e-waste, is the fastest growing global waste stream [59].

Currently, electronic products are made with a wide range of hazardous materials, which can cause harm at all stages of the lifecycle of the product, particularly during manufacturing and recycling, as well as when mining or extracting the resources to make the products [60]. The composition of e-waste is extremely distinct and varies in products across several classes. Generally, it consists of ferrous and non-ferrous metals, printed circuit boards (PCB), plastics, glass, rubber and other items [61].

Another worrisome fact is that e-waste is growing three times faster than any other waste stream [62], and the usable lifespan of electronic products keeps shrinking (average electronic lifespan used to be eight years, now it is down to two), because the faster we see technology advancing, the more we are getting rid of [62, 63]. This type of waste is an emerging problem given the volumes of e-waste being generated and the content of both toxic and valuable materials in them [61]. To overcome some of the problems, mentioned before, the European commission created the European Green Deal, in 2019, with the aim of making Europe climate neutral in 2050 through a set of initiatives, including a toxic free environment (Figure I-8) [64].

So, it is urgent a new approach in terms of solvents, like "green solvents" and, in addition, new techniques to produce, in this case, "cleaner" electronics, that allow a reduction on the environment impact, such as printing techniques [14, 65]. Green chemistry is made not only to meet certain performance goals, but also to meet health and safety goals [66]. The term green chemistry was coined by Paul Anastas in 1991 [65] in a program conducted by the US Environmental Protection Agency to implement sustainable development in chemistry and chemical industries.

Figure I-8- *European commission initiatives [64].*

There are twelve key principles formulated which ought to be implemented by all chemists at all levels towards attaining the goal of good human health and clean environment [67]:

1. **Waste Prevention**: It is better to prevent waste than to treat or clean up waste after it has been created;

2. **Atom Economy**: Synthetic methods should be designed to maximize incorporation of all materials used in the process into the final product;

3. **Less Hazardous Synthesis**: Wherever practicable, synthetic methods should be designed to use and generate substances that possess little or no toxicity to human health and the environment;

4. **Designing Safer Chemicals**: Chemical products should be designed to preserve efficacy of function while reducing toxicity;

5. **Safer Solvents and Auxiliaries**: The use of auxiliary substances (e.g., solvents, separation agents, etc.) should be made unnecessary wherever possible and, innocuous when used;

6. **Energy efficiency**: By conducting synthesis at ambient temperature and pressure, energy requirement of the synthesis can be minimized;

7. **Use of Renewable Feedstock**: Whenever and wherever possible feed stock or raw material should be renewable;

8. **Reduce Derivatives**: Use of enzymes;

9. **Catalysis**: Catalytic reagents (as selective as possible) are superior to stoichiometric reagents;

10. **Design for Degradation**: Designing of chemical product is done in a way that they break down into innocuous degradation product in the end, which does not remain in the environment for long;

11. **Real time Analysis for Pollution Prevention**: For proper functioning of chemical processes real time feedback is needed;

12. **Inherently safer chemistry for accident prevention**: Substances and the form of a substance used in a chemical process should be chosen to minimize the potential for chemical accidents, including releases, explosions, and fires.

On the other hand, printing techniques, have been in the focus for several applications as a green, efficient, energy-saving, environmentally friendly manufacturing method. The process is additive and drastically lowers not only the number of manufacturing steps, but also the need for energy, time, consumables, as well as the waste [67].

1.2 Towards printable magnetoactive materials and devices

The idea of flexible electronics has been around for several decades - printed electronics is a new way to manufacture electronics employing an old manufacturing method combined with novel materials [69].

In 1903, Albert Hanson, a German scientist, filed the first patent on printed wires, in England, and created the circuit board for telephone systems, which consisted of conductive pieces of foil attached to wires and bonded to a flat sheet of paraffin paper [70, 71]. The construction resembled modern PCBs, despite being "unrefined" by todays' standards.

From 1903 onwards, the production of PCBs was done via the use of stencils and electrically conductive inks, later produced via etching copper foils in 1943 (Figure I-9) and reinforced by soldering copper wires in 1961. This technique allowed 25 % additional room to contain more functionality within the same enclosure [72].

Figure I-9- *Radio with printed PCB, in 1943 [73].*

In the same period (1967), thin solar cell arrays (< 200 μm) were employed for aerospace and satellites [74] and the mechanical flexibility offered a convenient yet consistent means for compact stowage during launch and thereafter opened for deployment.

It can be discussed that PE "came of age" in the 1970s when the first conducting polymers were realized by Nobel Laureates Alan Heeger, Alan MacDiarmid, and Hideki Shirakawa – "*plastic can, after certain modifications, be made electrically conductive*" [75].

Through the years, a lot of investigation to improve and optimize printing techniques and materials development in PE field, has been made. Analyzing the printed electronics by its basic components, the printing of electrical conductors corresponds to the base for other applications [11] and it allows to obtain conductors with controlled widths and thicknesses below 1 μm [76].

Regarding to its conductivities, it possible to control this parameter using different materials and fillers. Depending on the used fillers, the obtained inks can be classified as metallic [77], organic [78], ceramic [79] or a combination of them.

Printed conductors with conductivities greater than 2.43×10^{7} S m^{-1} at temperature of 120 °C are reported in literature [80], and in a general way, this field of technology is already considered well consolidated among the industries.

Nowadays, the evolution of the conductors is passing through the concept of stretchability, being reported studies that present conductors with high deformations (> 200 %) [19, 81], using inks based on highly stretchable materials [82] and innovative designs that promote the elasticity [82].

Concerning to drivers, transparency is another point of interest, being reported remarkable solutions with a conductivity/transparency ratio at the level of Indium tin oxide (ITO) solutions [83].

Depending on the base material used, the mentioned sub-areas (conductors and drivers) are located, in terms of state of development, between the semicommercial (as graphene, CNT) and the market growth (as Silver Nanowires (Ag NW) and metal mesh) [84]. The development of conductors is the basis for the construction of printed antennas, not only for data communication, with frequencies between 10 MHz and 6 GHz [85], but also for power transition (10 to 50 MHz) [86].

In the field of data communication, there are currently numerous published works, as well as commercial products, of antennas with gains of up to 10 dBi [87, 88], for high frequencies. In addition, the fact that the printed antennas are typically smaller, decrease the influence of them in the conductivity in their response. For energy transmission antennas, there are some developments in terms of energy, however its design is quite inefficient when compared with traditional solutions, since the series resistance of the coils used to harvest energy is very high, dissipating a lot of energy on the coil itself [89].

The printed sensing can be considered one of the areas of greatest impact, and that greater visibility gives the printing technologies due the wide range of solutions reposted in basically all sensor areas of transduction: physical, chemical, biochemical, optical, biosensors, etc. [90]. Yet, the number of reported solutions based exclusively on printing solutions is insufficient, being mostly restricted to sensors of humidity, temperature, gas, photodetectors, piezoresistive (mapping force) piezoelectric (pressure), capacitive and biosensors [91, 92].

Right when the IoT and 4.0 revolution concepts started to be discussed more concretely and from a more application-oriented point of view, a disposable glucose biosensor, produced by drop coating/screen-printing was proposed [93]. The biosensor was composed of Fe_3O_4 nanoparticles (synthesized by co-precipitation) that were drop coated (in an ammonia solution) into carbon electrodes that were previously screen-printed. The innovative glucose sensor exhibited a fast response (within less than 15 s), high sensitivity (1.74 $\mu A\ mM^{-1}$) and a wide linear range up to 33.3 mM (600 mg dL^{-1}) suitable for applications such as clinical diabetes sensors and in the food industry for quality control and communication tools.

The first printing procedure of a magnetic material with potential application for sensing devices and taking advantage of the giant magnetoresistance effect (GMR) was demonstrated by Karnaushenko et al., [94]. To formulate the ink, 500 mg of the GMR powder were added to 1 mL of a binder solution (polymethyl methacrylate (PMMA) dissolved in a methyl isobutyl ketone (MIBK) carrier, Figure I-10a-c). The magnetic material after being printed was incorporated in an electronic circuitry (amplification cascade with a light emitting diode (LED)) produced on a postcard (Figure I-10d-e). The fabricated material showed a high room-temperature GMR (≈ 8 %) revealing high technological potential for wireless switching in hybrid electronic circuitry. It was also shown that such high-performance printed magnetic materials were applicable to flexible electronics [95]. The proposed printed GMR sensing elements showed a high variation of the electrical resistance (37 %) with a maximum sensitivity of 0.93 T^{-1} at an optimum magnetic field of 130 mT.

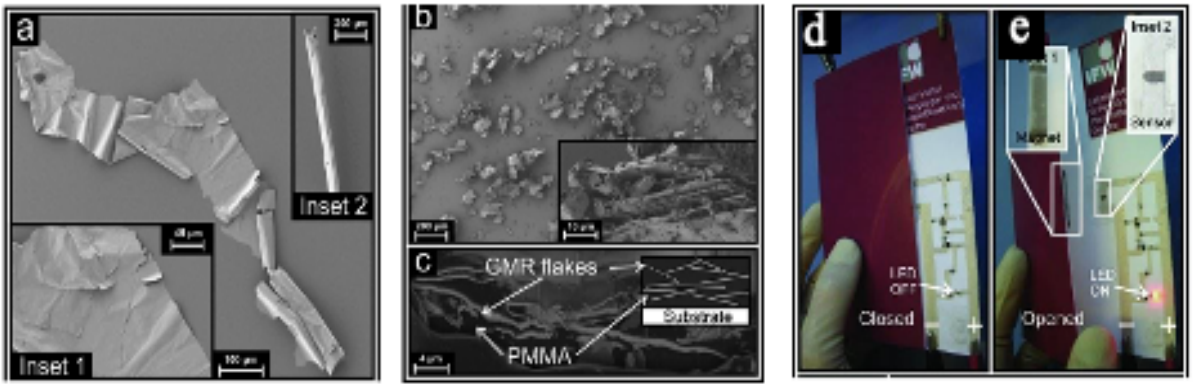

Figure I-10- *Images obtained through SEM of the GMR powder on different stages of ink preparation:* ***a)*** *Early GMR powder after the delamination from Si substrates, consisting of bulky metallic flakes (inset 1) and a high variety of tube-shaped structures (inset 2).* ***b)*** *Magnetic film milled with ceramic beads with the objective to develop magnetic powder composed of heterogeneously shaped flakes. The reported higher electrical conductivity is explained by the stacking of separated* $[Co/Cu]_{50}$ *flakes (inset 1).* ***c)*** *Cross-section image obtained through SEM of the printed. The inset reveals a schematic representation of the principle of flake percolation.* ***d)*** *and* ***e)*** *The LED ON/OFF status that is controlled with a magnet (inset 1) that changes the conductivity of the printed sensor (inset 2). Reproduced with permission from [94].*

A method to print magnetic field sensors based on colloidal nickel nanoparticles coated with polyvinylpyrrolidone (PVP) has been later presented [94]. The projected sensor achieved a significant Hall effect signal (≈ - 6 mΩ), low coercivity (≈ 10 mT), high conductivity (resistivity in magnetically saturated state in the range of 0.1 to 1.0 μΩ cm) and high sensitivity at magnetic fields close to 0 (5 $m\Omega\ T^{-1}$). The measured Hall resistance, under currents from 1 to 10 mA, were between 10 to 100 $m\Omega\ T^{-1}$ on a field range of 50 to 100 mT [96]. These printed magnetic field sensors allow applications such as contactless switches and linear or rotation motion sensors, needed in a 4.0 context.

In an attempt of monitoring Bisphenol A, a toxic and potent endocrine-disrupting compound in the environment, it was introduced a new idea to obtain electrochemical sensors [95] composed of screen-printed magnetic $CoFe_2O_4$/Multi-Walled Carbon Nanotubes (MWCNTs) nanoparticles electrodes combined with a magnetic-CoF_2O_4-solid phase microextraction for substance absorption. The sensor revealed high linearity in the 0.5 - 50 μM range with a 0.2 μM detection limit. The magnetic solid phase micro extractor fabricated by co-precipitation reaction, also presented an abstention capacity of 67.7 mg g^{-1} [97]. The printed sensor developed in this study provides a new tool for water pollution detection compatible with IoT environments.

By using a different type of CNT, SWCNTs (76 wt.%) and iron-based magnetic nanoparticles (11 wt.%), a magnetoactive composite has been inkjet-printed with the capability to be used on the IoT identification of genuine documents or a bank note [98]. The reported high conductance variation (from 10^{-8} S to 10^{-4} S) when a magnetic field of ≈ 1 mT was inputted was an obvious indicator of the suitability of this type of composites for smart sensing applications.

Magnetic filaments composed of Fe-based magnetic particles and acrylonitrile butadiene styrene (ABS) resin were also developed by fused deposition modeling method, being reported a relative permeability up to 1.7 for the sample with 70 wt.% of particle contents. According to this study, magnetic circuit with unusual and on-demand shapes for IoT-related magnetic field sensors can be envisioned [99].

The need for 3D printing of silicone-based magnetic materials by the 4.0 industries led to the production of Polydimethylsiloxane (PDMS)-SF13/carbonyl iron particles (with pure iron content of up to 99.8 %) composites with carbonyl iron content up to 30 wt.% [100]. The high magnetic permeability (5.5), normalized capacitance of 0.36 C_n at 0.5 T and the observed formation of cavities in the PDMS matrix that led to measurable magnetic-field-dependent changes in IR absorption at a wavelength of 4.255 μm (because of the interactions between diamagnetic atmospheric CO_2 and the magnetoactive composite) opened the application potential of this materials for IoT-related gas sensing devices.

Regarding ME materials, an up scalable and low-cost method for the development of ME materials based on spray-printing was presented [101], being suitable for cost-effective and large-scale sensor/actuator applications, namely in aerospace, automotive and recreational products [101]. With the addition of 20 wt.% of ferrite content to P(VDF-TrFE), the resulting composite exhibits a fibrillar-porous structure, an ≈ 1.8 GPa Young's Modulus, a saturation magnetization of 11.2 emu g^{-1}, a 6.0 emu g^{-1} magnetic remanence and a magnetic coercivity of 2050 Oe. The high dielectric (34 dielectric constant at 10 kHz) and piezoelectric (–27 pC N^{-1}) responses explain the high ME coupling of 21.2 mV cm^{-1} Oe^{-1} at an optimum magnetic field of 2450 Oe.

While many limitations still exist in nowadays, the successful printing of magnetic materials was accelerating in the recent years. As evidenced by the above-reviewed publications, new materials, processes, and applications are being explored for magnetoactive materials. The IoT context allows the "perfect storm" for this type of materials being fully implemented into a variety of advanced printed applications.

Following this technological wind, this thesis aims to develop a new generation of magnetoactive printable materials for device applications allying high-performance, compatibility with additive

manufacturing technologies and contributing towards environmental friendlier materials, processed and devices.

1.3 Objectives

The present work plan aims to develop a new generation of magnetoactive materials compatible with additive manufacturing and with reduced environmental impact. It is also intended to build a prototype, in which all components are fully printed. Thus, new magnetic and magnetoelectric inks will be developed, characterized and, later, integrated into a fully printed functional device.

In more detail, the objectives of this work are:

I) Formulation of inks (magnetic, magnetoelectric) using conventional approaches and environmentally friendly approaches; and functionalization of nanocomposites based on low-cost hydrophilic polymers, in order to be able to obtain adequate rheological properties (viscosity and surface tension) in addition to high chemical and colloidal stability;

II) Development of printed electronic components using printing techniques such as screen-printing and further characterization of the electrical and mechanical properties of electronic components, to identify the factors that limit the performance of the device for subsequent optimization, if necessary. The active layer of the magnetic and magnetoelectric sensor will be produced by screen-printing, to allow a thicker layer;

III) Construction of a fully printed and viable magnetic sensor for industrial use.

1.4 Structure of the work and methodology

This thesis is divided in six chapters, four of them based on already published research papers. In this way, a comprehensive and logic report is provided on the progress achieved during the present research as well as on the research methodology, as the chapters represent the sequential progress obtained during this work, involving the development of transparent materials (Chapter II), materials with improved ME response (Chapter III), green ME composites (Chapter IV) and magnetic proximity sensor application (Chapter V).

Thus, the present thesis is divided in the following chapters:

- **Chapter I** presents a general introduction to the work, the objectives, as well as the methodology and structure of the thesis. A brief state of the art on magnetoactive printable materials is presented. It is to notice that the specific state of the art is placed in each of the different chapters.
- **Chapter II** demonstrates the fabrication of a flexible and transparent ME composite, combining $Fe_{72.5}Si_{12.5}B_{15}$ microwires and poly (vinylidene fluoride-trifluoroethylene) – P(VDF-TrFE). It is based on the published research work "Transparent Materials for Advanced Invisible Electronic Applications".
- **Chapter III** presents the development of a novel screen-printed and flexible ME material based on P(VDF–TrFE) and PVDF–CFO. This chapter is based on the published scientific paper "All-printed multilayer materials with improved magnetoelectric response". A novel screen-printed and flexible ME material is developed based on P(VDF–TrFE) and PVDF–CFO.
- **Chapter IV** demonstrates that $CoFe_2O_4$/P(VDF-TrFE) nanocomposites can be successfully prepared from solution using three different environmental friendlier solvents: Dimethyl sulfoxide (DMSO), N, N′-Dimethylpropyleneurea (DMPU) and Triethyl phosphate (TEP) with different dipolar moments. This chapter is based on the published work "Greener solvent-based processing of polymer-based magnetoelectric nanocomposites".
- **Chapter V** reports magnetic proximity sensors based on magnetoelectric PVDF/Metglas® composites and an excitation-printed coil. This is based on the work "Magnetic Proximity Sensor Based on Magnetoelectric Composites and Printed Coils".
- **Chapter VI** presents the main conclusions of this thesis, as well some suggestions for future works.

1.5 References

1. Gomez, C., et al., Internet of Things for enabling smart environments: A technology-centric perspective. Journal of Ambient Intelligence and Smart Environments, 2019. 11(1): p. 23-43. DOI: 10.3233/AIS-180509
2. Ortiz, J., W. Marroquin, and L. Cifuentes, Industry 4.0: Current Status and Future Trends. 2019: IntechOpen. DOI: 10.5772/intechopen.90396. Available from: https://www.intechopen.com/chapters/70465
3. Costa, F., et al., A Review of RFID Sensors, the New Frontier of Internet of Things. Sensors, 2021. 21(9): p. 3138. DOI: https://doi.org/10.3390/s21093138

4. Moore, S.J., et al., IoT reliability: a review leading to 5 key research directions. CCF Transactions on Pervasive Computing and Interaction, 2020. 2(3): p. 147-163. DOI: https://doi.org/10.1007/s42486-020-00037-z

5. Haidine, A., et al., The role of communication technologies in building future smart cities, in Smart Cities Technologies. 2016: IntechOpen. DOI: 10.5772/64732. Available from: https://www.intechopen.com/chapters/52010

6. Martino, D., et al., Internet of Everything: Algorithms, Methodologies, Technologies and Perspectives. 1st ED. 2018. ISBN: 9789811058615

7. Dinc, E., et al., Internet of Everything: A Unifying Framework Beyond Internet of Things, in Harnessing the Internet of Everything (IoE) for Accelerated Innovation Opportunities. 2019, IGI Global. p. 1-30. DOI: 10.4018/978-1-5225-7332-6.ch001

8. Overmars, A. and S. Venkatraman, Towards a Secure and Scalable IoT Infrastructure: A Pilot Deployment for a Smart Water Monitoring System. Technologies, 2020. 8(4): p. 1-50. DOI: 10.3390/technologies8040050

9. Beedasy, V. and Smith, P.J., Printed Electronics as Prepared by Inkjet-Printing. Materials (Basel, Switzerland), 2020. 13(3): p. 704. DOI: https://doi.org/10.3390/ma13030704

10. Chang, J., et al., Fully printed electronics on flexible substrates: High gain amplifiers and DAC. Organic Electronics, 2014. 15(3): p. 701-710. DOI: https://doi.org/10.1016/j.orgel.2013.12.027

11. Liao, Y., Zhang, R., and Qian, J., Printed electronics based on inorganic conductive nanomaterials and their applications in intelligent food packaging. Royal Society of Chemistry, 2019(9): p. 29154-29172. DOI: DOI https://doi.org/10.1039/C9RA05954G

12. Cruz, S., Rocha, L. and Viana, J., printing Technologies in Flexible Substrates for Printed electronics, in Flexible Electronics, S. Rackauskas, Editor. 2017, IntechOpen. DOI: 10.5772/intechopen.76161. Available from: https://www.intechopen.com/chapters/61428

13. Huang, Q. and Y. Zhu, Printing Conductive Nanomaterials for Flexible and Stretchable Electronics: A Review of Materials, Processes, and Applications. Advanced Materials Technologies, 2019. 4: p. 1800546. DOI: https://doi.org/10.1002/admt.201800546

14. Nag, A., et al., Printed Electronics: Present and Future Opportunities, in 2015 9th International Conference on Sensing Technology. 2015, IEEE: New York. p. 380-389. DOI: 10.1109/ICSensT.2015.7438427

15. SCOPUS, Documents per year by year, 1950-2021. Available at https://www.scopus.com/term/analyzer.uri?sid=bc7cc08f45785418716d1cc30970ce64&origin=resultslist&src=s&s=TITLE-ABS-KEY%28printed+electronics%29&sort=cp-f&sdt=b&sot=b&sl=34&count=19431&analyzeResults=Analyze+results&txGid=632df940d0dd0cf6e97e6afabb308f30 (Access date: 10 June 2021).

16. Printed Electronics Market Research Report, By Component (Product; Visibility, Analytics, and Management Software; and Services), Industry Vertical (BFSI, government and defense, healthcare, retail, manufacturing) — Global Forecast till 2023.

17. Dahiya, A.S., et al., High-performance printed electronics based on inorganic semiconducting nano to chip scale structures. Nano Convergence, 2020. 7(1): p. 33. DOI: https://doi.org/10.1186/s40580-020-00243-6

18. Cano-Raya, C., et al., Chemistry of solid metal-based inks and pastes for printed electronics – A review. Applied Materials Today, 2019. 15: p. 416-430. DOI: 10.1016/j.apmt.2019.02.012

19. Suikkola, J., et al., Screen-Printing Fabrication and Characterization of Stretchable Electronics. Sci Rep, 2016. 6: p. 25784. DOI: https://doi.org/10.1038/srep25784

20. Søndergaard, R., et al., Roll-to-roll fabrication of polymer solar cells. Materials Today, 2012. 15(1): p. 36-49. DOI: https://doi.org/10.1016/S1369-7021(12)70019-6

21. Rincón-Iglesias, M., et al., Water-based 2D printing of magnetically active cellulose derivative nanocomposites. Carbohydrate Polymers, 2020. 233. DOI: 10.1016/j.carbpol.2020.115855

22. Krebs, F.C., Fabrication and processing of polymer solar cells: A review of printing and coating techniques. Solar Energy Materials and Solar Cells, 2009. 93(4): p. 394-412. DOI: 10.1016/j.solmat.2008.10.004

23. Sondhi, K., et al., Flexible screen-printed coils for wireless power transfer using low-frequency magnetic fields. Journal of Micromechanics and Microengineering, 2019. 29(8): p. 1-10. DOI: 10.1088/1361-6439/ab26ff

24. Ho, C.C. Dispenser Printed Electrochemical Capacitors for Power Management of Millimeter Scale Lithium-Ion Polymer Microbatteries for Wireless Sensors. in The Sixth International Workshop on Micro and Nanotechnology for Power Generation and Energy Conversion Applications, 2006. Berkeley, U.S.A.

25. De Vos, M., et al. Functional electronic screen-printing - Electroluminescent lamps on Fabric. in Procedia Engineering. 2014. 87: p. 1513-1516 DOI: https://doi.org/10.1016/j.proeng.2014.11.586

26. Oishi, A., et al. The power generation characteristics and durability of a vibration power generation device using piezoelectric thick film formed directly by screen printing on a stainless-steel substrate. in Journal of Physics: Conference Series. 2014.

27. Oliveira, J., et al., Polymer-based smart materials by printing technologies: Improving application and integration. Additive Manufacturing, 2018. 21: p. 269-283. DOI: https://doi.org/10.1016/j.addma.2018.03.012.

28. Sousa, R.E., C.M. Costa, and S. Lanceros-Mendez, Advances and Future Challenges in Printed Batteries. Chemsuschem, 2015. 8(21): p. 3539-3555. DOI: https://doi.org/10.1002/cssc.201500657

29. Mendes-Felipe, C., et al., State-of-the-Art and Future Challenges of UV Curable Polymer-Based Smart Materials for Printing Technologies. Advanced Materials Technologies, 2019. 4(3). DOI: https://doi.org/10.1002/admt.201800618

30. Shodeinde, A.B., et al., Recent Advances in Smart Biomaterials for the Detection and Treatment of Autoimmune Diseases. Advanced Functional Materials, 2020. 30(37). DOI: 10.1002/adfm.201909556

31. Galinski, H., et al., Functional Coatings on High-Performance Polymer Fibers for Smart Sensing. Advanced Functional Materials, 2020. 30(14). DOI: 10.1002/adfm.201910555

32. Correia, D.M., et al., Ionic Liquid–Polymer Composites: A New Platform for Multifunctional Applications. Advanced Functional Materials, 2020. 30(24). DOI: https://doi.org/10.1002/adfm.201909736

33. Farahani, R.D., M. Dubé, and D. Therriault, Three-Dimensional Printing of Multifunctional Nanocomposites: Manufacturing Techniques and Applications. Advanced Materials, 2016. 28(28): p. 5794-5821. DOI: https://doi.org/10.1002/adma.201506215

34. Ferreira, A., Nóvoa, and Marques A., Multifunctional Material Systems: A state-of-the-art review. Composite Structures, 2016. 151: p. 3-35. DOI: 10.1016/j.compstruct.2016.01.028

35. Roy, D., Cambre, J. and Sumerlin, B., Future perspectives, and recent advances in stimuli-responsive materials. Progress in Polymer Science (Oxford), 2010. 35(1-2): p. 278-301. DOI: 10.1016/j.progpolymsci.2009.10.008

36. Yao, X. and Lin, X., Emerging manufacturing paradigm shifts for the incoming industrial revolution. International Journal of Advanced Manufacturing Technology, 2016. 85(5-8): p. 1665-1676. DOI: https://doi.org/10.1007/s00170-015-8076-0

37. Jeong, U. and Y. Yin, Smart and Responsive Micro- and Nanostructured Materials. Advanced Functional Materials, 2020. 30(2).

38. Li, Z., F. Yang, and Y. Yin, Smart Materials by Nanoscale Magnetic Assembly. Advanced Functional Materials, 2020. 30(2). DOI: https://doi.org/10.1002/adfm.201903467

39. Nagarajan, B., P. Mertiny, and A.J. Qureshi, Magnetically loaded polymer composites using stereolithography—Material processing and characterization. Materials Today Communications, 2020. 25. DOI: 10.1016/j.mtcomm.2020.101520

40. Gottschall, T., et al., A Matter of Size and Stress: Understanding the First-Order Transition in Materials for Solid-State Refrigeration. Advanced Functional Materials, 2017. 27(32). DOI: https://doi.org/10.1002/adfm.201606735

41. Tang, S.Y., et al., Versatile Microfluidic Platforms Enabled by Novel Magnetorheological Elastomer Microactuators. Advanced Functional Materials, 2018. 28(8). DOI: https://doi.org/10.1002/adfm.201705484

42. Ikegawa, S., et al., Magnetoresistive Random Access Memory: Present and Future. IEEE Transactions on Electron Devices, 2020. 67(4): p. 1407-1419. DOI:10.1109/TED.2020.2965403

43. He, Y., et al., Interaction of Trace Rare-Earth Dopants and Nanoheterogeneities Induces Giant Magnetostriction in Fe-Ga Alloys. Advanced Functional Materials, 2018. 28(20). DOI: https://doi.org/10.1002/adfm.201800858

44. Martins, P. and S. Lanceros-Méndez, Polymer-based magnetoelectric materials. Advanced Functional Materials, 2013. 23(27): p. 3371-3385. DOI: https://doi.org/10.1002/adfm.201202780

45. Zhang, X., et al., Liquid Metal-Based Stretchable Magnetoelectric Films and Their Capacity for Mechanoelectrical Conversion. Advanced Functional Materials, 2020. 30(45): p. 2027–2034. DOI: https://doi.org/10.1021/acsnano.8b00147

46. Ma, J., et al., Recent progress in multiferroic magnetoelectric composites: from bulk to thin films. Adv Mater, 2011. 23(9): p. 1062-87. DOI: https://doi.org/10.1002/adma.201003636

47. Correia, D.M., et al., Low-field giant magneto-ionic response in polymer-based nanocomposites. Nanoscale, 2018. 10(33): p. 15747-15754. DOI: https://doi.org/10.1039/C8NR03259A

48. Landau, L.D. and E.M. Lifshitz Electrodynamics of Continuous Media, Course of Theoretical Physics. 1960, UK: Pergamon Press. 2nd ED. ISBN: 9780750626347

49. Nan, C.-W., et al., Multiferroic magnetoelectric composites: Historical perspective, status, and future directions. Journal of Applied Physics, 2008. 103(3): p. 031101.DOI: https://doi.org/10.1063/1.2836410

50. Palneedi, H., et al., Status and Perspectives of Multiferroic Magnetoelectric Composite Materials and Applications. Actuators 2015. 5(1). DOI: https://doi.org/10.3390/act5010009

51. Zheng, T., Development and Characterization of Polymer-based Magnetoelectric Nanofibers, in Intelligent Polymer Research Institute. 2017, Wollongong. https://ro.uow.edu.au/theses1

52. Tong, C., Introduction to Materials for Advanced Energy Systems. 2019: Springer. ISBN: 978-3-319-98002-7

53. Shi, Z., et al., Magnetoelectric Properties of Multiferroic Composites with Pseudo 1-3 Type Structure. Journal of Applied Physics, 2006. 99: p. 124108-124108. DOI: https://doi.org/10.1063/1.2208734

54. Lanceros-Méndez, S. and P. Martins, Magnetoelectric Polymer-based Composites: Fundamentals and Applications. 2017: John Wiley & Sons. DOI: https://doi.org/10.1002/adfm.201909736

55. Gil, K., et al. Experimental set up of a magnetoelectric measuring system operating at different temperatures. in Journal of Physics: Conference Series. 2016. DOI: 10.1088/1742-6596/687/1/012090

56. Aceto, G., V. Persico, and A. Pescapé, Industry 4.0 and Health: Internet of Things, Big Data, and Cloud Computing for Healthcare 4.0. Journal of Industrial Information Integration, 2020. 18: p. 100129. DOI: 10.1016/j.jii.2020.100129

57. Dalenogare, L.S., et al., The expected contribution of Industry 4.0 technologies for industrial performance. International Journal of Production Economics, 2018. 204: p. 383-394. DOI: 10.1016/j.ijpe.2018.08.019

58. Beier, G., et al., Industry 4.0: How it is defined from a sociotechnical perspective and how much sustainability it includes – A literature review. Journal of Cleaner Production, 2020. 259: p. 120856. DOI: https://doi.org/10.1016/j.jclepro.2020.120856

59. Semuels, A., The World Has an E-Waste Problem. 2019: Time Magazine. Available at https://time.com/5594380/world-electronic-waste-problem/ (Access date: 08 June 2021).

60. Pinto, V.N., E-waste hazard: The impending challenge. Indian journal of occupational and environmental medicine, 2008. 12(2): p. 65-70. DOI: 10.4103/0019-5278.43263

61. Needhidasan, S., M. Samuel, and R. Chidambaram, Electronic waste - an emerging threat to the environment of urban India. Journal of environmental health science & engineering, 2014. 12(1): p. 36-36. DOI: 10.1186/2052-336X-12-36

62. Abalansa, S., et al., Electronic Waste, an Environmental Problem Exported to Developing Countries: The GOOD, the BAD and the UGLY. Sustainability 2, 2021. 13(9): p. 5302. DOI: https://doi.org/10.3390/su13095302

63. Cucchiella, F., et al., Recycling of WEEEs: An economic assessment of present and future e-waste streams. Renewable and Sustainable Energy Reviews, 2015. 51: p. 263-272. DOI: https://doi.org/10.1016/j.rser.2015.06.010

64. European Commission, A European Green Deal: Striving to be the first climate-neutral Continent, 2019. Available at https://ec.europa.eu/info/strategy/priorities-2019-2024/european-green-deal_en (Access date: 07 June 2021).

65. Capello, C., U. Fischer, and K. Hungerbühler, What is a green solvent? A comprehensive framework for the environmental assessment of solvents. Green Chemistry, 2007. 9(9): p. 927-934. DOI: https://doi.org/10.1039/B617536H

66. Zuin, V.G., et al., Education in green chemistry and in sustainable chemistry: perspectives towards sustainability. Green Chemistry, 2021. 23(4): p. 1594-1608. DOI: https://doi.org/10.1039/D0GC03313H

67. Anastas, P. and J. Warner, Green Chemistry: Theory and Practice. American Chemical Society 1998: Oxford University Press: New York. 30.

68. Altay, B., M. Bolduc, and S. Cloutier, Sustainable Advanced Manufacturing of Printed Electronics: An Environmental Consideration, in Green Energy and Environment, Y. Hwa, Editor. 2019, IntechOpen. DOI: 10.5772/intechopen.91979. Available from: https://www.intechopen.com/chapters/71738

69. Keskinen, M., 16 - End-of-life options for printed electronics, in Waste Electrical and Electronic Equipment (WEEE) Handbook, V. Goodship and A. Stevels, Editors. 2012, Woodhead Publishing. p. 352-364. ISBN 9780081021583

70. Killeen K. and B. P, Flexible Circuit, EP1304911A1. 2003: European Patent.

71. Killeen K. and B. P., Extensible Spiral for Flex Circuit, US20030070833A1. 2003: United States Patent.

72. Reuss, R.H., G.B. Raupp, and B.E. Gnade, Special issue on advanced flexible electronics for sensing applications [Scanning the Issue]. Proceedings of the IEEE, 2015. 103(4): p. 491-496. DOI: 10.1109/JPROC.2015.2414486

73. Hills, J., Radio with the first Printed Circuit Board by Paul Eisler. Science Museum / Science & Society Picture Library.

74. Crabb, R.L. and F.C. Treble, Thin Silicon Solar Cells for Large Flexible Arrays. Nature, 1967. 213(5082): p. 1223-1224. DOI: https://doi.org/10.1038/2131223a0

75. The Nobel Prize in Chemistry 2000. NobelPrize.org. Nobel Prize Outreach AB 2021. Sun. Available at https://www.nobelprize.org/prizes/chemistry/2000/summary (Access date: 27 Jun 2021).

76. Suganuma, K., Introduction to Printed Electronics. 2014: Springer New York. ISBN: 978-1-4614-9625-0

77. R, V.K.R., et al., Conductive silver inks and their applications in printed and flexible electronics. RSC Advances, 2015. 5(95): p. 77760-77790. DOI: https://doi.org/10.1039/C5RA12013F

78. Saidina, D.S., et al., Recent Development of Graphene-based Ink and Other Conductive Material-based Inks for Flexible Electronics. Journal of Electronic Materials, 2019. 48(6): p. 3428-3450. DOI: https://doi.org/10.1007/s11664-019-07183-w

79. Lee, J.-H., et al., Formulation of a graft polymer-containing aqueous yellow ceramic ink for digital ink-jet printing. RSC Advances, 2020. 10(4): p. 2428-2436. DOI: https://doi.org/10.1039/C9RA09595K

80. Black, K., et al., Silver Ink Formulations for Sinter-free Printing of Conductive Films. Sci Rep, 2016. 6: p. 20814. DOI: 10.1038/srep20814 (2016).

81. Noh, J.-S., Conductive Elastomers for Stretchable Electronics, Sensors and Energy Harvesters. Polymers, 2016. 8(4): p. 123. DOI: https://doi.org/10.3390/polym8040123

82. Wu, W., Stretchable electronics: functional materials, fabrication strategies and applications. Science and Technology of Advanced Materials, 2019. 20(1): p. 187-224. DOI: https://doi.org/10.1080/14686996.2018.1549460

83. Hassan, G., J. Bae, and C.H. Lee, Inkjet-printed transparent and flexible electrodes based on silver nanoparticles. Journal of Materials Science: Materials in Electronics, 2018. 29(1): p. 49-55.

84. Wang, P., et al., Scalable Solution-Processed Fabrication Approach for High-Performance Silver Nanowire/MXene Hybrid Transparent Conductive Films. Nanomaterials, 2021. 11(6). DOI: https://doi.org/10.3390/nano11061360

85. Khan, Y., et al., A New Frontier of Printed Electronics: Flexible Hybrid Electronics. Advanced Materials, 2020. 32(15): p. 1905279. DOI: https://doi.org/10.1002/adma.201905279

86. Singh, R., E. Singh, and H.S. Nalwa, Inkjet-printed nanomaterial based flexible radio frequency identification (RFID) tag sensors for the internet of nano things. RSC Advances, 2017. 7(77): p. 48597-48630. DOI: DOIhttps://doi.org/10.1039/C7RA07191D

87. Babar, A.A., et al. Inkjet-printable UHF RFID tag antenna on a flexible ceramic- polymer composite substrate. in 2012 IEEE/MTT-S International Microwave Symposium Digest. 2012. DOI: 10.1109/MWSYM.2012.6259566

88. Subbaraman, H., et al., Inkjet-Printed Two-Dimensional Phased-Array Antenna on a Flexible Substrate. IEEE Antennas and Wireless Propagation Letters, 2013. 12: p. 170-173. DOI: 10.1109/LAWP.2013.2245292

89. Curry, J. and N. Harris, Powering the Environmental Internet of Things. Sensors (Basel, Switzerland), 2019. 19(8): p. 1940. DOI: https://doi.org/10.3390/s19081940

90. Naresh, V. and N. Lee, A Review on Biosensors and Recent Development of Nanostructured Materials-Enabled Biosensors. Sensors, 2021. 21(4). DOI: https://doi.org/10.3390/s21041109

91. Senthil Kumar, K., P.-Y. Chen, and H. Ren, A Review of Printable Flexible and Stretchable Tactile Sensors. Research, 2019. 2019: p. 3018568. DOI: https://www.mdpi.com/1424-8220/21/4/1109

92. He, S., et al., Recent Progress in 3D Printed Mold-Based Sensors. Sensors, 2020. 20(3): p. 703. DOI: https://doi.org/10.3390/s20030703

93. Lu, B.W. and W.C. Chen, A disposable glucose biosensor based on drop-coating of screen-printed carbon electrodes with magnetic nanoparticles. Journal of Magnetism and Magnetic Materials, 2006. 304(1): p. 400-402. DOI: 10.1016/j.jmmm.2006.01.222

94. Karnaushenko, D., et al., Printable giant magnetoresistive devices. Adv Mater, 2012. 24(33): p. 4518-4522. DOI: 10.1002/adma.201201190

95. Karnaushenko, D., et al., High-performance magnetic sensorics for printable and flexible electronics. Advanced Materials, 2015. 27(5): p. 880-885. DOI: 10.1002/adma.201403907

96. Ben Gur, L., et al., Extraordinary Hall-effect in colloidal magnetic nanoparticle films. Journal of Magnetism and Magnetic Materials, 2017. 426: p. 178-182. DOI:10.1016/j.jmmm.2016.11.106

97. Asiye Aslihan, A. and F. Hayati, $CoFe_2O_4$-MWCNTs Modified Screen Printed Carbon Electrode Coupled with Magnetic $CoFe_2O_4$-MWCNTs Based Solid Phase Microextraction for the detection of Bisphenol A. Current Nanoscience, 2018. 14(3): p. 199-208. DOI: 10.2174/1573413713666171109160816

98. Tanaka, S., et al., Investigation of Inkjet-Printed Composites Based on Single-Walled Carbon Nanotubes with Superparamagnetic Nanoparticles. IEEE Transactions on Applied Superconductivity, 2021. DOI: 10.1109/TASC.2021.3051297

99. Ikeda, S. and S. Yamada. Magnetic particle composite materials for magnetic sensor made by fused deposition method. in Proceedings of the International Conference on Sensing Technology, ICST. 2019. DOI: 10.1109/ICST46873.2019.9047742

100. Monkman, G.J., et al., Dielectric behaviour of magnetic hybrid materials. Physical Sciences Reviews, 2020. DOI: DOI: 10.1515/psr-2019-0121

101. Martins, P., et al., Spray-printed magnetoelectric multifunctional composites. Composites Part B: Engineering, 2020. 187: p. 107829. DOI: https://doi.org/10.1016/j.compositesb.2020.107829

CHAPTER II

TRANSPARENT MATERIALS FOR ADVANCED INVISIBLE ELECTRONIC APPLICATIONS

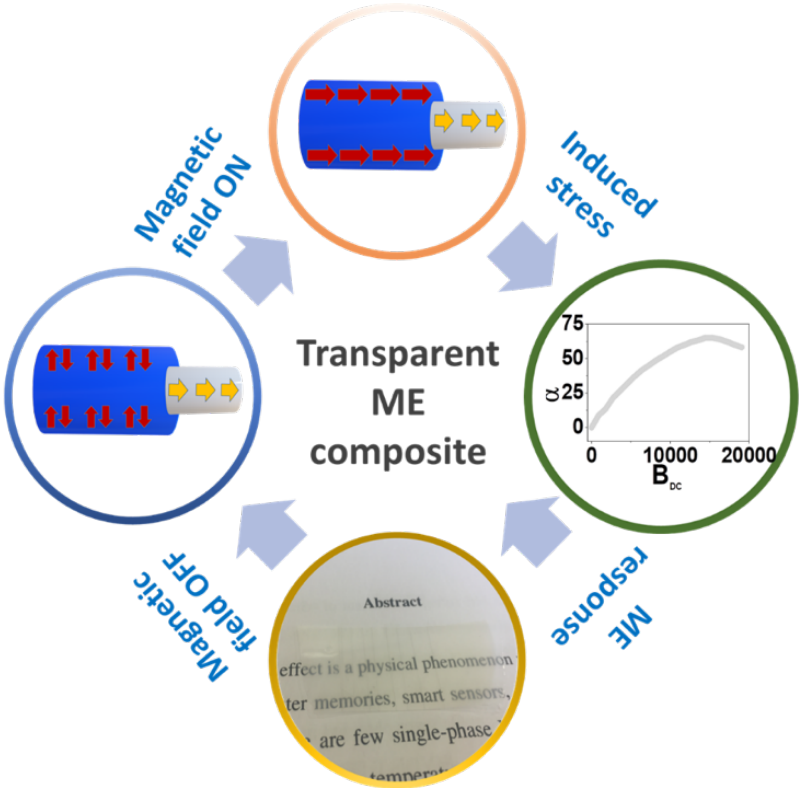

Chapter II – Transparent Materials for Advanced Invisible Electronic Applications

The need for flexible and transparent smart materials is leading to substantial advances in principles, material combinations, and technologies. Particularly, the development of optically transparent ME materials will open the range of applications to new directions such as transparent sensors, touch display panels, multifunctional flat panel displays, and optical magnetic coatings. In this work, a flexible and transparent ME composite is made of magnetostrictive $Fe_{72.5}Si_{12.5}B_{15}$ microwires and piezoelectric P(VDF-TrFE). The high magnetostriction of $Fe_{72.5}Si_{12.5}B_{15}$ (35 ppm) enables superior ME voltage response (65 mV cm^{-1} Oe^{-1}) obtained at the critical longitudinal magnetic field equating the transverse anisotropy (14500 A m^{-1}) on the external shell of the microwire.

This chapter is based on the following scientific publication:

R. Polícia, **A. C. Lima**, N. Pereira, E. Calle, M. Vázquez, S. Lanceros-Méndez, and P. Martins, Transparent Materials for Advanced Invisible Electronic Applications; Adv. Electronic Materials, vol. 5, 12, 2019. DOI: https://doi.org/10.1002/aelm.201900280

2.1 Introduction

ME materials present large potential in scientific and technological applications due to their ability to change the electric polarization in response to an external magnetic field or to change their magnetization in response to an applied electric field [1, 2]. Single-phase ME materials [3-5] are sparse in nature and have limited applications, since they show weak ME response at very low operating temperatures [6-8].

Alternatively, multiferroic composite materials, with an extrinsically ME effect, are suitable for practical applications due to the simplicity of the manufacturing process, and, more importantly, large magnitude of ME response at room temperature [9, 10]. These ME heterostructures [11] enable the conversion between magnetic and electrical energies through mechanical coupling between magnetostrictive and piezoelectric phases [12], allowing a high number of applications including magnetic sensors, actuators, switches, energy harvesters, inductors and data storage devices for smart electronic applications [13, 14].

However, despite the large potential of ME materials and the extensive research in this field in the last few years, the search for a flexible and resistant composite with high ME response, low-cost and simple fabrication continues to be a scientific/technological challenge [15]. Flexible materials allow to expand the boundaries of design and packaging, being suitable for a new generation of electronic device applications [16-18]. Polymer-based composites are the obvious choice to develop this kind of materials [19, 20].

Although ceramic-based ME composites present ME coefficients three orders of magnitude higher than polymer-based ME materials, piezoelectric ceramics are more expensive, rigid, and fragile, which makes them inadequate for several applications [21]. In contrast, polymer-based composites are flexible, lightweight, able to conform into a variety of forms, cheap, require low temperatures to process, and their fabrication can be scaled up, since the production methods are compatible with industrial requirements [22, 23].

Among polymeric piezoelectric materials, P(VDF-TrFE), a co-polymer of PVDF has been widely studied and used as organic matrix in ME composites since it exhibits high piezoelectric coefficient, stable mechanical properties, high breakdown strength, easy processing, high thermal stability, optical transparency and biocompatibility [24]. Recent results demonstrate the increased potential of polymer-based ME materials, and a strong effort is being made to develop new devices such as energy harvesters, actuators, low-temperature spintronics and magnetic sensors, among others [19, 25, 26].

As a disruptive approach in this field, the development of optically transparent materials will expand the range of applications of ME materials [27-32]. Different flexible and transparent smart materials have already been studied and developed. Thus, magnetic, conductive, semiconductive, and piezoelectric materials which are also flexible and transparent to the visible light are mentioned in the literature [33-38], however, transparent and flexible ME materials capable of combining magnetic and electrical properties on a single compound are still under-explored.

A first approach was presented in [39], where transparent ME nanocomposites based on magnetostrictive nanowires (NWs) of Fe, Ni and Galfenol dispersed and magnetically aligned inside of a piezoelectric polymer matrix of P(VDF-TrFE) were produced. Yet, the transparency of the material was not quantified and the use of nanowires instead of glass-coated microwires cause difficulties in the production of large number of nanowires, biocompatibility problems and loss of mechanical, electrical and chemical stability [40]. Additionally, the junction of polymer composites and magnetic microwires exhibits three additional merits, namely a remarkable magnetic field and mechanical stress tunability in the microwave regime that ensures excellent sensing properties, minimum disturbance of the mechanical properties compatibility with cost-effective fabrication techniques that don't demand magnetic alignment of the fillers [41].

The main difficult in developing a flexible transparent ME material is related to the magnetostrictive phase. Magnetic particles with high magnetostrictive values, such as $CoFe_2O_4$, for example, are opaque from a certain concentration (higher than 10 weight percentage (wt.%)) hindering the development of a material with high ME response and significant transparency, simultaneously.

Herein, we introduce magnetic microwires (MWs) that can be a solution to this scenario due to their excellent magnetic properties and unique geometrical features [42] that allow the development of transparent composites. These microwires, particularly those based on Iron-Silicon- Boron (FeSiB) alloy composition, exhibit a high saturation magnetic polarization (i.e., $J_s \approx 1.65$ T) and relatively high magnetostriction value ($\lambda_s \approx 35$ ppm). Their cylindrical geometry is characterized by a high aspect ratio (i.e., up to meters long and typically, 5-10 μm diameter), that favours the mechanical coupling with the piezoelectric polymer phase. In addition, these microwires, being structurally amorphous, present a strong uniaxial longitudinal magnetoelastic anisotropy determined by the coupling between the internal mechanical stresses and the magnetostriction constant that adds to their shape anisotropy. The magnetization process consists essentially in the nucleation and fast propagation of a single domain wall at relatively low applied field [43, 44].

The combination of the geometrical and mechanical properties together with the soft magnetic behavior makes them suitable for smart applications [42, 45]. Indeed, polymer composites incorporating ferromagnetic microwires reveal a series of potential applications due to the flexibility and sensitive response towards external stimuli, such as magnetic field, temperature, or mechanical stress, among others [46].

In this paper, we present the first flexible and transparent ME material made up of FeSiB amorphous microwires embedded and magnetically aligned inside a piezoelectric matrix of P(VDF-TrFE).

2.2 Experimental Section

2.2.1 Materials

N, N-dimethylformamide (DMF), pure grade was supplied by Fluka and P(VDF-TrFE) (Solef 1010) was supplied by Solvay. All the chemicals and particles were used as received from the suppliers. Poly (3,4-ethylenedioxythiophene) – poly (styrenesulfonate) (PEDOT/PSS) 5.0 wt.% conductive screen-printable ink was purchased from Sigma-Aldrich.

2.2.2 Preparation of magnetic microwires and magnetoelectric composite

Glass-coated amorphous microwires were fabricated by quenching and drawing technique having nominal composition of $Fe_{72.5}Si_{12.5}B_{15}$ (X-ray Diffraction-XRD- analysis can be found on [47]), with 9.2 μm metallic diameter and coated by Pyrex to a total diameter of 26.2 μm. 20 pieces of microwires (≈ 4 cm) have been placed in parallel and with a 2 mm spacing on a clean glass substrate. 2 g of P(VDF-TrFE) (XRD analysis can be found on [48]) have been added to DMF and mechanical agitation has been performed until a complete dissolution of the polymer.

The resulting solution was homogeneously distributed with a spreader over the aligned microwires. After the spreading step, the samples were placed inside an oven (JP Selecta, Model 2000208) for 10 minutes at a temperature of 210 °C, following the protocol presented in [49], for polymer melting and complete removal of the solvent. Then, the films (≈ 90 μm) were removed from the oven and allowed to cool at room temperature. The detachment of the flexible composite was obtained after the glass substrate was immersed in a vat for 20 minutes.

The transparent conductive ink, PEDOT/PSS, was screen-printed with a polyester mesh with 120 wires in both sides of the ME composite and cured on an oven at 130 °C for 3 minutes.

2.2.3 Characterization

The poling of the samples was achieved (before PEDOT deposition), after an optimization procedure [50], after 60 minutes of corona poling at 120 °C in a home-made chamber. In order to optimize the piezoelectric response, the electric field was kept applied when the samples were cooled to room temperature. The piezoelectric response (d_{33}) of the poled samples was obtained with a wide range d_{33}-meter (model 8000, APC Int. Ltd).

The magnetic characterization of the microwires was performed in a vibrating sample magnetometer (VSM) (ADE system EV7 KLA-Tencor) under a maximum applied magnetic field of ± 1.44 M A m^{-1}, parallel to the microwire axis.

The X-ray diffraction (XRD) data were taken by Esther Calle in a Bruker Diffractometer (D8 Advance A25), Cu Kα radiation (wavelength of 1.54 Å).

ME effect was characterized by measuring the transversal ME voltage coefficient (α_{33}) using the dynamic lock-in amplifier method [50]. A pair of Helmholtz coils was used to generate an AC magnetic field with amplitude of 63 A m^{-1} and frequency of ≈ 17-28 kHZ (resonance of the composites) that is superimposed to a DC bias field driven by an electromagnet.

Both fields are applied out of plane of the nanocomposite film and the generated voltage across the sample thickness is measured using a digital Lock-in amplifier (Stanford Research SR530).

The α_{33} was calculated from the measured voltage (across the PEDOT layers) using the Equation I.1.

The optical transmittance of the samples was obtained by a double beam spectrophotometer UV-2501PC UltravioleteVisible (UVeVIS) set up in the 350-700 nm range with a 1 nm step.

2.3 Results and Discussion

Figure II-1 depicts the ferromagnetic behavior of the FeSiB microwires under longitudinal applied field characterized by a squared hysteresis loop with a 182 A m^{-1} coercivity and a giant Barkhausen jump at around 200 A m^{-1} applied magnetic field.

The square hysteresis loop is characteristic of a bistable magnetic configuration, meaning that at remanence the microwire consists of a large magnetic domain with axial magnetization, and a smaller region (close to the external shell) remaining transversely magnetized. Upon application of a critical field (± 200 A m^{-1}), the magnetization reverses in that domain by the fast propagation of a single domain wall.

At higher applied field, magnetization increases reversibly at that external shell with small magnetic susceptibility until reaching apparent saturation at above 1.1 M A m^{-1} applied field. Additionally, the FeSiB microwires show the typical wide spectrum for an amorphous structure.

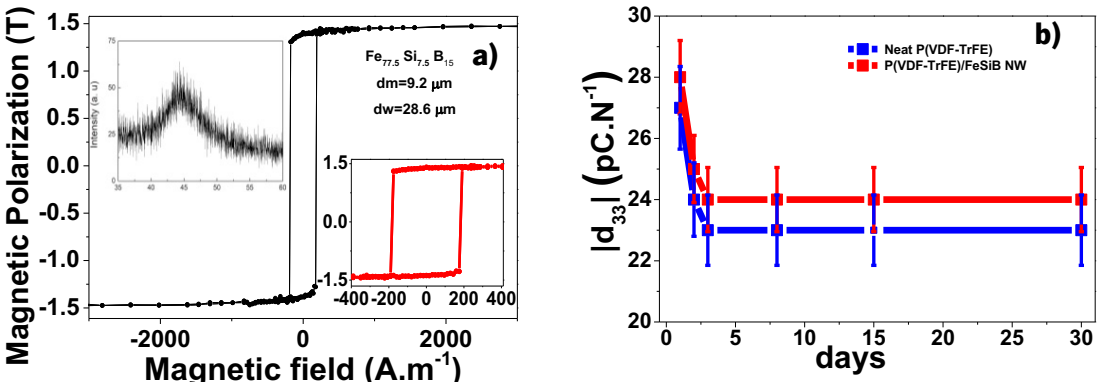

Figure II-1- a) *Room-temperature magnetic response of the FeSiB microwires (the top inset displays the XRD data of the FeSiB microwires); and* ***b)*** *room-temperature piezoelectric response of the P(VDF-TrFE)/FeSiB composite.*

As the P(VDF-TrFE) matrix has no influence in the type of magnetic response of the magnetostrictive inclusions [19, 51], the FeSiB microwires have been introduced in P(VDF-TrFE) and the $|d_{33}|$ of the resulting composite has been studied (Figure II-1b). It is observed that the piezoelectric response of the piezoelectric layer is not affected by the introduction of the magnetic fillers once it is similar to the one obtained in the neat P(VDF-TrFE) (24 – 28 pC N^{-1}) [49].

After the magnetic and piezoelectric behavior has been verified, the optical transmittance was studied (Figure II-2).

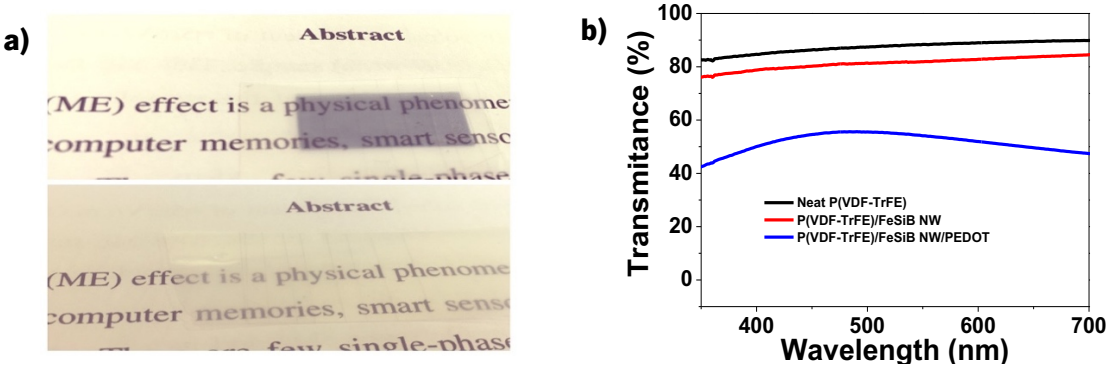

Figure II-2- a) *Photographs of the composite placed on a written page, with (TOP) and without (DOWN) the PEDOT conductive layers, serving as electrodes;* ***b)*** *Optical transmittance of the composites measured from 350 nm to 700 nm.*

Figure II.2b quantifies the optical transmittance loss from, ≈ 82 % to ≈ 50 %, observed when the two PEDOT conductive layers are printed in the composite. The difference on the optical transmittance between the neat P(VDF-TrFE) (≈ 88 %) and the P(VDF-TrFE)/FeSiB ME composite (≈ 82 %) is almost negligible, showing that the optimization of the transmittance in this type of material passes through the optimization of the conductive material and not so much through the optimization of the ME composites composition.

To validate the use of the flexible P(VDF-TrFE)/FeSiB/PEDOT composite as a ME material for sensor or energy harvesting applications, among others, the room-temperature ME response of the P(VDF-TrFE)/FeSiB/PEDOT was studied as a function of the B_{AC} frequency and DC (B_{DC}) magnetic field (Figure II-3).

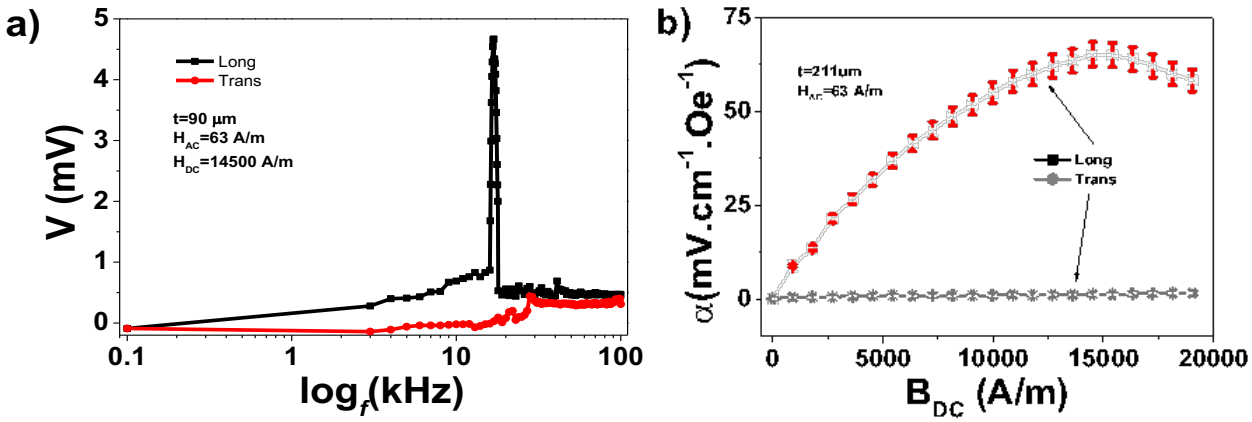

Figure II-3- a) *ME voltage coefficient of the sample measured longitudinally (in-plane) and transversally (out-of-plane) as a function of the resonance frequency;* ***b)*** *ME coefficient of the sample measured in-plane and out-of-plane as a function of the DC magnetic field.*

It is observed that the resonance frequency of the composites is ≈ 17 kHz when the measurement is performed longitudinally and ≈ 28 kHz when it is performed transversely. It is also observed that the ME voltage response is highly dependent on the direction of the applied magnetic field, reaching a maximum response of 65 mV cm^{-1} Oe^{-1} at 14500 A m^{-1} DC magnetic field and 60 A m^{-1} AC magnetic field for the sample, when characterized longitudinally.

The transversal ME response is negligible. Such distinct response is fully attributed to the small transversal susceptibility of the microwires because of the strong uniaxial longitudinal magnetic anisotropy of the microwire. Thus, a quite large transverse applied field is required to observe an even small magnetic response.

The bistable magnetic configuration of the microwires (a large magnetic domain with axial magnetization and an axial magnetization in relatively small region, close to the external shell), Figure II-4, ensures that the reversal occurring at 200 A m^{-1} by the fast propagation of a domain wall does not induce any magnetostrictive effect which is activated only by magnetization rotation mechanisms.

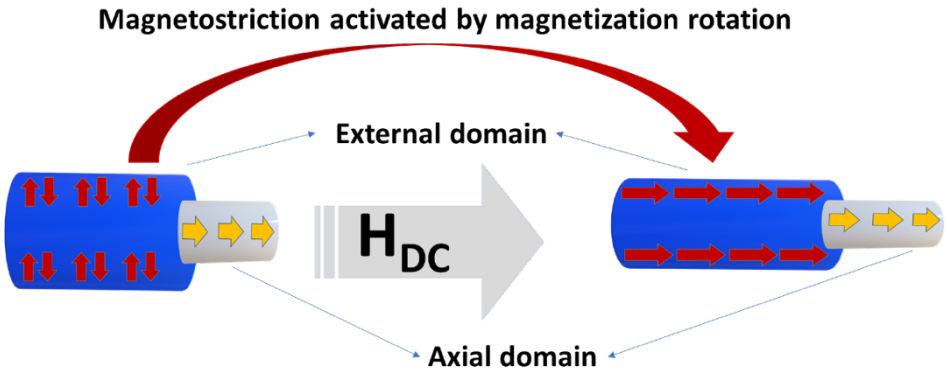

Figure II-4 - *Representation of the origin of magnetostriction on the FeSiB microwire.*

To compare the ME response reported in this work with the ones found in the literature we will introduce a new figure of merit α/H_{DC} aiming to correlate the ME voltage coefficient with the size of DC magnetic field needed to generate it (Table II-1).

Table II-1- Higher α/H_{DC} ratios reported in the literature.

Composite		**α (mV cm^{-1} Oe^{-1})**	**H_{DC} (Oe)**	**α/H_{DC} (mV cm^{-1} Oe^{-2})**	**Ref.**
Polymer	**Filler**				
P(VDF-TrFE)	$CoFe_2O_4$ NP	40	2500	0.02	[51]
	Galfenol NW	80	2000	0.04	[39]
	$Fe_{72.5}Si_{12.5}B_{15}$ MW	65	182	0.36	Our

Table II-1 reveals that the present work has the best α/H_{DC} ratio reported in the literature regarding polymer-based ME composites, being one order higher than the best ones. Finally, from a simple analysis of the longitudinal applied field at which maximum ME response is obtained we derive an interesting additional conclusion: the applied field can be correlated with the transverse magnetoelastic anisotropy

field ($H_{t,max} \approx 14500$ A m^{-1}) of the microwire that arises from the transverse mechanical stress frozen-in during the quenching fabrication process. Thus, the transverse magnetoelastic anisotropy energy density can be expressed as

$$K_t = (1/2)\, J_s \times H_{t,max} = (3/2)\, I_s \times \langle \sigma \rangle \qquad \text{(Equation II.1)}$$

where $\langle \sigma \rangle$ denotes the average compressive stresses in the external shell. From the experimental data we obtain $\langle \sigma \rangle \approx 230$ MPa which is a quite reasonable value for glass-coated microwires.

2.4 Conclusions

In conclusion, a flexible and transparent ME composite composed of P(VDF-TrFE) and $Fe_{72.5}Si_{12.5}B_{15}$ exhibited a maximum ME voltage response of 65 mV cm^{-1} Oe^{-1} obtained at the critical longitudinal applied field of at 14500 A m^{-1} that equals the transverse anisotropy field at the external shell of the microwire.

That allows us to anticipate that such a maximum ME can be engineered by the designed choice of the magnetostrictive character of the amorphous microwire (given by the alloy composition), with the value of the internal mechanical stresses (that can be tailored by suitable thermomagnetic annealing) and with the use of a conductive ink with higher transparency.

Transparent magnetic sensors (useful for anti-theft sensors and for optical modulators), actuators (in which the magnetization/actuation can be controlled by photo illumination), multifunctional touch displays (in which the transparent screen may incorporate transparent magnetic smart materials), and transparent optical magnetic coatings are obvious advantages of the composite reported in this work.

2.5 References

1. Palneedi, H., et al., Status and Perspectives of Multiferroic Magnetoelectric Composite Materials and Applications. Actuators, 2016. 5(1). DOI: https://doi.org/10.3390/act5010009
2. Nan, T., et al., A Strain-Mediated Magnetoelectric-Spin-Torque Hybrid Structure. Advanced Functional Materials, 2019. 29(6). DOI: https://doi.org/10.1002/adfm.201806371
3. Cong, J., et al., Spin-induced multiferroicity in the binary perovskite manganite Mn_2O_3 Nature Communications, 2018. 9(1). DOI: https://doi.org/10.1038/s41467-018-05296-0
4. Zhai, K., et al., Room-Temperature Nonvolatile Memory Based on a Single-Phase Multiferroic Hexaferrite. Advanced Functional Materials, 2018. 28(9). DOI: 10.1002/adfm.201705771

5. Shi, X., X.Q. Liu, and X.M. Chen, Readdressing of Magnetoelectric Effect in Bulk $BiFeO_3$, Advanced Functional Materials, 2017. 27(12). DOI: https://doi.org/10.1002/adfm.201604037

6. Folen, V.J., G.T. Rado, and E.W. Stalder, Anisotropy of the Magnetoelectric Effect in Cr_2O_3. Physical Review Letters, 1961. 6(11): p. 607-608. DOI: https://doi.org/10.1103/PhysRevLett.6.607

7. Rado, G.T. and V.J. Folen, Observation of the Magnetically Induced Magnetoelectric Effect and Evidence for Antiferromagnetic Domains. Physical Review Letters, 1961. 7(8): p. 310-311. DOI: https://doi.org/10.1103/PhysRevLett.7.310

8. Schmid, H., Multi-ferroic magnetoelectrics. Ferroelectrics, 1994. 162(1): p. 317-338. DOI: https://doi.org/10.1080/00150199408245120

9. Nan, C.-W., et al., Multiferroic magnetoelectric composites: Historical perspective, status, and future directions. Journal of Applied Physics, 2008. 103(3): p. 031101. DOI: https://doi.org/10.1063/1.2836410

10. Chen, J., et al., Symmetry Modulation and Enhanced Multiferroic Characteristics in $Bi1_{-x}NdxFeO_3$ Ceramics. Advanced Functional Materials, 2019. 29(3). DOI: https://doi.org/10.1002/adfm.201806399

11. Evrard, Q., et al., Layered Simple Hydroxides Functionalized by Fluorene-Phosphonic Acids: Synthesis, Interface Theoretical Insights, and Magnetoelectric Effect. Advanced Functional Materials, 2017. 27(41). DOI: 10.1002/adfm.201703576

12. Fernández-Posada, C.M., et al., The Polar/Antipolar Phase Boundary of BiMnO3–$BiFeO_3$–$PbTiO_3$: Interplay among Crystal Structure, Point Defects, and Multiferroism: Interplay among Crystal Structure, Point Defects, and Multiferroism. Advanced Functional Materials, 2018. 28(35). DOI: https://doi.org/10.1002/adfm.201802338

13. Verma, K.C., et al., Multiferroic $Ni_{0.6}Zn_{0.4}Fe_2O_4$-$BaTiO_3$ nanostructures: Magnetoelectric coupling, dielectric, and fluorescence. Journal of Applied Physics, 2014. 116(12): p. 124103. DOI: https://doi.org/10.1063/1.4896118

14. Yan, Y., et al., Colossal tunability in high frequency magnetoelectric voltage tunable inductors. Nature Communications, 2018. 9(1). DOI: https://doi.org/10.1038/s41467-018-07371-y

15. Kambale, R.C., D.-Y. Jeong, and J. Ryu, Current Status of Magnetoelectric Composite Thin/Thick Films. Advances in Condensed Matter Physics, 2012. 2012: p. 15. DOI: https://doi.org/10.1155/2012/824643

16. Oliveira, J., et al., Polymer-based smart materials by printing technologies: Improving application and integration. Additive Manufacturing, 2018. 21: p. 269-283. DOI: https://doi.org/10.1016/j.addma.2018.03.012

17. Guan, M., et al., Ionic Modulation of Interfacial Magnetism in Light Metal/Ferromagnetic Insulator Layered Nanostructures. Advanced Functional Materials, 2019. 29(1). DOI: https://doi.org/10.1002/adfm.201805592

18. Huang, S., et al., Flexible Electronics: Stretchable Electrodes and Their Future. Advanced Functional Materials, 2019. 29(6). DOI: https://doi.org/10.1002/adfm.201805924

19. Martins, P., and S. Lanceros-Méndez, Polymer-based magnetoelectric materials. Advanced Functional Materials, 2013. 23(27): p. 3371-3385. DOI: https://doi.org/10.1002/adfm.201202780

20. Zong, Y., et al., Cellulose-based magnetoelectric composites. Nature Communications, 2017. 8(1). DOI: https://doi.org/10.1038/s41467-017-00034-4

21. Lin, Y., et al., Giant magnetoelectric effect in multiferroic laminated composites. Physical Review B, 2005. 72(1): p. 012405. DOI: https://doi.org/10.1103/PhysRevB.72.012405

22. Maceiras, A., et al., High-temperature polymer-based magnetoelectric nanocomposites. European Polymer Journal, 2015. 64: p. 224-228. DOI: 10.1016/j.eurpolymj.2015.01.020

23. Buchanan, G.R., Layered versus multiphase magneto-electro-elastic composites. Composites Part B: Engineering, 2004. 35(5): p. 413-420. DOI: https://doi.org/10.1016/j.compositesb.2003.12.002

24. Ling, Q.-D., et al., Polymer electronic memories: Materials, devices and mechanisms. Progress in Polymer Science, 2008. 33(10): p. 917-978. DOI: https://doi.org/10.1016/j.progpolymsci.2008.08.001

25. Fusil, S.G., V.; Barthélémy, A.; Bibes, M., Magnetoelectric Devices for Spintronics, Annual Review of Materials Research, 2014. 44: p. 91-116. DOI: https://doi.org/10.1146/annurev-matsci-070813-113315

26. Phuoc, K., Electric field modulation of ultra-high resonance frequency in obliquely deposited $[Pb(Mg_{1/3}Nb_{2/3})O_3]0.68$-$[PbTiO_3]_{0.32}$(011)/FeCoZr heterostructure for reconfigurable magnetoelectric microwave devices. Applied Physics Letters, 2014. 105(2): p. 022905. DOI: https://doi.org/10.1063/1.4890411

27. Al-Dahoudi, N., et al., Transparent Conducting, Anti-static and Anti-static–Anti-glare Coatings on Plastic Substrates, 2001. 392(2): p. 299-304. DOI: 10.1016/S0040-6090(01)01047-1

28. Cesarini, G., et al., Optical and photoacoustic investigation of AZO/Ag/AZO transparent conductive coating for solar cells. Physica Status Solidi (C) Current Topics in Solid State Physics, 2016. 13(10-12): p. 998-1001. DOI: https://doi.org/10.1002/pssc.201600118

29. Liu, S.Y., et al., Highly Sensitive and Optically Transparent Resistive Pressure Sensors Based on a Graphene/Polyaniline-Embedded PVB Film. IEEE Transactions on Electron Devices, 2018. 65(5): p. 1939-1945. DOI: 10.1109/TED.2018.2814204

30. Xu, M., et al., Transparent and flexible tactile sensors based on graphene films designed for smart panels. Journal of Materials Science, 2018. 53(13): p. 9589-9597. DOI: 10.1007/s10853-018-2216-5

31. Zhang, D. and R.I. Murakami, Manipulation of optical and electrical properties of ZnO thin films via embedded nano structure. International Journal of Modern Physics B, 2018. 32(19). DOI: https://doi.org/10.1142/S0217979218400398

32. Luo, C.S., et al., Healable Transparent Electronic Devices. Advanced Functional Materials, 2017. 27(23). DOI: https://doi.org/10.1002/adfm.201606339

33. Neves, A.I.S., et al., Transparent conductive graphene textile fibers. Scientific Reports, 2015. 5: p. 9866. DOI: 0.1038/srep09866

34. Bagal, A., et al., Multifunctional nano-accordion structures for stretchable transparent conductors. Materials Horizons, 2015. 2(5): p. 486-494. DOI: https://doi.org/10.1039/C5MH00070J

35. Kobayashi, N., et al., Optically Transparent Ferromagnetic Nanogranular Films with Tunable Transmittance. Scientific Reports, 2016. 6: p. 34227. DOI: https://doi.org/10.1038/srep34227

36. MoolKyul, K., et al., Fully flexible and transparent piezoelectric touch sensors based on ZnO nanowires and $BaTiO_3$-added SiO_2 capping layers. physica status solidi (a), 2015. 212(9): p. 2005-2011.

37. Yamada, N., Y. Kondo, and R. Ino, Low-Temperature Fabrication and Performance of Polycrystalline CuI Films as Transparent p-Type Semiconductors. Physica Status Solidi (A) Applications and Materials Science, 2019. 216(5). DOI: https://doi.org/10.1002/pssa.201700782

38. Tsay, C.Y. and W.T. Hsu, Comparative studies on ultraviolet-light-derived photoresponse properties of ZnO, AZO, and GZO transparent semiconductor thin films. Materials, 2017. 10(12). DOI: https://doi.org/10.3390/ma10121379

39. Alnassar Mohammed, Y., P. Ivanov Yurii, and J. Kosel, Flexible Magnetoelectric Nanocomposites with Tunable Properties. Advanced Electronic Materials, 2016. 2(6): p. 1600081. DOI: https://doi.org/10.1002/aelm.201600081

40. Zhukov, A., High Performance Soft Magnetic Materials. 1st ed. Springer Series in Materials Science, ed. A. Zhukov. Vol. 252. 2017: Springer International Publishing AG, part of Springer Nature. DOI: https://doi.org/10.1007/978-3-319-49707-5

41. Zhukov, A., Novel Functional Magnetic Materials: Fundamentals and Applications. Vol. 231. 2016: Springer. DOI: https://doi.org/10.1007/978-3-319-26106-5

42. Pirota, K., et al., Multilayer microwires: Tailoring magnetic behavior by sputtering and electroplating. Advanced Functional Materials, 2004. 14(3): p. 266-268. DOI: 10.1002/adfm.200304432

43. Vázquez, M., et al., Trapping and injecting single domain walls in magnetic wire by local fields. Physical Review Letters, 2012. 108(3). DOI: https://doi.org/10.1103/PhysRevLett.108.037201

44. Calle, E., et al., Time-resolved velocity of a domain wall in a magnetic microwire. Journal of Alloys and Compounds, 2018. 767: p. 106-111. DOI: 10.1016/j.jallcom.2018.07.015

45. Vázquez, M., Advanced Magnetic Microwires, in Handbook of Magnetism and Advanced Magnetic Materials. 2007. p.2193-2226

46. Qin, F. and H.-X. Peng, Ferromagnetic microwires enabled multifunctional composite materials. Progress in Materials Science, 2013. 58(2): p. 183-259. DOI: http://dx.doi.org/10.1016/j.pmatsci.2012.06.001

47. Alvarez, K.L., et al., Magnetic Properties of Annealed Amorphous Alloys (Fe-rich) Obtained by Gas Atomization Technique. IEEE Transactions on Magnetics, 2018. 54(11). DOI: 10.3390/nano10050884

48. Shamsudeen, R.K., et al. Studies on piezosheets of P(VDF-TrFE) and its nanocomposites. in AIP Conference Proceedings. 2019. DOI: 10.1063/1.5093845

49. Ribeiro, C., et al., Electroactive poly (vinylidene fluoride)-based structures for advanced applications. Nature Protocols, 2018. 13(4): p. 681-704. DOI: 10.1038/nprot.2017.157

50. Martins, P., et al., Optimizing piezoelectric and magnetoelectric responses on $CoFe_2O_4$/P(VDF-TrFE) nanocomposites. Journal of Physics D: Applied Physics, 2011. 44(49): p. 495303. DOI: 10.1088/0022-3727/44/49/495303

51. Martins, P., et al., Effect of filler dispersion and dispersion method on the piezoelectric and magnetoelectric response of $CoFe_2O_4$/P(VDF-TrFE) nanocomposites. Applied Surface Science, 2014. 313: p. 215-219. DOI: 10.1016/j.apsusc.2014.05.187

CHAPTER III

ALL PRINTED MULTILAYER WITH IMPROVED MAGNETOELECTRIC RESPONSE

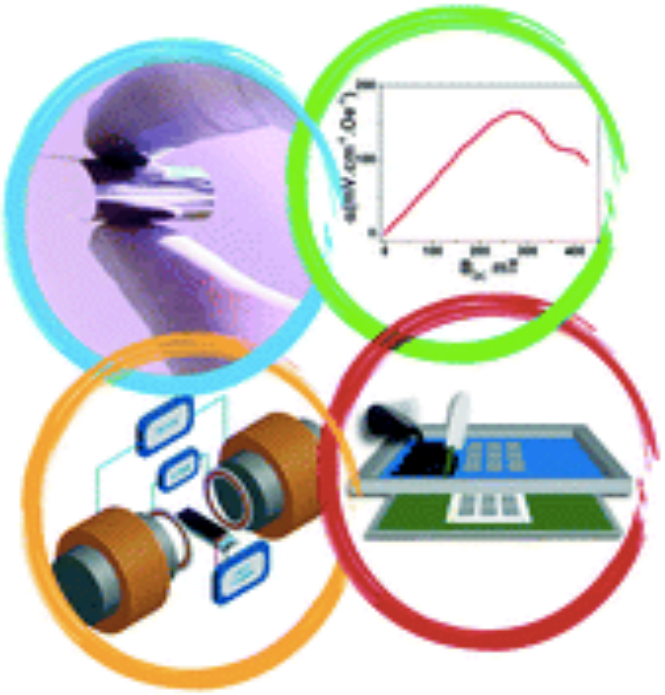

Chapter III – All Printed Multilayer with Improved ME Response

A decade ago, the "polymer-based magnetoelectric" idea changed thinking in multiferroic ME materials research, resulting in a new generation of high-performance materials and an increased focus on controlling structure, flexibility, and electrical output, as well as in the implementation into proof-of-concept applications. Nowadays, the successful implementation of those materials is closely related to the processing and integration of ME materials by additive manufacturing techniques on the cutting-edge interface of materials science with chemistry, physics, biology, and engineering. Here a novel screen-printed, and flexible ME material is developed based on P(VDF-TrFE) as the piezoelectric phase and PVDF/$CoFe_2O_4$ as the magnetostrictive phase. The all-printed ME composite exhibits a ferromagnetic behavior with 16 emu g^{-1} saturation magnetization, -26 pC N^{-1} piezoelectric response and a ME voltage coefficient of 164 mV cm^{-1} Oe^{-1} at a longitudinal resonance frequency of 16.2 kHz. Such optimized magnetic, piezoelectric and ME behavior associated to the reduced cost of assembly, easy integration into devices and the possibility to be obtained over flexible and large areas trough screen-printing demonstrates the suitability of the developed material for applications such as printed electronics, sensors, actuators, and energy harvesters.

This chapter is based on the following scientific publication:

A. C. Lima, N. Pereira, R. Polícia, C. Ribeiro, V. Correia, S. Lanceros-Méndez, and P. Martins, All-printed multilayer materials with improved magnetoelectric response, Journal of Materials Chemistry C, 7, 5394-5400, 2019. DOI: https://doi.org/10.1039/C9TC01428D

3.1 Introduction

The smart materials research area is a multidisciplinary field that explores the development and implementation of novel materials with increased functionality [1, 2]. These material types include shape memory, piezoelectric, piezoresistive, magnetorheological, magnetostrictive, micromachines, magnetoelectric, electrorheological and chromic materials, among others [3-5].

ME materials are particularly interesting as they provide effective coupling between electric and magnetic orders [6, 7], allowing additional degrees of freedom in the design of devices such as sensors, scaffolds, actuators, and information storage, among other interesting application areas [8-11]. Additionally, the processing of smart materials, including ME materials, by additive manufacturing processes, such as printing technologies, allows improved integration into devices and to explore novel applications in low-power, flexible and wearable electronics [12]. Regarding the ME coupling two distinct forms have been reported/explored: single-phase ME materials [13] and ME composites [14].

Single-phase ME materials, also known as intrinsic ME materials, usually show a low temperature and small ME coupling, hindering in this way their incorporation into technological applications [15]. In the case of ME composite materials with an extrinsic effect, the magnetic field induces a dimensional change in the magnetostrictive material that is transferred to the adjacent piezoelectric material, which in turn undergoes a mechanically induced change in its polarization, and vice-versa [16].

This ME-product property leads to output signals at room temperature that are 2-4 orders of magnitude higher than the ones observed in single-phase materials, making the materials suitable for device applications [17].

ME composite materials are divided into ceramic-based or polymer-based. Although ceramic-based ME materials show ME coefficients higher than the ones observed in polymer-based ME materials, piezoelectric ceramics are affected by reactions at the interface regions, feature low electrical resistance and high dielectric losses [8, 14].

Polymer-based ME materials allow overcoming these limitations. Further, polymers show a strain coupling that typically does not deteriorate with the operation, their processing is at low-temperature and allows a large variety of shapes and morphologies [18], are flexible [8], without large leakage currents [19], can exhibit optimized tailored mechanical properties [20] and in some cases biocompatibility [21].Depending on the interface between the magnetic phase and the polymer matrix, two main types of multiferroic polymer composites can be found in the literature: nanocomposites and laminate composites [20].

The ME response of nanocomposites is generally lower than in laminates. Thus, the ME response of P(VDF-TrFE)/$CoFe_2O_4$ nanocomposite [19] (42 mV cm^{-1} Oe^{-1}) is four orders of magnitude lower than the ME response (383 V cm^{-1} Oe^{-1}) reported for P(VDF-TrFE)/Metglas® 2605SA1 laminates. Nevertheless, its flexibility, simple fabrication (solvent-based), easy shaping, the possibility of miniaturization and/or to the ability produce large uniform areas and the absence of degradation at the piezoelectric/magnetostrictive interface are obvious advantages of nanocomposites [22].

Additionally, ME nanocomposites can support the expansion of the Internet of Things (IoT) concept once they allow the engineering of devices and systems to new environments and scales [23] that can allow the development of sustainable, wireless, and interconnected autonomous smarter devices, systems, and cities [1]. This interrelation of the IoT and ME composites is continuously developing, becoming an important research topic where new and fascinating innovation devices/opportunities will emerge [1] such wearable sensors (wearable magnetic field sensors for flexible electronics) [12], injectable and implantable bio-scaffolds/bio-actuators/bio-sensors [24], interconnected smart phones with improved battery life [25], wireless communication gadgets with miniaturized ME antennas working at their acoustic resonance frequencies [26] and smart energy harvesters capable of harvesting energy from dual-stimulus: mechanical vibrations and magnetic fields [27].

As a result, the printing of ME smart materials, not will just allow a more environmentally friendly production and implementation into devices, but also offers several advantages over other large-scale production methods, namely high speed, and low-cost production, patterning ability, compatibility with room temperature processes and suitability for large area production on flexible substrates [1].

Being the cost/efficiency ratio optimization of printing technologies, and their use in ME smart materials production a catalyst for the emergence of new device applications [28], it is highly surprising that, to our knowledge, the only report regarding the printing of polymer-based ME materials is the one of Chlaihawi et al. [29]. Nevertheless, such ME material was produced by screen-printing PVDF piezoelectric polymer into a magnetostrictive Metglas® substrate, not being in this way, a fully printed ME material and therefore limiting the aforementioned advantages of printed devices.

In this work, we present the first fully printed ME composite. The printed ME is based on PVDF, P(VDF–TrFE), $CoFe_2O_4$ (CFO) nanoparticles and silver conductive ink. P(VDF–TrFE) will be used as piezoelectric polymer due to its highest piezoelectric response among polymers [19], PVDF as a binder for the high magnetostrictive CFO nanoparticles [14] and silver as the electrode.

Screen-printing, one of the most used techniques for smart materials production, is used due to its high velocity and versatility [30].

3.2 Experimental Section

3.2.1 Materials

CFO nanoparticles (≈ 30-55 nm) were purchased from Nanoamor (Houston, TX, USA). N, N-dimethylformamide (DMF), pure grade was supplied by Fluka (Milwaukee, WI, USA), (PVDF Solef 1010) and P(VDF-TrFE) 70/30 were supplied by Solvay (West Deptford, NJ, USA). HPS-021LV – Silver ink was purchased from Novacentrix (Austin, TX, USA). All chemicals and particles were used as received from the suppliers.

3.2.2 Ink and magnetoelectric printed sample preparation

For production for the hybrid ME composite the following steps were followed (Figure III-1):

i) A P(VDF-TrFE) ink suitable for screen-printing was developed by adding 4 g of the polymer powder to 10 mL of DMF. The mixture was magnetically stirred during 2 hours at room temperature (≈ 25 °C) until complete dissolution of the polymer.

ii) The Novacentrix HPS-021LV – Silver ink (top electrode: 1000 Pa s viscosity) was screen-printed with a polyester mesh with 64 wires on a Teflon flexible substrate. The resulting 2-layer laminate was placed in an oven at 80 °C for one hour.

iii) The P(VDF-TrFE) ink was screen-printed with a polyester mesh with 64 wires on the previous laminate. The resulting 3-layer laminate was placed on an oven at 210 °C for 10 minutes.

iv) The Novacentrix HPS-021LV – Silver ink (bottom electrode) was screen-printed with a polyester mesh with 64 wires on the previous laminate. The resulting (4-layer) laminate was placed on an oven at 80 °C for one hour.

v) A PVDF/CFO magnetostrictive ink was obtained by adding 11.3 g of CFO to 9 mL of DMF. 2 g of PVDF polymer was then added to the former mixture as a binder and mechanically stirred during 2 hours at room temperature with a Teflon stirrer. After solvent evaporation, the CFO content on the PVDF matrix will be 85 % in weight percentage (wt.%). Such content was selected to obtain a high magnetostrictive layer [14]. Two other contents of CFO (20 wt.% and 40 wt.%) were also used in the

development of the magnetostrictive layer to study the influence of the CFO in the rheology of the resulting inks.

vi) The previous PVDF/CFO magnetostrictive ink was screen-printed with a polyester mesh with 64 wires on the laminate of step **iv)**. The resulting (5-layer) laminate was placed on an oven at 210 °C for one hour.

The transversal poling of the piezoelectric layer was achieved after step **iii)**, subsequently to an optimization procedure: 60 minutes of corona poling at 120 °C in a home-made chamber [18]. The electric field was kept applied when the samples were cooled to room temperature. The composite sample was magnetized along the length direction for 60 minutes at 3000 Oe DC magnetic field.

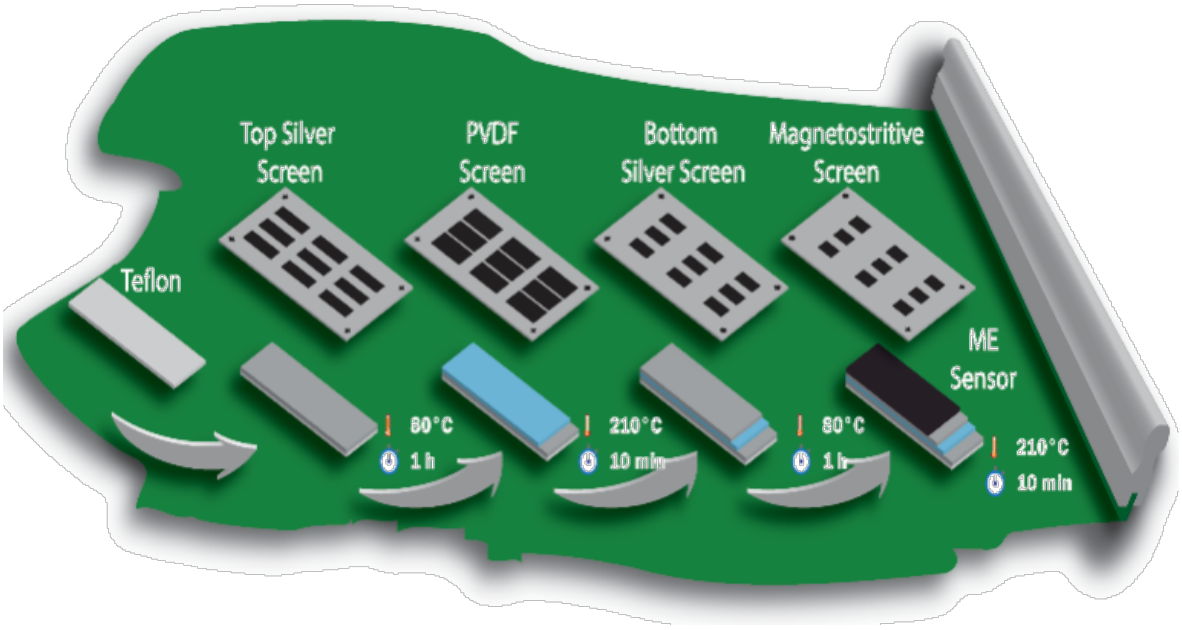

Figure III-1- *Schematic representation of the experimental procedure used to: obtain the hybrid ME composite.*

3.2.3 Ink and magnetoelectric printed sample characterization

The morphology of the ME sample was evaluated *via* scanning electron microscopy (SEM) with a NanoSEM - FEI Nova 200 (FEG/SEM) scanning electron microscope at 10 kV. Before SEM, samples were gold coated by magnetron sputtering using a Polaron SC502 sputter coater. The thicknesses values were calculated from 5 images with 10 measurements by using an Image J software.

Magnetic hysteresis loops were measured at room temperature using an ADE Technologies 3473-70 vibrating sample magnetometer (VSM).

The piezoelectric response of the poled samples was obtained with a wide range d_{33}-meter (model 8000, APC Int. Ltd).

The ME effect was characterized by measuring the transversal ME voltage coefficient (α_{33}) and longitudinal ME coefficient (α_{31}) using the dynamic lock-in amplifier method. A pair of Helmholtz coils was used to generate an AC magnetic field with an amplitude of 1 Oe and frequency equal to the resonance of the ME sample that is superimposed to a DC bias field driven by an electromagnet. The generated voltage across the sample thickness direction was measured using a digital Lock-in amplifier (Stanford Research SR530).

Both ME voltage coefficients were calculated from the measured voltage using Equation I.1 [31].

Rheological measurements were performed using an AresG2 rheometer equipped with a flat plate geometry (40 mm) and a GAP of 1000 μm. The different solutions were transferred onto the rheometer plate (preheated at 40 °C) immediately after the polymer dissolution and incorporation of the particles. Flow curves were obtained by a three-shear rate sweeps (up-down-up) program (to eliminate the time-dependence) using a continuous ramp and shear rate range between 0 and 300 s^{-1}.

The apparent viscosity at low shear rate (3 s^{-1}) was evaluated from curve 1 (unsteady-state) since the structure was less disturbed at this condition; and from curve 3 for the others shear rate values (steady-state).

The viscosity of the different solutions was compared at different shear rates if the solutions follow a power-law model (Equation III.1) [32].

$$\eta = K \gamma^{N-1} \qquad \text{(Equation III.1)}$$

where the coefficients K and N are determined experimentally.

3.3 Results and Discussion

3.3.1 Inks properties

Knowing that the ink viscosity range for screen-printing can vary between ≈ 0.1 Pa s and ≈ 1000 Pa s, the rheological measurements, and the viscosity of the inks as a function of magnetic filler content of both piezoelectric and magnetostrictive inks are presented in Figure III-2

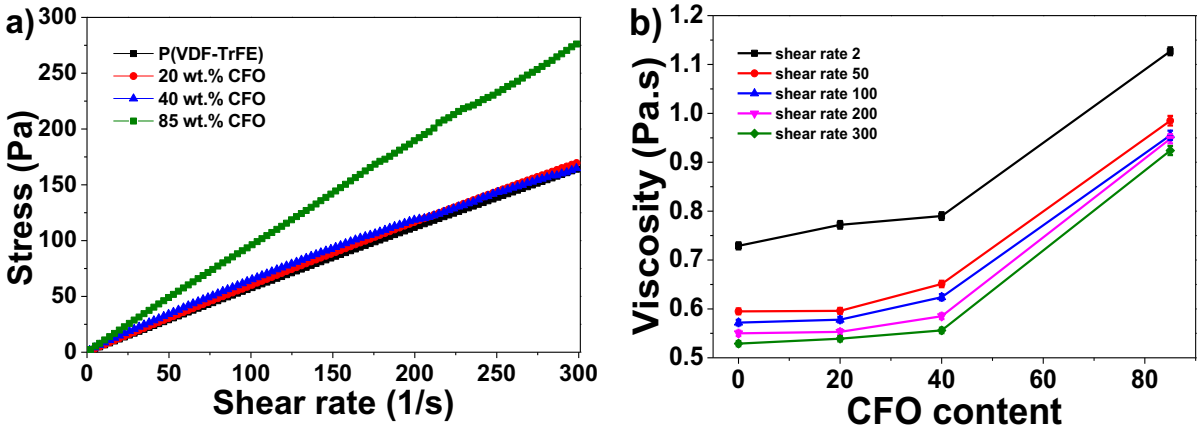

Figure III-2- a) *Shear stress versus shear rate of the different inks;* ***b)*** *Viscosity values of the different inks as a function of magnetostrictive filler content for different shear rates.*

It is verified that the shear stress increases almost linearly with the shear rate for all the inks, being observed a higher slope in the sample with higher content of CFO nanoparticles, due to the higher viscosity on those formulations. Data from Figure III-2a were used to determine the viscosity as a function of the CFO content and shear rate (Figure III-2b), being verified a slight increase in the viscosity, for all shear rates, with the introduction of magnetic particles for CFO contents lower than 20 wt.%.

The same does not happen when 85 wt.% of magnetic nanoparticles are added, being detected a significant increase of the viscosity values for all shear rates. Based on the results of Figure III-2, the 85 wt.% of CFO composition was selected for the development of the magnetostrictive ink, since the high concentration of particles will give rise to a higher magnetostriction [14] and by the fact that its maximum viscosity (1100 Pa s) is compatible with the screen-printing process.

3.3.2 Printed Layers

After checking the viscosity of the inks, the ME laminate was produced, and the cross-sectional SEM image of the multilayer film is shown in Figure III-3a.

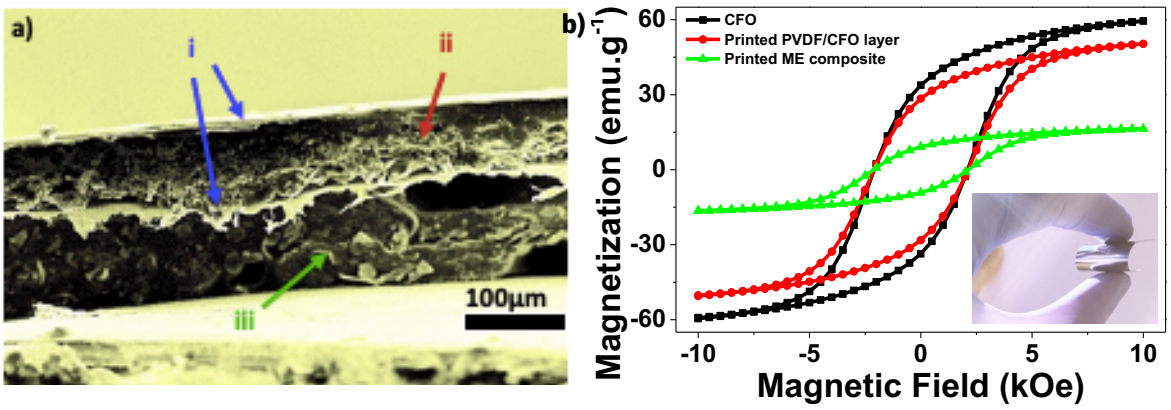

Figure III-3 - a) *SEM image of the printed ME sample: i) silver electrodes, ii) P(VDF-TrFE) piezoelectric layer, iii) PVDF/CFO magnetostrictive layer;* ***b)*** *Room-temperature magnetic hysteresis loops for the pure CFO nanoparticles, printed PVDF-CFO layer and all-printed.*

Figure III-3a exhibits a thin film multilayered structure revealing thicknesses of 100 (± 10) nm, 108 (± 11) µm, 122 (± 12) µm and 250 (± 15) µm, for the silver electrodes layers (i), P(VDF-TrFE) piezoelectric layer (ii), magnetostrictive PVDF/CFO layer (iii) and all-printed ME, APME, composite, respectively. VSM measurements (Figure III-3b) were used to determine the room-temperature magnetic response of the APME composite and to calculate the CFO content on the magnetostrictive PVDF/CFO magnetostrictive layer and in the APME laminate, by the method proposed in [33]. The proper interface between the magnetostrictive and piezoelectric layers is also indirectly demonstrated by the stability of the ME response after repeated material manual bending (inset of Figure III-3b).

The CFO nanoparticles exhibit room-temperature ferromagnetism with a saturation magnetization of 59 emu g^{-1}, 34 emu g^{-1}, remanence and coercivity of 2030 Oe. The hysteresis loops of the PVDF/CFO layer and APME composite also reveal ferromagnetic nature which confirms that the PVDF matrix and printing process have no influence on the ferromagnetism of the nanoparticles.

The saturation magnetization of the printed PVDF/CFO layer (50 emu g^{-1}) and APME composite (16 emu g^{-1}) allowed to determine their CFO content as 84 wt.% and 27 wt.%, respectively.

3.3.3 Smart Response

The piezoelectric response of the P(VDF-TrFE) layer and ME behavior of the all-printed P(VDF-TrFE)/PVDF/CFO ME composite can be found in Figure III-4.

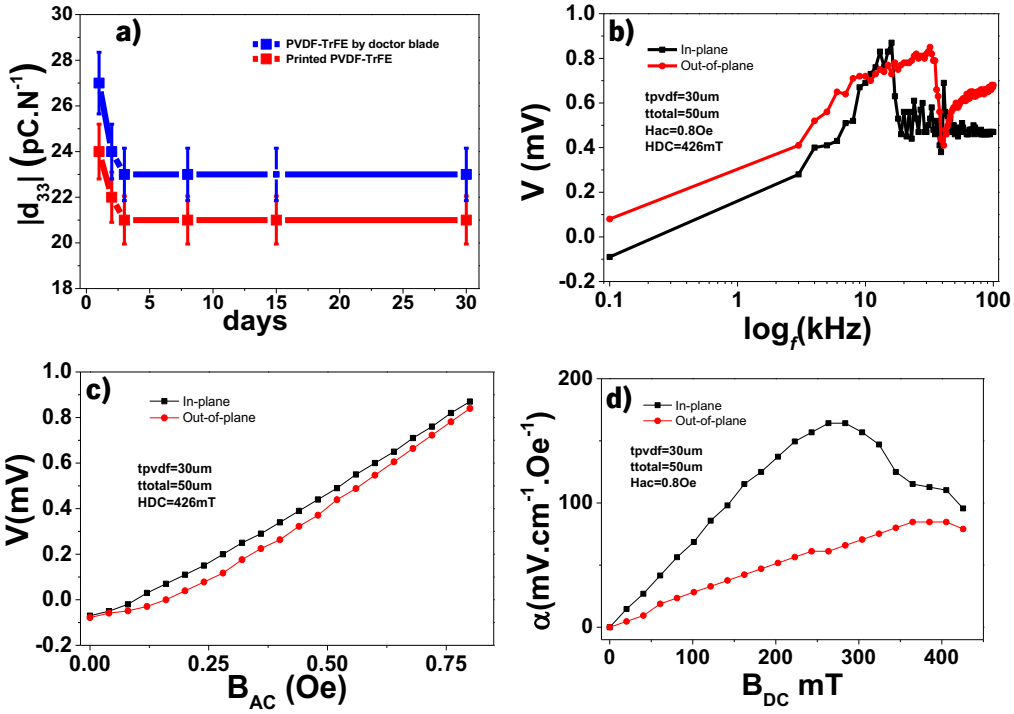

Figure III-4- a) *Room-temperature piezoelectric response of the ME sample compared with the one obtained on a P(VDF-TrFE) prepared by doctor blade;* ***b)*** *magnetoelectric voltage of the sample measured longitudinally (in-plane) and transversally (out-of-plane) as a function of the frequency;* ***c)*** *ME coefficient (α) of the sample measured in-plane and out-of-plane as a function of the AC magnetic field;* ***d)*** *ME coefficient of the sample measured in-plane and out-of-plane as a function of the DC magnetic field.*

Figure III-4a shows that the piezoelectric response of the piezoelectric layer is not affected by the printing process once the $|d_{33}|$ value of the printed P(VDF-TrFE) is like the one obtained by the traditional doctor blade technique (-24 to -28 pC N^{-1}).

After a correct magnetic and piezoelectric behavior has been verified in the different layers, ME evaluation has been performed in the multilayered composite. The resonance of the composite was found to be 16.2 kHz on the longitudinal direction and 32.1 kHz on the transversal direction.

The ME voltage response as a function on the AC magnetic field and DC magnetic field was performed for those frequencies (Figure III-4c-d). Despite the ME response as a function of the AC field be very similar in both directions, the ME coefficient as a function of the DC field is highly dependent on the direction of the applied magnetic field, reaching a maximum response of 164 mV cm^{-1} Oe^{-1} at 260 mT and 83 mV cm^{-1} Oe^{-1} at 405 mT for the sample characterized longitudinally and transversely, respectively.

Such distinct response is fully attributed to the anisotropic behavior of the magnetostriction on the PVDF/CFO magnetostrictive layer, that strongly depends on the magnetic alignment achieved in the magnetization procedure [34].

Once the CFO on the PVDF matrix is magnetically aligned along the longitudinal direction, in such direction the ME response is higher and occurs for lower DC magnetic fields. When the ME behavior is induced along the perpendicular direction, there is a need to reorganize the magnetic moments in such direction, leading the emergence of demagnetizing effects, with the consequence of smaller ME voltage response occurring at higher DC magnetic fields [34, 35].

In this way, by changing the thickness of the PVDF/CFO layer or by changing the exciting modes (longitudinal or transversal), the maximum of the ME voltage response can be tuned, and its amplitude further tailored [35].

Table III-1 shows that the obtained ME values are the highest on polymer/CFO composites, both laminate and nanocomposites. Further, the ME coefficient is in the same order of magnitude of the ones observed on PVDF/Metglas® laminates and piezoceramics/CFO nanocomposites.

Table III-1- *Comparison between α_{ME} obtained in this work for an all-printed multi-layered structure and the ones reported in the literature for similar compositions but in laminated and nanocomposite form.*

Sample		**Type**	**α (mV cm^{-1} Oe^{-1})**	**Ref.**
Piezoelectric	**Magnetic**			
PVDF	Metglas ®	Laminate-piezo printed	686	[29]
Pb ($Fe_{1/2}Nb_{1/2}$) O_3	CFO particles	Laminate-tape cast	206	[36]
		Nanocomposite-ball mill	76	
P(VDF-TrFE)	CFO ellipsoids	Nanocomposite-doctor blade	1.5	[34]
	CFO particles		40	[19]
		Hybrid-all printed	164	Our

The highest ME response of the developed printed hybrid composite when compared to the traditional nanocomposites reported in the literature is explained by the improved elastic coupling between piezoelectric and magnetostrictive phases. Such coupling is less effective in the case of nanocomposites once the movement of domain walls under applied external magnetic field is expected to progress easier in highly concentrated ferrite layers than in nanocomposites with less concentration of ferrite [36]. In this way, the progress of approaching magnetic domain wall may be hindered by amorphous polymer chains surrounding a ferrite particle due to their non-ferromagnetic character. Additionally, on nanocomposites the ME coupling is often suppressed due to leakage current in the magnetostrictive nanoparticles that affect the piezoelectric matrix, in the case of the reported hybrid composite, the resistivity of the material is improved with the existence of a neat piezoelectric dielectric layer [19, 36].

Such high ME response allied to the simplicity and scalability of the screen-printing technique demonstrate the suitability of the all-printed P(VDF-TrFE)/PVDF-CFO ME multilayer structure for technology transfer and implementation into flexible sensors, actuators and energy harvesting applications [1, 17].

3.4 Conclusions

A hybrid ME composite was successfully printed with P(VDF-TrFE)/DMF as piezoelectric ink (0.53 Pa s viscosity at 300 s^{-1} shear rate), PVDF-CFO/DMF (1.13 Pa s viscosity at 300 s^{-1} shear rate) as magnetic ink and silver ink as electrodes.

The resulting composite exhibits a ferromagnetic behavior with 16 emu g^{-1} saturation magnetization, -26 pC N^{-1} piezoelectric response and a ME voltage coefficient of 164 mV cm^{-1} Oe^{-1} at a longitudinal resonance frequency of 16.2 kHz, the highest reported in the literature in this kind of composite.

The additive manufacturing nature of the printing process results in improved usage of material and integration and, consequently, more efficient production of the ME material for sensor and actuator applications.

3.5 References

1. J. Oliveira, V. Correia, H. Castro, P. Martins and S. Lanceros-Mendez, Additive Manufacturing, 2018, 21: p. 269-283. DOI: 10.1016/j.addma.2018.03.012

2. Y. S. Kim, R. Tamate, A. M. Akimoto and R. Yoshida, Materials Horizons, 2017, 4, p. 38 54.

3. A. Jain, K. J. Prashanth, A. K. Sharma, A. Jain, Polymer Engineering and Science, 2015, 55, p. 1589-1616. DOI: https://doi.org/10.1002/pen.24088

4. H. P. Phan, D. V. Dao, K. Nakamura, S. Dimitrijev and N. T. Nguyen, Journal of Microelectromechanical Systems, 2015, 24, p. 1663-1677. DOI: 10.1109/JMEMS.2015.2470132

5. I. S. Song, W. Y. Kim, C. Y. Kim, B. H. Kim, H. K. Kim and T. J. Ahn, Sensors and Actuators, A: Physical, 2015, 232, 223-228. DOI: https://doi.org/10.1016/j.sna.2015.06.013

6. J. Ma, J. Hu, Z. Li and C. W. Nan, Advanced Materials, 2011, 23, p. 1062-1087. https://doi.org/10.1002/adma.201003636

7. L. Zhang, W. Hou, G. Dong, Z. Zhou, S. Zhao, Z. Hu, W. Ren, M. Chen, C. W. Nan, J. Ma, H. Zhou, W. Chen, Z. G. Ye, Z. D. Jiang and M. Liu, Materials Horizons, 2018, 5, p. 991-999. DOI: https://doi.org/10.1039/c8mh00763b

8. P. Martins and S. Lanceros-Méndez, Advanced Functional Materials, 2013, 23, p. 3371-3385. DOI: https://doi.org/10.1002/adfm.201202780

9. D. M. Correia, P. Martins, M. Tariq, J. M. S. S. Esperança and S. Lanceros-Méndez, Nanoscale, 2018, 10, p. 15747-15754. DOI: https://doi.org/10.1039/C8NR03259A

10. X. Z. Chen, N. Shamsudhin, M. Hoop, R. Pieters, E. Siringil, M. S. Sakar, B. J. Nelson and S. Pané, Materials Horizons, 2016, 3, p. 113-118. DOI: https://doi.org/10.1039/C5MH00259A

11. R. Bernasconi, F. Cuneo, E. Carrara, G. Chatzipirpiridis, M. Hoop, X. Chen, B. J. Nelson, S. Pané, C. Credi, M. Levi and L. Magagnin, Materials Horizons, 2018, 5, p. 699-707. DOI: https://doi.org/10.1039/C8MH00206A

12. Y. Cheng, B. Peng, Z. Hu, Z. Zhou and M. Liu, Physics Letters, Section A: General, Atomic and Solid-State Physics, 2018, 382, p. 3018-3025. DOI: https://doi.org/10.1016/j.physleta.2018.07.014

13. J. Wang, Z. Fu, R. Peng, M. Liu, S. Sun, H. Huang, L. Li, R. J. Knize and Y. Lu, Materials Horizons, 2015, 2, p. 232-236. DOI: https://doi.org/10.1039/C4MH00202D

14. P. Martins, Y. V. Kolen'Ko, J. Rivas and S. Lanceros-Mendez, ACS Applied Materials and Interfaces, 2015, 7, 15017-15022. DOI: https://doi.org/10.1021/acsami.5b04102

15. T. N. Yang, J. M. Hu, C. W. Nan and L. Q. Chen, Applied Physics Letters, 2014, 104. DOI: https://doi.org/10.1063/1.4863941

16. N. Castro, S. Reis, M. P. Silva, V. Correia, S. Lanceros-Mendez and P. Martins, Smart Materials and Structures, 2018, 27. DOI: 10.1088/1361-665X/aab969

17. S. Lanceros-Mendez and P. Martins, Magnetoelectric Polymer-Based Composites: Fundamentals and Applications, Wiley, 2017. DOI: 10.1002/9783527801336

18. C. Ribeiro, C. M. Costa, D. M. Correia, J. Nunes-Pereira, J. Oliveira, P. Martins, R. Gonçalves, V. F. Cardoso and S. Lanceros-Méndez, Nature Protocols, 2018, 13, p. 681-704. DOI: 10.1038/nprot.2017.157

19. P. Martins, R. Gonçalves, S. Lanceros-Mendez, A. Lasheras, J. Gutiérrez and J. M. Barandiarán, Applied Surface Science, 2014, 313, p. 215-219. DOI: 10.1016/j.apsusc.2014.05.187

20. M. Alnassar, A. Alfadhel, Y. P. Ivanov and J. Kosel, Journal of Applied Physics, 2015, 117.DOI: https://doi.org/10.1063/1.4913943

21. C. Ribeiro, V. Correia, P. Martins, F. M. Gama and S. Lanceros-Mendez, Colloids and Surfaces B: Biointerfaces, 2016, 140, p. 430-436. DOI: 10.1016/j.colsurfb.2015.12.055

22. J. Jin, S. G. Lu, C. Chanthad, Q. Zhang, M. A. Haque and Q. Wang, Advanced Materials, 2011, 23, p. 3853-3858. DOI: https://doi.org/10.1002/adma.201101790

23. I. F. Akyildiz, M. Pierobon, S. Balasubramaniam and Y. Koucheryavy, IEEE Communications Magazine, 2015, 53, p. 32-40. DOI: 10.1109/MCOM.2015.7060516

24. Y. Zong, T. Zeng, P. Martins, S. Lanceros-Mendez, Z. Yue, M. Higgins, in Magnetoelectric Polymer-Based Composites, ed. S. L. M. P. Martins, Wiley, 2017, DOI: 10.1002/9783527801336.ch6b.

25. J. A. Mundy, C. M. Brooks, M. E. Holtz, J. A. Moyer, H. Das, A. F. Rébola, J. T. Heron, J. D. Clarkson, S. M. Disseler, Z. Liu, A. Farhan, R. Held, R. Hovden, E. Padgett, Q. Mao, H. Paik, R. Misra, L. F. Kourkoutis, E. Arenholz, A. Scholl, J. A. Borchers, W. D. Ratcliff, R. Ramesh, C. J. Fennie, P. Schiffer, D. A. Muller and D. G. Schlom, Nature, 2016, 537, p. 523-527. DOI: 10.1038/nature19343.

26. T. Nan, H. Lin, Y. Gao, A. Matyushov, G. Yu, H. Chen, N. Sun, S. Wei, Z. Wang, M. Li, X. Wang, A. Belkessam, R. Guo, B. Chen, J. Zhou, Z. Qian, Y. Hui, M. Rinaldi, M. E. McConney, B. M. Howe, Z. Hu, J. G. Jones, G. J. Brown and N. X. Sun, Nature Communications, 2017, 8. DOI: doi: 10.1038/s41467-017-00343-8.

27. Z. Chu, V. Annapureddy, M. Pourhosseiniasl, H. Palneedi, J. Ryu and S. Dong, MRS Bulletin, 2018, 43, p. 199-205. DOI: https://doi.org/10.1557/mrs.2018.31

28. D. S. Thomas and S. W. Gilbert, in Additive Manufacturing: Costs, Cost Effectiveness and Industry Economics, 2015, p. 1-96. DOI: http://dx.doi.org/10.6028/NIST.SP.1176

29. A. A. Chlaihawi, S. Emamian, B. B. Narakathu, M. M. Ali, D. Maddipatla, B. J. Bazuin and M. Z. Atashbar, 2016. DOI: https://doi.org/10.1016/j.proeng.2016.11.247

30. R. E. Sousa, J. Oliveira, A. Gören, D. Miranda, M. M. Silva, L. Hilliou, C. M. Costa and S. Lanceros-Mendez, Electrochimica Acta, 2016, 196, p. 92-100. DOI: 10.1016/j.electacta.2016.02.189

31. G. Srinivasan, Magnetoelectric Composites, Annual Review of Materials Research, 2010, 40, p. 153-178. DOI: https://doi.org/10.1146/annurev-matsci-070909-104459

32. Z. L. Chen, P. Y. Chao and S. H. Chiu, Journal of Applied Polymer Science, 2003, 88, p. 3045-3057. DOI: https://doi.org/10.1002/app.11768

33. J. Gutiérrez, P. Martins, R. Gonçalves, V. Sencadas, A. Lasheras, S. Lanceros-Mendez and J. M. Barandiarán, European Polymer Journal, 2015, 69, p. 224-231. DOI: 10.1016/j.eurpolymj.2015.06.012

34. M. M. Fernandes, H. Mora, E. D. Barriga-Castro, C. Luna, R. Mendoza-Reséndez, C.Ribeiro, S. Lanceros-Mendez and P. Martins, Journal of Physical Chemistry C, 2018,

122, p. 19189-19196. DOI: https://doi.org/10.1021/acs.jpcc.8b04910

35. V. Loyau, V. Morin, G. Chaplier, M. Lobue and F. Mazaleyrat, Journal of Applied Physics, 2015, 117.DOI: https://doi.org/10.1063/1.4919722

36. J. Kulawik, D. Szwagierczak and P. Guzdek, Journal of Magnetism and Magnetic Materials,2012, 324, p. 3052-3057.DOI: https://doi.org/10.1016/j.jmmm.2012.04.056

CHAPTER IV

GREENER SOLVENT-BASED PROCESSING OF POLYMER-BASED MAGNETOELECTRIC NANOCOMPOSITES

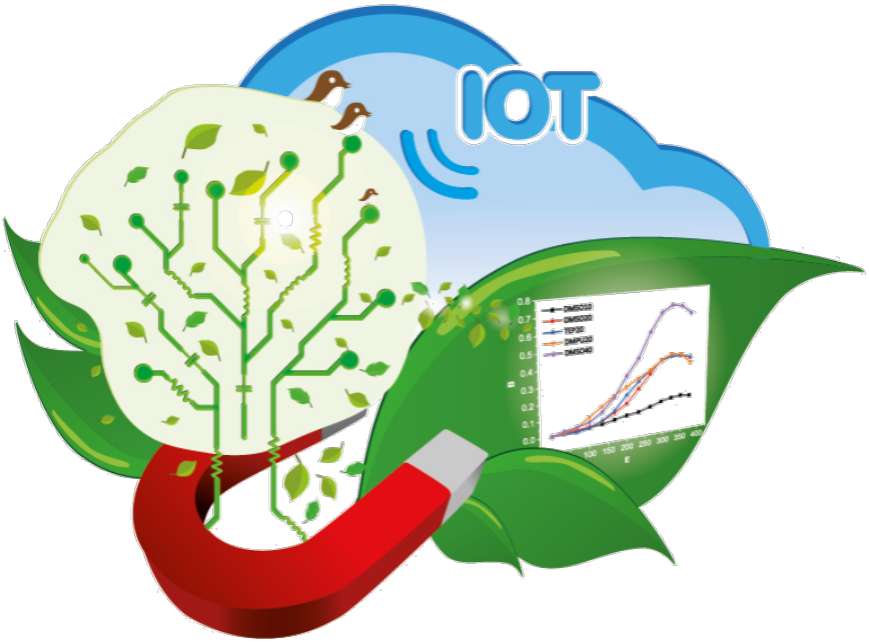

Chapter IV – Greener solvent-based processing of polymer-based magnetoelectric nanocomposites

Polymer-based magnetoelectric (ME) nanocomposites are an enabling material technology for a wide range of applications in the area of digitalization strategies. Due to its highest piezoelectric response among polymers, poly (vinylidene fluoride-trifluoroethylene) (PVDF-TrFE) is the piezoelectric matrix most used in polymer-based ME materials with over 80% of the total reports, with the resulting composites typically processed from solutions with N, N-dimethylformamide (DMF), a toxic solvent. Nevertheless, environmentally friendlier approaches and sustainable technologies are increasingly being required. This work demonstrates that P(VDF-TrFE)/$Co_2Fe_2O_4$ nanocomposites can be successfully prepared from solution using three different environmentally friendlier solvents: dimethyl sulfoxide (DMSO), N, N'-Dimethylpropyleneurea (DMPU), and triethyl phosphate (TEP) with different dipole moments. It is shown that the prepared composite films, with a maximum ME voltage coefficient of 35 mV cm^{-1} Oe−1 and a maximum sensitivity of 2.2 mV T^{-1}, are suitable for applications, highlighting the path for a new generation of more sustainable ME sensors.

This chapter is based on the following scientific publication:

A. C. Lima, N. Pereira, S. Lanceros-Méndez, and P. Martins, Greener solvent-based processing of polymer based magnetoelectric nanocomposites, ACS Sustainable Chemistry & Engineering, 2021, 10, 13, 4122-4132, DOI: https://doi.org/10.1021/acssuschemeng.1c06967.

4.1 Introduction

The link between the physical world and the internet has been a driving force in enhancing people's quality of life which has culminated on the Internet of Things (IoT) concept [1-3]. This technology allows a more effective and ubiquitous interrelation between humans and electronic devices, modifying the paradigm of the user's interactions. In such human-machine connectivity, the user that previously interacted with a physical object in a voluntary way, starts to interact with the object simply by using it: the "I-user" [4,5] In addition, the rapid evolution of the digitalization wave leading to the interconnection in real time of every possible "Things" (home appliances, mobile phones, cars, or smart houses, among others) demands also a new generation of materials [6] that allow lightness, flexibility and improved integration, at reasonable prices [4,7]. Thus, a new generation of materials called "smart materials", are being developed to be integrated in a variety of objects and devices with the objective to sense temperature, pressure, impact, deformation and other relevant parameters [8-10]. Additionally, some of those types of materials can also act as energy harvesters [11,12] or actuators [13,14].

Magnetoactive smart materials contribution to the IoT is particularly relevant since they will trigger the fabrication of antennas, bioelectronics devices, proximity, magnetic and current sensors, as well as actuators, among others [5,15]. Magnetoactive materials can be produced by combining magnetic fillers and polymeric/ceramic matrices and, in such systems, the application of an external AC/DC magnetic field trigger a physical change in the composite [16]. Among those materials, magnetoelectric (ME) structures are among the most exciting ones once they allow an efficient coupling between the electrical and magnetic orders of the matter [17]. In addition, ME materials permit the development of novel and conventional applications, the latter based on new approaches, such as in the case of magnetic sensors, that match the current requirements of the IoT-related industries in terms of cost, size, flexibility, detection limits and noise [18,19]. ME materials can also solve problems related with the powering of conventional sensors (periodic replacement, capacity limitations and maintenance costs) due to their aptitude to harvest surrounding energy from harsh/inaccessible locations, exhibiting the same harvesting benefits of piezoelectric materials but with improved power output and higher mechanical stress [20].

ME composites, with ME coupling coefficients ≈1000 times higher than single-phase MEs, are usually categorized according to the connectivity of the two components into 0–3 (nanocomposites) and 2–2 (laminated composites) [21,22]. Laminated composites have been largely explored based on their superior ME coefficient (≈ some V cm^{-1} Oe^{-1}), though, the stress transfer of the coupling layer between piezoelectric and magnetostrictive layers brings undesired relaxation and electrical loss problems [23].

Nanocomposites despite exhibiting a lower ME coupling coefficient (≈some mV cm^{-1} Oe^{-1}), do not exhibit the abovementioned performance limitations, once the magnetostrictive nanoparticles can be equally dispersed in the piezoelectric matrix [24]. Polymer-based ME nanocomposites also offer optimized features with respect to low temperature processing, compatibility with additive manufacturing technologies, tunable mechanical features for flexible and/or large area devices [25,26], thus permitting the manufacture of products that are eco-friendlier and safer [23].

Due to their highest dielectric constant and electroactive response, including piezoelectric ($|d_{33}| \approx$ 30 pc N^{-1}) effect, and the capability to crystallize directly in the β-phase (the phase that displays optimized ferroelectric, pyroelectric and piezoelectric properties) poly(vinylidene fluoride–trifluoroethylene), P(VDF-TrFE), with molar ratios of vinylidene fluoride (VDF) between 50 % and 80 %, is the copolymer preferentially used (≈80 % of the total published papers [23,27] for the fabrication of ME nanocomposites.

For most applications, P(VDF-TrFE) is processed from the melt, such as by extrusion or injection molding, where the material is converted from a liquid melt into a solid form with a defined structure and shape [28,29], being melt extrusion a common method to produce oriented flexible chain polymers [30,31]. Nevertheless, in the growing area of printed electronics and advanced coatings, increasingly requiring sensors and/or actuators, piezoelectric materials in general and P(VDF-TrFE) in particular, need to be processed from solutions [32], being required in some cases a specific post processing treatment [24]. The most utilized printing/coating techniques include screen- and ink-printing or doctor blade [17,23].

In the subject of printed electronics, P(VDF-TrFE) is mostly prepared after dissolution in N, N-dimethylformamide (DMF), methyl ethyl ketone (MEK), tetrahydrofuran (THF) or N-methyl-2-pyrrolidone (NMP), all of them hazardous, toxic, and dangerous to be used at large scale, and consequently, should be avoided [27,33].

In this way, one of the keys enabling challenges in printable polymer-based MEs, is to change the abovementioned solvents by less hazardous and environmentally friendlier ones, the so called “green” solvents, aiming to decrease the environmental footprint of the materials [23,34].

The choice of solvent must also take into account its dipole moment once such a value significantly influences its polarizability which in turn affects the piezoelectricity, pyroelectricity, triboelectricity, crystallinity, and dipole alignment capability of the polymer that is obtained from solutions [35,36].

Thus, in this work P(VDF-TrFE)/$CoFe_2O_4$ ME nanocomposites have been developed using three different green solvents - Dimethyl sulfoxide (DMSO), N, N′-Dimethylpropyleneurea (DMPU) and Triethyl

phosphate (TEP) aiming sensing applications (Figure IV-1). Further, the different dipolar moments of the solvents also allow to assess the solvent-polymer interactions allowing to improve final materials properties.

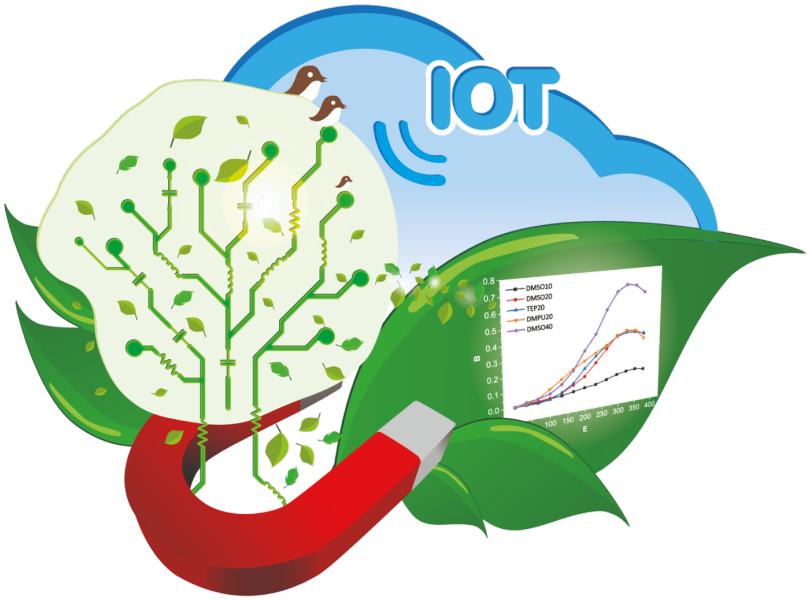

Figure IV-1- *Scheme of the main issues addressed in this work: environmentally friendly approaches regarding the development of ME smart materials for IoT-related applications.*

Once minable deposits of heavy rare-earth elements such as dysprosium (Dy), terbium (Tb) or neodymium (Nd), are heterogeneously and sparsely distributed over the planet, thus being important to diminish the quantities used to solve supply issues, material cost limitations and environmental problems [37,38], those materials should be suppressed from ME nanocomposites. Thus, $CoFe_2O_4$ will be used once along with its hysteresis (coercivity of ≈0.25 T), high magnetostrictive coefficient (up to ≈ 220 ppm), and chemical stability can also be produced through eco-friendly green methods [39,42].

4.2 Experimental Section

4.2.1 Materials

35-55 nm $CoFe_2O_4$ nanoparticles were acquired from Nanostructured & Amorphous Materials, Inc. (Texas, USA). Dimethyl sulfoxide (DMSO), N, N′-Dimethylpropyleneurea (DMPU) and Triethyl Phosphate (TEP) were obtained from (Charlotte, USA), LaborSpirit (Lisboa, Portugal) Sigma-Aldrich (Missouri, USA), respectively. P(VDF-TrFE) (Solvene 250, VDF/TrFE = 70/30) was provided by Solvay (Brussels, Belgium). All the chemicals, polymers and magnetic nanoparticles were utilized as received from the suppliers. The characteristics of each solvent can be found on Table IV-1.

Table IV-1 *- Relevant properties of different solvents used to dissolve P(VDF-TrFE) [43-46].*

	DMF	**DMSO**	**DMPU**	**TEP**
Dipole moment (D)	3.90	3.96	4.17	2.86
Boiling point (° C)	153°C	189°C	247°C	215 °C
Hazard Statement[a]	-Highly Flammable liquid and vapor; -Harmful in contact with skin or if inhaled; -Causes serious eye irritation.	-Combustible, but will not ignite readily; -Slightly irritant to eyes, but not relevant; -No effects known after inhalation.	-Flammable liquid and vapor; -Eye contact may result in permanent eye damage; -Harmful if swallowed.	-Non-flammable; -Harmful if swallowed; -Causes serious eye irritation.
Environmental impact/usability[b]	High: Undesirable use	Some: Usable	Some: Usable	None: Recommended

[a] According to Regulation (EC) No. 1272/2008

[b] According to CHEM21 method and GSK's solvent selection [47-50]

4.2.2 Processing

Nanocomposite films with thickness around 40–60 μm, were prepared by adding the desired amount of CFO to DMSO, DMPU or TEP solvents and later placed (5 hours) in ultrasounds (ATU ATM 3LCD) to ensure that CFO was well dispersed in the solvent and to prevent aggregation [51]. Next, the polymer in the powder form, was added and the resulting blend was mixed with a Teflon mechanical stirrer (Heidolph instruments – Schwabach, Germany) until the complete dissolution of P(VDF-TrFE). Flexible multiferroic films were obtained by spreading (at room temperature) the mixture on a very-clean

glass substrate. P(VDF-TrFE) crystallization and solvent evaporation were achieved in a post processing step by maintaining the samples inside a convection forced oven (JP Selecta 2005165) for:

i) 30 minutes at 230 °C for DMPU films;

ii) 30 minutes at 165 °C for DMSO films;

iii) 30 minutes at 180 °C for TEP films.

Each solvent evaporation temperature was selected considering the following premises: temperature should be lower (≈ 10 %) than the solvent's boiling point (Table IV-1) to allow slow solvent evaporation, leading to non-porous compact films and temperature should be the lowest promoting a compact, homogeneous, and non-brittle film.

After the specific/optimized time in the oven, the films were cooled to room temperature under ambient atmosphere. Two sets of samples were prepared, one with 20 wt.% of $CoFe_2O_4$ and prepared with different solvents, allowing to understand the effect of the used solvent on the ME performance, and other, with varying CFO wt.% (0, 10, 20 and 40 wt.%) on the same solvent (DMSO), to understand the effect of increasing filler content (Table IV-2).

Table IV-2- *P(VDF-TrFE)-based composite samples and respective nomenclature.*

Solvent	**$CoFe_2O_4$ (wt.%)**			
	0	10	20	40
DMSO	P@DMSO	P@DMSO/CFO10	P@DMSO/CFO20	P@DMSO/CFO40
DMPU	X	X	P@DMPU/CFO20	X
TEP	X	X	P@DMSO/TEP20	X

4.2.3 Characterization techniques

Sample morphology was evaluated by scanning electron microscopy (SEM - NanoSEM – FEI Nova 200) using an accelerating voltage of 10 kV. Previously, all samples have been coated (using a sputter coating Polaron, model SC502) with a very thin (≈30nm) conductive (Au) layer.

Sample thickness was calculated by using the Image J software on SEM images (5 measurements for each sample).

The wt.% of the polymer at the polymer-CFO interphase (m_I) was determined using Equation IV.1:

$$m_I = \frac{m(x)_{I0} - m_{I0}}{m_{I0}} \times 100 \qquad \text{(Equation IV.1)}$$

where m_{I0} is the mass of pristine P(VDF-TrFE) at the temperature upon which the mass loss rate is maximum and $m(x)_{I0}$ is the mass of the composite containing a given wt.% of CFO nanoparticles that has not degraded at the temperature at which the mass loss rate of the pristine P(VDF-TrFE) is maximum [52].

Differential scanning calorimetry (DSC) was performed using a Perkin-Elmer DSC 8000 under a flowing N_2 atmosphere from 25 °C to 200 °C (with a 10°C min^{-1} heating rate). The samples have been placed in aluminum pans (≈30 μL) with perforated lids to permit the release/removal of volatiles. The degree of crystallinity (χ_c) of the samples was determined using Equation IV.2:

$$\chi_c = \frac{\Delta H_f}{\Delta H_{100}} \times 100 \qquad \text{(Equation IV.2)}$$

Where ΔH_f is the melting enthalpy and ΔH_{100} is the melting enthalpy for a 100 % crystalline sample (103.4 J g^{-1}) [53].

Thermogravimetric analysis (TGA) with a heating rate of 10 °C min^{-1} was executed on a Q600 TGA TA thermobalance, from 40 °C to 800 °C under a N_2 atmosphere (flow of 50 mL min^{-1}). Samples (≈ 10 mg) have been previously placed in open ceramic crucibles.

The room-temperature stress–strain measurements in tensile mode at a deformation rate of 0.5 mm min^{-1} were performed with an Autograph AG-IS (Shimadzu) 500 N to assess the mechanical properties of samples. The elastic modulus, Y, was calculated in the linear regime of the stress–strain curves after Hooke's law (Equation IV.3):

$$\sigma = Y \cdot \varepsilon \qquad \text{(Equation IV.3)}$$

For both dielectric and electrical conductivity experiments circular gold electrodes (5 mm diameter) were deposited onto both sides of the films on a Polaron model SC502 sputter coater.

The capacity (C) and the dielectric losses (tan(δ)) of the films were evaluated at room temperature from 1 Hz to 1 MHz and with an applied voltage of 0.5 V in a Quadtech 1920 apparatus. Gold electrodes (5 mm diameter) were vacuum evaporated on both sides of each sample. Then, the real part of the complex permittivity (ε') was obtained using the parallel plate capacitor approximation considering the geometry and dimension of each sample (thickness t and Area A), using Equation IV.4:

$$\varepsilon' = \frac{C \times t}{A} \qquad \text{(Equation IV.4)}$$

The DC volume electrical conductivity of the films was obtained by assessing the room temperature characteristic IV curves with a Keithley 6487 picoammeter & voltage source. The electrical resistivity (ρ) was then calculated considered the geometrical parameters according to Equation IV.5:

$$\rho = R \times \frac{A}{t} \qquad \text{(Equation IV.5)}$$

where R is the film resistance, calculated by the inverse of the slope of the I (V) function, t is the thickness, and A is the area of the electrodes. The electrical conductivity (σ) is calculated as the inverse of the resistivity.

For the assessment of the d_{33} piezoelectric coefficient, the samples were first poled by corona discharge, after a previously optimized procedure (temperature of 120 °C, inside a homemade chamber, 10 kV applied voltage, ≈ 2 cm distance between sample and tip, 1 hour poling time and cooling to room temperature under applied electric field). Then, the piezoelectric d_{33} coefficients were measured with a d_{33} meter (model 8000, APC int, Ltd).

To obtain the out-of-plane ME coefficient (α_{33}), DC (bias) and AC magnetic fields (H_{AC}) were applied simultaneously along the same direction of the electric polarization of the P(VDF-TrFE) composite film, that is, perpendicular to the surface. The α_{33} was calculated using Equation I.1.

The AC driving magnetic field (with a maximum of 3.98 Oe) was provided by a pair of Helmholtz coils. The external bias field was provided by an electromagnet with a maximum value of 1.2 T. The induced ME voltage (V) in the samples was measured using a Standford Research Lock-in amplifier.

4.3 Results and Discussion

4.3.1 Morphological features

SEM has been used to reveal possible effects of the processing on the final thickness of the resulting samples and on the agglomeration/dispersion state of the magnetic nanoparticles within the polymer matrix (Figure IV-2).

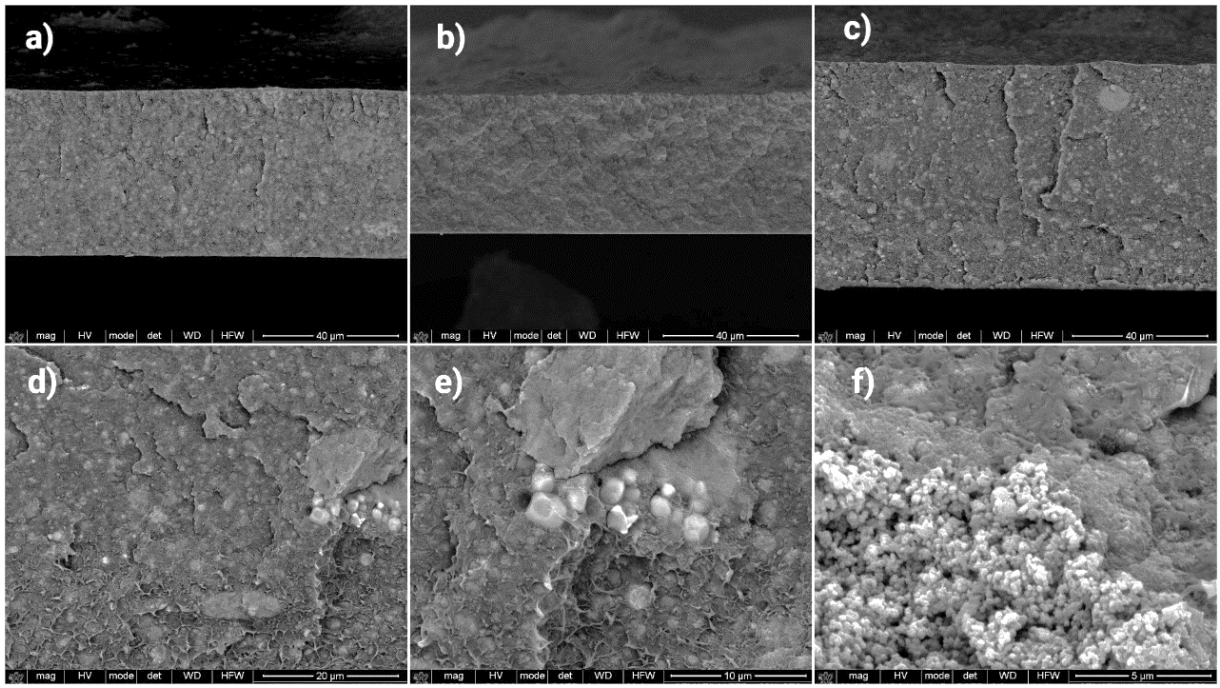

Figure IV-2 - *Representative SEM images of:* ***a)*** *P@DMPU/CFO20;* ***b)*** *P@DMSO/CFO20; and* ***c)*** *P@TEP/CFO20. SEM images of the P@TEP/CFO20 at different magnifications:* ***d)*** *5000x;* ***e)*** *10000x; and* ***f)*** *20000x.*

Figure IV-2a-c displays characteristic SEM images of the samples with 20 wt.% of CFO processed using three different solvents (a: DMPU; b: DMSO; and c: TEP). No substantial differences are detected between the different composites, all revealing a suitable distribution of cluster of nanoparticles with a maximum size of 3 µm (Figure IV-2d-f), compatible with a proper ME response [54].

4.3.2 Thermal characteristics and degree of crystallinity

To study the influence of the solvent, processing conditions and CFO nanoparticle content on the thermal stability of the nanocomposites, TGA has been used, and the representative curves for the different P(VDF-TrFE)/CFO composites are shown in Figure IV-3.

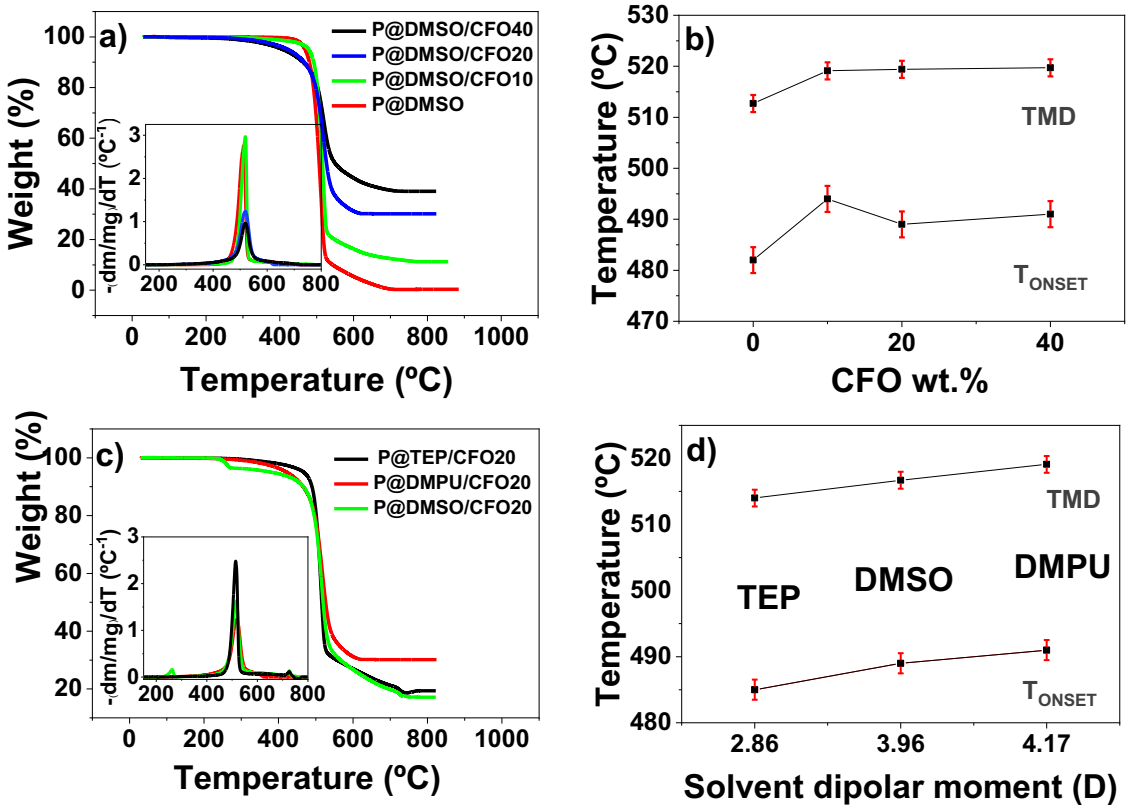

Figure IV-3 - *TGA thermograms* ***a), c)*** *and corresponding first derivatives (insets) for nanocomposites with different CFO wt.% content* ***a),*** *and nanocomposites prepared with different solvents and under different processing conditions* ***c).*** *Temperature of maximum rate of weight loss (TMD) for the samples with different CFO wt.% content* ***b)*** *and prepared with different solvents and under different processing conditions* ***d).***

It was found that, independently of the CFO wt.% content or the solvent and processing conditions, the thermal degradation behavior of P(VDF-TrFE) occurs in a one main weight loss step, corresponding to the scission of the carbon-hydrogen (C–H) bonds, followed by the carbon-fluorine (C–F) bonds due to the higher strength of the C–F bonds comparatively to the C–H bonds [55].

Figure IV-3c compares the composite samples with 20 wt.% processed with the different solvents, revealing a slight weight loss immediately above the solvent's evaporation temperature in all samples (also observed in the DTGA curves), which can be related to trapped solvent at the filler-polymer interfaces and determining also the crystallization (Figure IV-4) and the morphology of the films (Figure IV-2), based on the different dipolar moments of the solvents. The possibility of the existence of trapped solvent at the filler-polymer interface at crystallization is strengthened by the increased weight loss with increasing CFO wt.% (from 0 % to ≈ 2 % with increasing wt.% from 0 to 40).

The differential thermogravimetric, DTG, analysis (insets of Figure IV-3 a) and c)) allows to identify the temperature of maximum rate of weight loss, which is approximately 513 °C for P@DMSO, being this value increased to 519 °C – 520 °C with the introduction of CFO nanoparticles.

The increase of CFO wt.%, from 10 to 40 has no appreciable effect on the TMD. Similarly, the onset temperature is increased from 482 °C to 489 – 494 °C with the introduction of CFO nanoparticles. Such behaviors can be related with the emergence of an interphase (≈ 60 % of the sample weight, as calculated after Equation IV.1) in the interface between nanoparticles and polymer resulting from electrostatic interactions among the partially positive C–H bonds of the polymer and the negatively charged CFO (after the solvent trapped at the polymer-particle interface being evaporated), providing larger thermal stability to the polymer chains closer to the ferrite surface [52,56,57]. The total interface value is similar for P(VDF-TrFE) composites with CFO wt.% between 10 and 40 [52].

Regarding the effect of the solvent on the thermal properties of the composites, TEP, DMSO and DMPU led to TMD values of 514 °C, 517 °C and 519 °C and T_{ONSET} 485 °C, 489 °C, and 491 °C, respectively, being all variations within experimental error [55].

Figure IV-4 shows the heating DSC thermograms for the different P(VDF-TrFE)-based composite films.

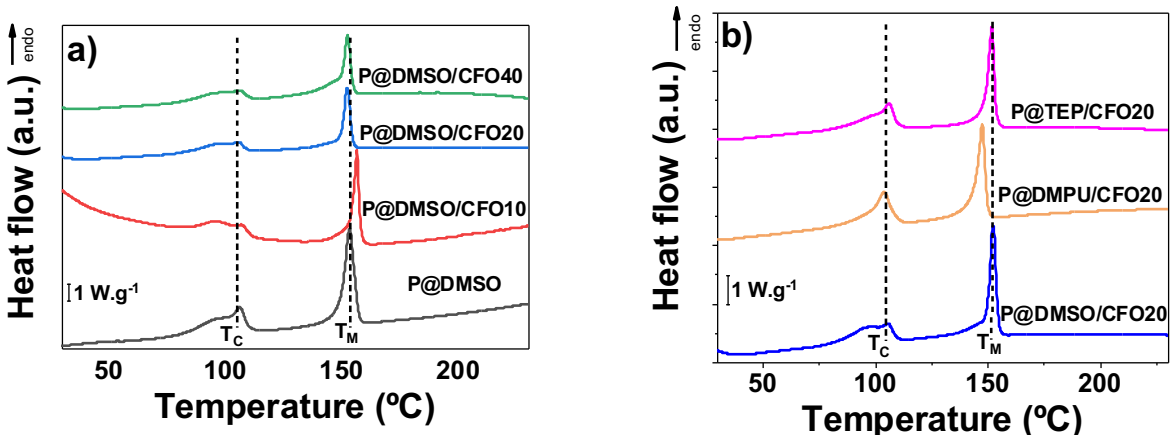

Figure IV-4 - *DSC thermograms for samples with different* ***a)*** *wt.% of CFO and* ***b)*** *different processing conditions and solvents for a filler content of 20 wt.% of CFO.*

The peak at lower temperature (≈105 °C), corresponds to the ferroelectric–paraelectric transition (Curie transition- T_c), and the higher temperature transition peak, at 147–153 °C, corresponds to the melting temperature, T_M of the paraelectric phase [55]. Regardless the used solvent or the wt.% of CFO,

the reference temperatures of the copolymer are not significantly affected (≈100 °C for T_c and ≈145 °C for T_M) [55, 58].

The degree of crystallinity values, calculated from the DSC thermograms by Equation IV.2, are presented in Table IV-3.

Table IV-3 - *Effect of solvent and CFO wt.% on the T_M and X_c values.*

Solvent	CFO wt.%	T_M (°C) ±1	X_c (%) ±1
DMSO	0	153	44
	10	156	26
	20	153	25
	40	153	25
DMPU	20	148	31
TEP	20	152	26

Values from Table IV-3 reveal that the X_c of the sample without magnetic nanoparticles is ≈ 40 % higher than the ones traditional reported on P(VDF-TrFE) produced using other solvents (26 % - 32 %) [27, 55]. Despite previous studies suggested that the strength of the solvent's dipole moment has less impact on the crystal's formation than the annealing process [59]., for samples with similar annealing it was reported that a solvent with higher dipole moment such as DMSO contributes to an improved dipole alignment in P(VDF-TrFE) that results in an augmented X_c [36, 60]. The same effect is also seen on samples prepared with 20 wt.% of CFO with the different solvents, being the degree of crystallinity larger for the samples prepared with DMPU, the solvent with the highest dipolar moment [36, 60].

4.3.3 Mechanical characteristics

To verify whether the P(VDF-TrFE) mechanical properties were changed by the addition of CFO, processing or by solvent dipolar moment, stress–strain measurements (Figure 5a-b) have been performed and the corresponding Young's modulus was calculated (Figure IV-5c-d).

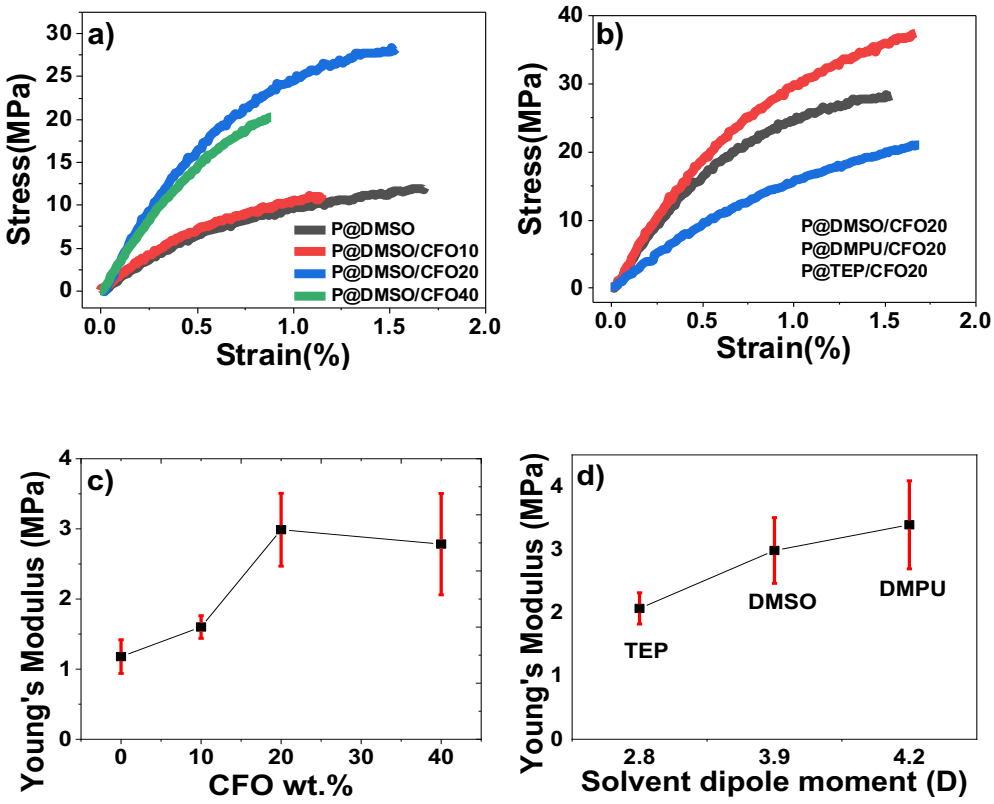

Figure IV-5 *- Stress–strain characteristic curves obtained for samples with varying:* ***a)*** *the wt.% content of ferrites; and* ***b)*** *processing conditions and solvent. Young's Modulus as a function of* ***c)*** *wt.% content of ferrites and* ***d)*** *solvent's dipole moment.*

Figure IV-5a-b reveals that all samples exhibit the usual mechanical behavior of thermoplastics, with a linear relation between stress and strain, for strains below 1%, followed by a plastic deformation stage before the sample undergoes fracture.

Figure IV-5b-c shows that the Young's modulus increase with the introduction of the CFO fillers, being this increase more significant for composites with higher CFO wt.%, fact that can be related to the mechanical enhancement resulting from interaction of CFO nanoparticles and the P(VDF-TrFE) chains, and also with the higher Y_Y of CFO (≈ 150 GPa) [22, 61]. In a similar way a solvent with a high dipole moment creates larger solvent/ - polymer chain interactions, leading to improved chain orientation and therefore higher Y values (Figure IV-5d) [36, 62].

4.3.4 Dielectric Response and electrical conductivity

Figure IV-6 shows the variation of the real part of the complex permittivity, ε', (Figure IV-6a) and the dielectric losses, tg (δ) at room temperature, (Figure IV-6b) as a function of the frequency and CFO wt.%, for the P(VDF-TrFE)/CFO composites.

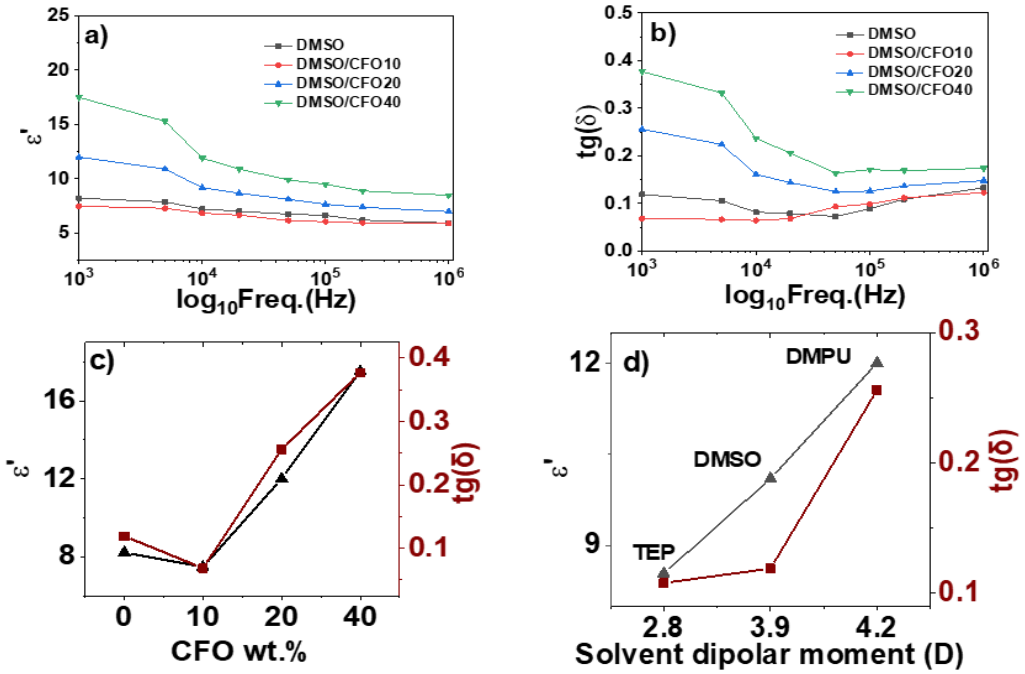

Figure IV-6 *– Real* ***a)*** *and imaginary* ***b)*** *part of the complex permittivity as a function of frequency for P@DMSO composites with different wt.%. Variation of the dielectric constant (black triangles) and dielectric losses (red squares) for the P@DMSO nanocomposites as a function of CFO wt.%* ***c);*** *and for the nanocomposites with 20 wt.% as a function of solvent dipolar moment* ***d)****, at room temperature and for a frequency of 10 kHz.*

For all composite films (independently of the CFO wt.%), it is noted that ε' decreases with increasing frequency in a similar way (Figure IV-6a) because of the cooperative relaxation of the orientational movement of the dipoles with strong contributions from the crystalline–amorphous interphases [53, 63]. The calculated values of the dielectric constant are characteristics of this polymer [64]. Also, the dielectric losses decrease as the frequency increases for all composites (Figure IV-6) due to the relaxation dynamics of the polymer [65]. At low frequencies, tg (δ) is superior because of the semicrystalline character of the polymer that led to interfacial polarization contributions.

Figure IV-6c-d, displays the variation of the dielectric constant of the samples with different CFO wt.% and different solvents, respectively, for a frequency of 10 kHz. This analysis demonstrates that the dielectric response strongly increases with increasing CFO wt.%, due both to the dielectric contribution of the filler and to the increased number of polymer-filler interfaces (Figure IV-6c).

The dielectric losses show an analogous tendency as that of the dielectric constant. Concerning to the variation of dielectric response and dielectric loss with different solvents at 10 kHz, the sample with higher ε' is the one prepared with DMPU (≈ 12), and the sample prepared with TEP presents a lower value (≈ 8.5). The high dipole moment of DMPU leads to improved chain orientation and therefore higher dielectric response (Figure IV-6d) [36]. Further, as indicated in discussion of Figure IV-3, the solvent seems to remain in the polymer-filler interfaces, making the solvents with higher dipolar moments contributing more to the dielectric response. The DC conductivity of all composites was evaluated, and the results are shown in Figure IV-7.

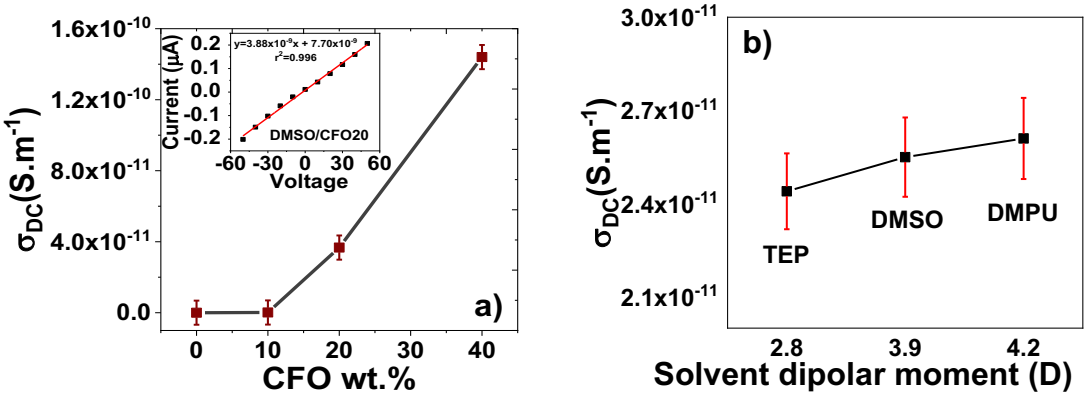

Figure IV-7 - *Electrical DC conductivity (σ_{DC}) of pristine P(VDF-TrFE) and the different nanocomposites as a function of* ***a)*** *CFO wt.% and* ***b)*** *solvent dipolar moment.*

The representative I-V plots (inset of Figure IV-7a) reveal a typical ohmic behavior in all P(VDF-TrFE)/CFO composites, with the electric current increasing linearly with the applied voltage. The slope of the I-V plots and consequently the DC conductivity of the composites increases with CFO content, from 2.0×10^{-12} S m^{-1} for neat P (VDF-TrFE to 1.4×10^{-8} S m^{-1} for the sample with 40 wt.% of CFO (Figure IV-7a).

The introduction of magnetic nanoparticles within the P(VDF-TrFE) significantly increases its electrical conductivity (Figure IV-7a), being this increase related with the interfacial charges, the defective interfaces and the corresponding increase of the conduction paths within the P(VDF-TrFE) matrix as a result of the introduction of the fillers [66]. Additionally, no substantial effect on the electric conductivity was detected when the solvent was changed (Figure IV-7b).

For low CFO content, the composites (less than 40 wt.%) show good distribution of CFO nanoparticles in the P(VDF-TrFE) matrix leading also to high dielectric permittivity (Figure IV-5), optimized Young's modulus (Figure IV-6) and low DC conductivity (Figure IV-7), that are advantageous for ME device applications [66, 67].

4.3.5 Piezoelectric and magnetoelectric response

Being the d_{33} piezoelectric coefficient a key parameter for ME materials, the piezoelectric response of the films has been evaluated as a function of the solvent dipole moment (Figure IV-8a) and CFO wt% (Figure IV-8a).

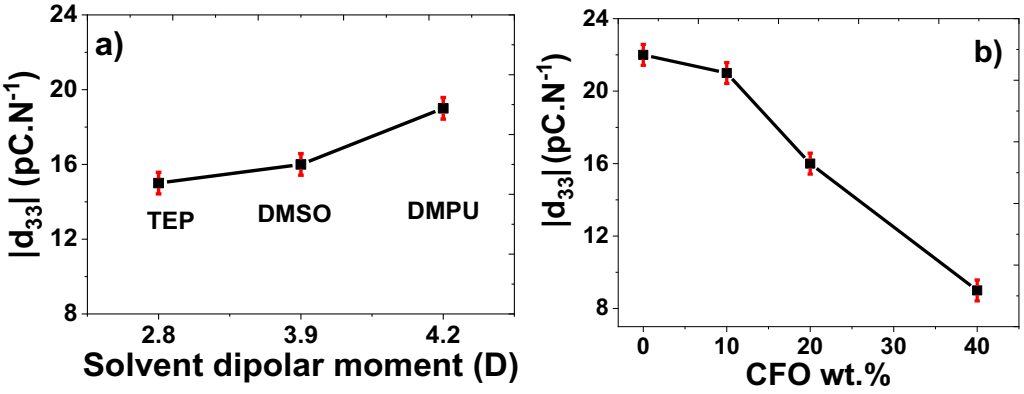

Figure IV-8 – a) *Variation of the piezoelectric d_{33} coefficient for the P(VDF-TrFE)/CFO samples with 20 wt.% of CFO as a function of the solvent dipolar moment.* ***b)*** *Variation of the piezoelectric d_{33} coefficient for P@DMSO samples as a function of the CFO wt.%.*

The solvent dipole moment seems to have only a slight effect on the $|d_{33}|$ values of composites, with the ones found in P@TEP/CFO20 and P@DMSO/CFO20 (15-16 pC N^{-1}) increased to 19 pC N^{-1} for the samples prepared with DMPU due to its higher crystallinity (Table IV-3). Additionally, the presence of the CFO nanoparticles substantially influences the piezoelectric response of the composites. (Figure IV-8b) reveals a decrease of $|d_{33}|$ from 22 pC N^{-1} to 9 pC N^{-1}, with increasing CFO content, caused by a disruption of the connectivity of the piezoelectric matrix, interfacial mechanical defects, increased stiffness of the sample and reduced crystallinity [66].

Finally, the ME properties have been studied as a function of frequency, DC magnetic field intensity, CFO wt.% content and sample preparation method (Figure IV-9).

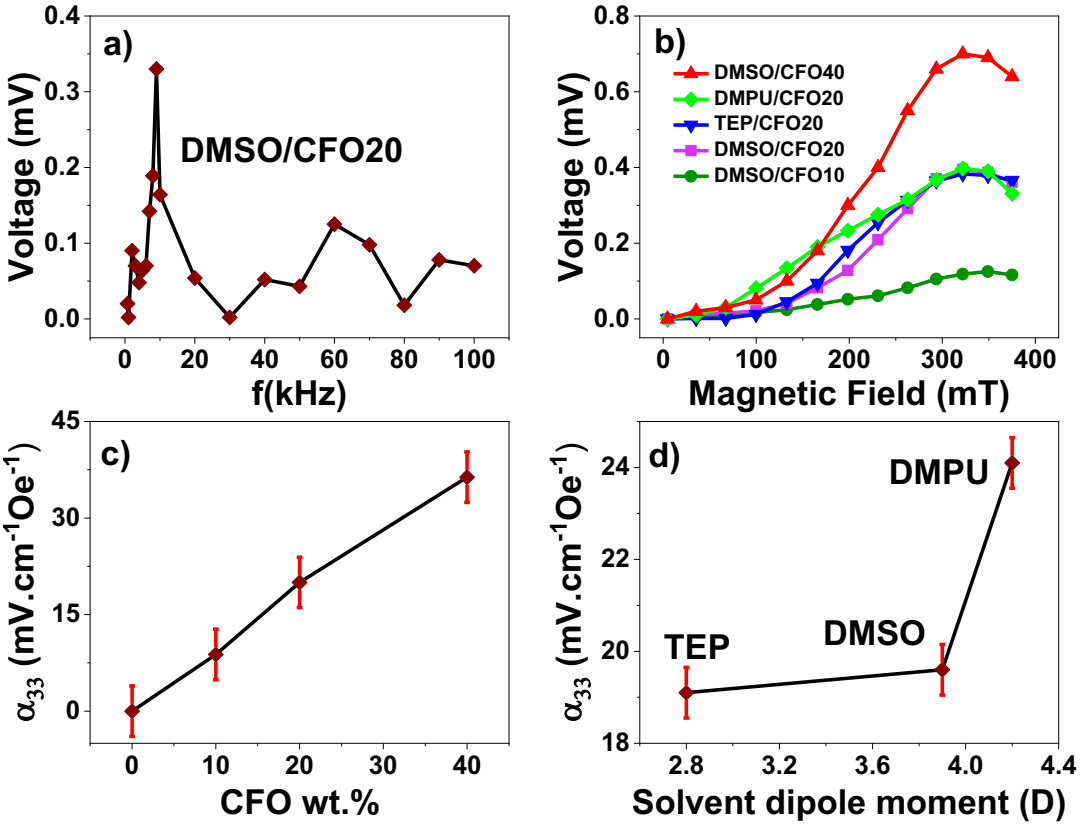

Figure IV-9 - *ME voltage as a function of frequency* ***a)*** *and DC magnetic field intensity* ***b)****. ME voltage coefficient (a_{33}) as a function of the CFO wt.% content* ***c)*** *and solvent dipole moment* ***d)****.*

Figure IV-9a shows a typical voltage-frequency plot that reveals that the resonance frequency of the P@DMSO/CFO20 sample is ≈ 9 kHz. The harmonic mode, thickness of the composites, in-plane Young's modulus, and volumetric mass density of the composites [22] set the resonance of all P(VDF-TrFE)/CFO composites on the 7 – 9 kHz range, being the subsequent characterization performed at such frequencies (8 kHz, 8 kHz, 9 kHz, and 7 kHz for the P@DMSO/CFO10, P@DMSO/CFO40, P@TEP/CFO20 and P@DMPU/CFO20 composites, respectively).

In all composites, the ME voltage increases with increasing magnetic field, until the optimum magnetic field is reached (≈330 mT) as a result of the higher striction at such magnetic field (Figure IV-9b). The following decrease of the ME voltage can be explained by the saturation of the magnetostrictive effect on the magnetostrictive CFO nanoparticles [21, 22].

After the calculation of the ME coefficient (α) it is observed that α increases with increasing CFO content on the P(VDF-TrFE)-DMSO/CFO composites (Figure IV-9c) with increasing solvent dipole moment on the samples with 20 wt.% of CFO (Figure IV-9d). By increasing CFO content from 10 wt.% to 40 wt.% the α value also increases, almost linearly, from 8.8 mV cm^{-1} Oe^{-1} to 36.4 mV cm^{-1} Oe^{-1}, because of the

increase in the magnetostriction due to the increase of the magnetostrictive phase on the ME composite. Further increase in the CFO wt.% should decrease the α value due to the partial disruption of the piezoelectric phase [53]. Once for the same CFO wt.% content, α is directly proportional to the $|d_{33}|$ piezoelectric coefficient and Young's modulus values [69], the composite that has both of those values optimized (P(VDF-TrFE)-DMPU/CFO20) has also the highest ME response on Figure IV-9d (24 mV cm^{-1} Oe^{-1}). Additionally, the sample with the highest CFO wt.% (P(VDF-TrFE)-DMSO/CFO40) exhibited the highest α (35 mV cm^{-1} Oe^{-1}) among the studied samples due to higher content of magnetostrictive phase, and the highest sensitivity reported in the literature for nanocomposites with similar composition (Table IV-4).

Table IV-4 - *Comparison of the ME response of P(VDF-TrFE)/CFO composites exhibiting the highest ME coupling reported in the literature.*

CFO wt.%	**H_{DC} (T)**	**Thickness (μm)**	**H_{AC} (Oe)**	**α (mV cm^{-1} Oe^{-1})**	**V (μV)**	**Sensitivity (μV T^{-1})**	**Ref.**
66	0.25	50	0.008	40	1.6	8	[50]
72	0.25	80	0.1	42	320	1280	[41]
40	0.32	50	3.98	35	700	2188	Our

It is show that whereas α, is similar to the ones reported in the literature for samples prepared with solvents with environmental concerns, the sensitivity, one of the key parameters for the development of ME materials [23, 26], was optimized under specific applied field conditions, for a more effective implementation of these materials in sensing applications.

4.4 Conclusions

This study, in addition to show that it is possible to prepare ME composites using greener solvents, also reveals how some properties of the resulting ME composite such as the maximum degradation temperature, dielectric constant, Young's modulus, piezoelectric coefficient and ME voltage coefficient depend on the processing conditions, including solvent selection. The magnetoelectric coupling is similar to the ones reported in the literature for samples prepared with environmentally problematic solvents, and the sensitivity of the proposed ME nanocomposites under specific H_{AC} conditions (2188 μV T^{-1}) is almost double the highest values reported in the literature (1280 μV T^{-1}).

4.5 References

1. Syed, A. S. Sierra-Sosa, D. Kumar, A. Elmaghraby, A. IOT in Smart Cities: A Survey of Technologies, Practices and Challenges Smart Cities 2021, 4(2): p. 429–475. DOI: https://doi.org/10.3390/smartcities4020024

2. Messerli, P., Murniningtyas, E., Eloundou-Enyegue, P., Foli, E.G., Furman, E., Glassman, A., Hernández Licona, G., Kim, E.M., et al. (2019). Global Sustainable Development Report 2019: The Future is Now – Science for Achieving Sustainable Development. United Nations, New York.

3. Glogic, E., Futsch, R. Thenot, V. Iglesias, A. Joyard-Pitiot, B. Depres, G. Rougier, A. Sonnemann, G. Development of Eco-Efficient Smart Electronics for Anticounterfeiting and Shock Detection Based on Printable Inks ACS Sustainable Chemistry and Engineering 2021, 9(35), p. 11691-11704. DOI: 10.1021/acssuschemeng.1c02348.

4. Dias, D., Paulo Silva Cunha, J. Wearable Health Devices-Vital Sign Monitoring, Systems and Technologies Sensors (Basel)Sensors (Basel) 2018, 18(8): 2414, DOI: 10.3390/s18082414.

5. Ghosh, S., K. Roy, K. Mishra, H. K. Sahoo, M. R. Mahanty, B. Vishwakarma, P. N. Mandal, D. Rollable Magnetoelectric Energy Harvester as a Wireless IOT Sensor ACS Sustainable Chemistry and Engineering 2020, 8(2), p. 864-873, DOI: 10.1021/acssuschemeng.9b05058.

6. Cadilha Marques, G., Garlapati, S. K. Dehm, S. Dasgupta, S. Hahn, H. Tahoori, M. Aghassi-Hagmann, J. Digital Power and Performance Analysis of Inkjet-Printed Ring Oscillators Based on Electrolyte-Gated Oxide Electronics Applied Physics Letters 2017,10: DOI: 111, 10.1063/1.4991919.

7. Xu, Y., Lu, Y. Zhu, X. Toward Plant Energy Harvesting for 5G Signal Amplification ACS Sustainable Chemistry and Engineering 2021, 9(3): p. 1099-1104, DOI: 10.1021/acssuschemeng.0c08453.

8. Basheer, A. A. Advances in the Smart Materials Applications in the Aerospace Industries Aircraft Engineering and Aerospace Technology 2020, 92, p. 1027-1035, DOI: 10.1108/AEAT-02-2020-0040.

9. Tzou, H. S., Lee, H.-J., Arnold, S. M., Smart Materials, Precision Sensors/Actuators, Smart Structures, and Structronic Systems. In Mechanics of Advanced Materials and Structures, Taylor & Francis Inc.: 2004, p. 367–393. DOI: https://doi.org/10.1080/15376490490451552

10. Becherini, S., Mitmoen, M., Tran, C. D. Biocompatible and Smart Composites from Cellulose, Wool, and Phase-Change Materials Encapsulated in Natural Sporopollenin Microcapsules ACS Sustainable Chemistry and Engineering 2020, 8(27), p. 10089-10101, DOI: 10.1021/acssuschemeng.0c02001.

11. Soh, C.-K., Yang, Y. Bhalla, S. Smart Materials in Structural Health Monitoring, Control and Biomechanics Springer Science & Business Media 2012, DOI: DOI: 10.1007/978-3-642-24463-6

12. Song, L., Dai, R., Li, Y. Wang, Q. Zhang, C. Polyvinylidene Fluoride Energy Harvester with Boosting Piezoelectric Performance through 3D Printed Biomimetic Bone Structures ACS Sustainable Chemistry and Engineering 2021, 9(22), p. 7561-7568, DOI: 10.1021/acssuschemeng.1c01305.

13. Palneedi, H., Annapureddy, V., Priya, S., Ryu, J. Status and Perspectives of Multiferroic Magnetelectric Composite Materials and Applications Actuators 2015, 5(1). DOI: https://doi.org/10.3390/act5010009

14. Chen, Z., Wang, J., Qi, H. J., Wang, T., Naguib, H. E. Green and Sustainable Layered Chitin-Vitrimer Composite with Enhanced Modulus, Reprocessability, and Smart Actuator Function ACS Sustainable Chemistry and Engineering 2020, 8, p. 15168-15178, DOI: 10.1021/acssuschemeng.0c04235.

15. Jiang, J., Liu, Y. Li, L. Zhu, J. Xu, M. Li, C. M. Smart Magnetic Interaction Promotes Efficient and Green Production of High-Quality Fe_3O_4@Carbon Nanoactives for Sustainable Aqueous Batteries ACS Sustainable Chemistry and Engineering 2018, 6, p. 757-765, DOI: 10.1021/acssuschemeng.7b03078.

16. Ferreira, A. D. B. L., Nóvoa, P. R. O., Marques, A. T. Multifunctional Material Systems: A State-of-the-Art Review Composite Structures 2016, 151, p. 3-35, DOI: 10.1016/j.compstruct.2016.01.028.

17. Lima, A. C., Pereira, N., Policia, R., Ribeiro, C., Correia, V., Lanceros-Mendez, S., Martins, P. All-Printed Multilayer Materials with Improved Magnetoelectric Response Journal of Materials Chemistry C 2019, 7, p. 5394-5400, 1DOI: 0.1039/c9tc01428d.

18. Cheng, Y., Peng, B., Hu, Z., Zhou, Z., Liu, M. Recent Development and Status of Magnetoelectric Materials and Devices Physics Letters A 2018, 382, p. 3018-3025, DOI: https://doi.org/10.1016/j.physleta.2018.07.014.

19. Correia, D. M., Martins, P., Tariq, M., Esperança, J. M. S. S., Lanceros-Méndez, S. Low-Field Giant Magneto-Ionic Response in Polymer-Based Nanocomposites Nanoscale 2018, 10, p. 15747-15754, DOI: 10.1039/C8NR03259A.

20. Narita, F., Fox, M. A Review on Piezoelectric, Magnetostrictive, and Magnetoelectric Materials and Device Technologies for Energy Harvesting Applications Advanced Engineering Materials 2018, 20, DOI: 10.1002/adem.201700743.

21. Martins, P., Fernandez, C. S. L., Silva, D., Lanceros-Méndez, S. Theoretical Optimization of Magnetoelectric Multilayer Laminates Composites Science and Technology 2021, 204, DOI: 10.1016/j.compscitech.2020.108642.

22. Martins, P., Nunes, J. S., Oliveira, J., Peřinka, N., Lanceros-Mendez, S. Spray-Printed Magnetoelectric Multifunctional Composites Composites Part B: Engineering 2020, 187, DOI: 10.1016/j.compositesb.2020.107829.

23. Martins, P., Lanceros-Méndez, S. Polymer-Based Magnetoelectric Materials: To Be or Not to Be Applied Materials Today 2019, 15, p. 558-561. DOI: 10.1016/j.apmt.2019.04.004.

24. Fernandes, M. M., Mora, H., Barriga-Castro, E. D., Luna, C.; Mendoza-Reséndez, R., Ribeiro, C., Lanceros-Mendez, S., Martins, P. Improving Magnetoelectric Contactless Sensing and Actuation through Anisotropic Nanostructures Journal of Physical Chemistry C 2018, 122, p. 19189-19196, DOI: 10.1021/acs.jpcc.8b04910.

25. Mu, X., Zhang, H., Zhang, C., Yang, S., Xu, J., Huang, Y., Xu, J., Zhang, Y., Li, Q., Wang, X., Cao, D., Li, S. Poly(Vinylidene Fluoride-Trifluoroethylene)/Cobalt Ferrite Composite Films with a Self-

Biased Magnetoelectric Effect for Flexible Ac Magnetic Sensors Journal of Materials Science 2021, 56, p. 9728-9740, DOI: 10.1007/s10853-021-05937-8.

26. Liang, X., Matyushov, A., Hayes, P., Schell, V., Dong, C., Chen, H., He, Y., Will-Cole, A., Quandt, E., Martins, P., McCord, J., Medarde, M., Lanceros-Mendez, S., Van Dijken, S.,Sun, N. X., Sort, J. Roadmap on Magnetoelectric Materials and Devices IEEE Transactions on Magnetics 2021, DOI: 10.1109/TMAG.2021.3086635.

27. Nunes-Pereira, J., Martins, P., Cardoso, V. F., Costa, C. M., Lanceros-Méndez, S. A Green Solvent Strategy for the Development of Piezoelectric Poly(Vinylidene Fluoride-Trifluoroethylene) Films for Sensors and Actuators Applications Materials and Design 2016, 104, p. 183-189, DOI: 10.1016/j.matdes.2016.05.023.

28. Francis, L. F., Chapter 3 - Melt Processes. In Materials Processing, Francis, L. F., Ed. Academic Press: Boston, 2016, 105-249.

29. Guo, J., Nie, M., Wang, Q. Self-Poling Polyvinylidene Fluoride-Based Piezoelectric Energy Harvester Featuring Highly Oriented β-Phase Structured at Multiple Scales ACS Sustainable Chemistry and Engineering 2021, 9, p. 499-509, DOI: 10.1021/acssuschemeng.0c07802.

30. Wang, S., Li, Q. Design, Synthesis and Processing of PVDF-Based Dielectric Polymers IET Nanodielectrics 2018, 1, p. 80-91, DOI: 10.1049/iet-nde.2018.0003.

31. Wang, M., Dong, X., Escobar, I. C., Cheng, Y. T. Lithium Ion Battery Electrodes Made Using Dimethyl Sulfoxide (DMSO) - a Green Solvent ACS Sustainable Chemistry and Engineering 2020, 8, p. 11046-11051, DOI: 10.1021/acssuschemeng.0c02884.

32. Haque, R. I., Vié, R., Germainy, M., Valbin, L., Benaben, P., Boddaert, X. Inkjet-Printing of High Molecular Weight P(VDF-TrFE) for Flexible Electronics Flexible and Printed Electronics 2016, 1, DOI: 10.1088/2058-8585/1/1/015001.

33. Russo, F., Galiano, F., Pedace, F., Aricò, F., Figoli, A. Dimethyl Isosorbide as a Green Solvent for Sustainable Ultrafiltration and Microfiltration Membrane Preparation ACS Sustainable Chemistry and Engineering 2020, 8, p. 659-668, DOI: 10.1021/acssuschemeng.9b06496.

34. Meringolo, C., Mastropietro, T. F., Poerio, T., Fontananova, E., De Filpo, G., Curcio, E., Di Profio, G. Tailoring PVDF Membranes Surface Topography and Hydrophobicity by a Sustainable Two-Steps Phase Separation Process ACS Sustainable Chemistry and Engineering 2018, 6, p. 10069-10077, DOI: 10.1021/acssuschemeng.8b01407.

35. Kong, D. S.; Lee, T. K.; Ko, Y. J.; Jung, J. H. Dielectric and Ferroelectric Properties of P(Vdf-Trfe) Films with Different Polar Solvents. J. Korean Phys. Soc. 2019, 74, 78–81.DOI: 10.3938/jkps.74.78

36. Kim, J.; Lee, J. H.; Ryu, H.; Lee, J. H.; Khan, U.; Kim, H.; Kwak, S. S.; Kim, S. W. High-Performance Piezoelectric, Pyroelectric, and Triboelectric Nanogenerators Based on P(VDF-TrFE) with Controlled Crystallinity and Dipole Alignment. Adv. Funct. Mater. 2017, 27, No. 1700702.

37. Brito-Pereira, R., Ribeiro, C., Peřinka, N., Lanceros-Mendez, S., Martins, P. Reconfigurable 3D-Printable Magnets with Improved Maximum Energy Product Journal of Materials Chemistry C 2020, 8, DOI: 952-958, 10.1039/c9tc06072c.

38. Tian, L., Chang, H., Tang, P., Li, T., Zhang, X., Liu, S., He, Q., Wang, T., Yang, J., Bai, Y., Vidic, R. D., Crittenden, J. C., Liu, B. Rare Earth Elements Occurrence and Economical Recovery Strategy from Shale Gas Wastewater in the Sichuan Basin, China ACS Sustainable Chemistry and Engineering 2020, 8, p. 11914-11920, DOI: 10.1021/acssuschemeng.0c04971.

39. Routray, K. L., Saha, S., Behera, D. Green Synthesis Approach for Nano Sized $CoFe_2O_4$ through Aloe Vera Mediated Sol-Gel Auto Combustion Method for High Frequency Devices Materials Chemistry and Physics 2019, 224, p. 29-35, DOI: https://doi.org/10.1016/j.matchemphys.2018.11.073.

40. Mohamed, M. A., El-Badawy, F. M., El-Desoky, H. S., Ghoneim, M. M. Magnetic Cobalt Ferrite Nanoparticles $CoFe_2O_4$ Platform as an Efficient Sensor for Trace Determination of Cu(Ii) in Water Samples and Different Food Products New Journal of Chemistry 2017, 41,DOI: 11138-11147, 10.1039/c7nj01857f.

41. Kombaiah, K., Vijaya, J. J., Kennedy, L. J., Bououdina, M., Ramalingam, R. J., Al-Lohedan, H. A. Okra Extract-Assisted Green Synthesis of $CoFe_2O_4$ Nanoparticles and Their Optical, Magnetic, and Antimicrobial Properties Materials Chemistry and Physics 2018, 204, p. 410-419, DOI: 10.1016/j.matchemphys.2017.10.077.

42. Martins, P., Kolen'Ko, Y. V., Rivas, J., Lanceros-Mendez, S. Tailored Magnetic and Magnetoelectric Responses of Polymer-Based Composites ACS Applied Materials and Interfaces 2015, 7, p. 15017-15022, DOI: 10.1021/acsami.5b04102.

43. Sigma-Aldrich, Triethyl Phosphate Safety Data Sheet (Sds), Generic Eu Msds. 2021.

44. Sigma-Aldrich, Dimethyl Sulfoxide Safety Data Sheet (Sds). 2021.

45. Sigma-Aldrich, N, N′-Dimethylpropyleneurea Safety Data Sheet (Sds), Generic Eu Msds. 2021.

46. N, N -Dimethylformamide Safety Data Sheet (Sds), Generic Eu Msds. 2021.

47. Thi, H. Y. N., Nguyen, B. T. D., Kim, J. F. Sustainable Fabrication of Organic Solvent Nanofiltration Membranes Membranes 2021, 11, p. DOI: 1-21, DOI: 10.3390/membranes11010019.

48. Doolin, A. J., Charles, R. G., De Castro, C. S. P., Rodriguez, R. G., Péan, E. V., Patidar, R., Dunlop, T., Charbonneau, C., Watson, T., Davies, M. L. Sustainable Solvent Selection for the Manufacture of Methylammonium Lead Triiodide (Mapbi3) Perovskite Solar Cells Green Chemistry 2021, 23, p. 2471-2486, DOI: 10.1039/d1gc00079a.

49. Byrne, F. P., Jin, S., Paggiola, G., Petchey, T. H. M., Clark, J. H., Farmer, T. J., Hunt, A. J., Robert McElroy, C., Sherwood, J. Tools and Techniques for Solvent Selection: Green Solvent Selection Guides Sustainable Chemical Processes 2016, 4, 7, DOI: 10.1186/s40508-016-0051-z.

50. Henderson, R. K., Jiménez-González, C., Constable, D. J. C., Alston, S. R., Inglis, G. G. A., Fisher, G., Sherwood, J., Binks, S. P., Curzons, A. D. Expanding Gsk's Solvent Selection Guide – Embedding Sustainability into Solvent Selection Starting at Medicinal Chemistry Green Chemistry 2011, 13, p. 854-862, DOI: 10.1039/C0GC00918K.

51. Martins, P., Gonçalves, R., Lanceros-Mendez, S., Lasheras, A., Gutierrez, J., Baradiaran, J. M. Effect of Filler Dispersion and Dispersion Method on the Piezoelectric and Magnetoelectric Response of $CoFe_2O_4$/P(VDF-TrFE) Nanocomposites Applied Surface Science 2014, 313, p. 215-219

52. Martins, P., Costa, C. M., Benelmekki, M., Botelho, G. Lanceros-Méndez, S. Interface Characterization and Thermal Degradation of Ferrite/ Poly(Vinylidene Fluoride) Multiferroic Nanocomposites Journal of Materials Science 2013, 48, p. 2681-2689, DOI: 10.1007/s10853-012-7063-1.

53. Nakagawa, K., Ishida, Y. Dielectric Relaxations and Molecular Motions in Poly (Vinylidene Fluoride) with Crystal Form Ii Polymer Physics 1973, 11

54. Martins, P., Gonçalves, R., Lanceros-Mendez, S., Lasheras, A.; Gutiérrez, J., Barandiarán, J. M. Effect of Filler Dispersion and Dispersion Method on the Piezoelectric and Magnetoelectric Response of $CoFe_2O_4$/P(VDF-TrFE) Nanocomposites Applied Surface Science 2014, 313, p. 215-219, DOI: 10.1016/j.apsusc.2014.05.187.

55. C. M. Costa, M. N. T. M., J. L. Gomez Ribelles, S. Lanceros-Méndez Composition-Dependent Physical Properties of Poly[(Vinylidene Fluoride)- Co -Trifluoroethylene]–Poly(Ethylene Oxide) Blends Journal of Materials Science 2013,

56. Martins, P.; Costa, C. M.; Benelmekki, M.; Botelho, G.; Lanceros-Mendez, S. On the Origin of the Electroactive Poly(Vinylidene Fluoride) B-Phase Nucleation by Ferrite Nanoparticles Via Surface Electrostatic Interactions CrystEngComm 2012, 14, p. 2807-2811, DOI: 10.1039/c2ce06654h.

57. Manna, S., Batabyal, S. K., Nandi, A. K. Preparation and Characterization of Silver-Poly(Vinylidene Fluoride) Nanocomposites: Formation of Piezoelectric Polymorph of Poly(Vinylidene Fluoride) Journal of Physical Chemistry B 2006, 110, p. 12318-12326, DOI: 10.1021/jp061445y.

58. Hafner, J. Teuschel, M., Schneider, M., Schmid, U. Origin of the Strong Temperature Effect on the Piezoelectric Response of the Ferroelectric (Co-)Polymer P(VDF-TrFE) 70-30) Polymer 2019, 170, p. 1-6, DOI: https://doi.org/10.1016/j.polymer.2019.02.064.

59. Ng, C. Y. B., Gan, W. C., Velayutham, T. S., Goh, B. T., Hashim, R. Structural Control of the Dielectric, Pyroelectric and Ferroelectric Properties of Poly(Vinylidene Fluoride-: Co -Trifluoroethylene) Thin Films Physical Chemistry Chemical Physics 2020, 22, p. 2414-2423, DOI: 10.1039/c9cp01556f.

60. Kim, M., Lee, S., Kim, Y. I. Solvent-Controlled Crystalline Beta-Phase Formation in Electrospun P(VDF-TrFE) Fibers for Enhanced Piezoelectric Energy Harvesting APL Materials 2020, 8, DOI: 10.1063/5.0011686.

61. Zhang, J. X., Dai, J. Y., So, L. C., Sun, C. L., Lo, C. Y.; Or, S. W., Chan, H. L. W. The Effect of Magnetic Nanoparticles on the Morphology, Ferroelectric, and Magnetoelectric Behaviors of CFO/P(VDF-TrFE) 0-3 Nanocomposites Journal of Applied Physics 2009, 105, DOI: 10.1063/1.3078111.

62. Tung, K.-L., Lu, K.-T., Ruaan, R.-C., Lai, J.-Y. Molecular Dynamics Study of the Effect of Solvent Types on the Dynamic Properties of Polymer Chains in Solution Desalination 2006, 192, p. 380-390, DOI: https://doi.org/10.1016/j.desal.2005.07.043.

63. Hahn, B., Wendorff, J., Yoon, D. Y. Dielectric Relaxation of the Crystal-Amorphous Interphase in Poly(Vinylidene Fluoride) and Its Blends with Poly(Methyl Methacrylate) Macromolecules 1985, 18, p. 718-721, DOI: 10.1021/ma00146a024.

64. Heiler, B. P., B Dielectric Nonlinearities of P(VDF-TrFE) International Symposium on Electrets 1994, p. 662-667

65. Helfand, E. Static and Dynamic Properties of the Polymeric Solid-State Journal of Polymer Science: Polymer Letters Edition 1983, 21,

66. Brito-Pereira, R., Ribeiro, C., Lanceros-Mendez, S., Martins, P. Magnetoelectric Response on Terfenol-D/ P(VDF-TrFE) Two-Phase Composites Composites Part B: Engineering 2017, 120: p. 97-102, DOI: https://doi.org/10.1016/j.compositesb.2017.03.055.

67. Zhang, C., Chi, Q., Dong, J., Cui, Y., Wang, X., Liu, L., Lei, Q. Enhanced Dielectric Properties of Poly(Vinylidene Fluoride) Composites Filled with Nano Iron Oxide-Deposited Barium Titanate Hybrid Particles Scientific Reports 2016, 6, 33508, DOI: 10.1038/srep33508.

68. Martins, P., Silva, M., Lanceros-Mendez, S. Determination of the Magnetostrictive Response of Nanoparticles Via Magnetoelectric Measurements Nanoscale 2015, 7, p. 9457-9461, DOI: 10.1039/c5nr01397f.

CHAPTER V

MAGNETIC PROXIMITY SENSOR BASED ON MAGNETOELECTRIC COMPOSITES AND PRINTED COILS

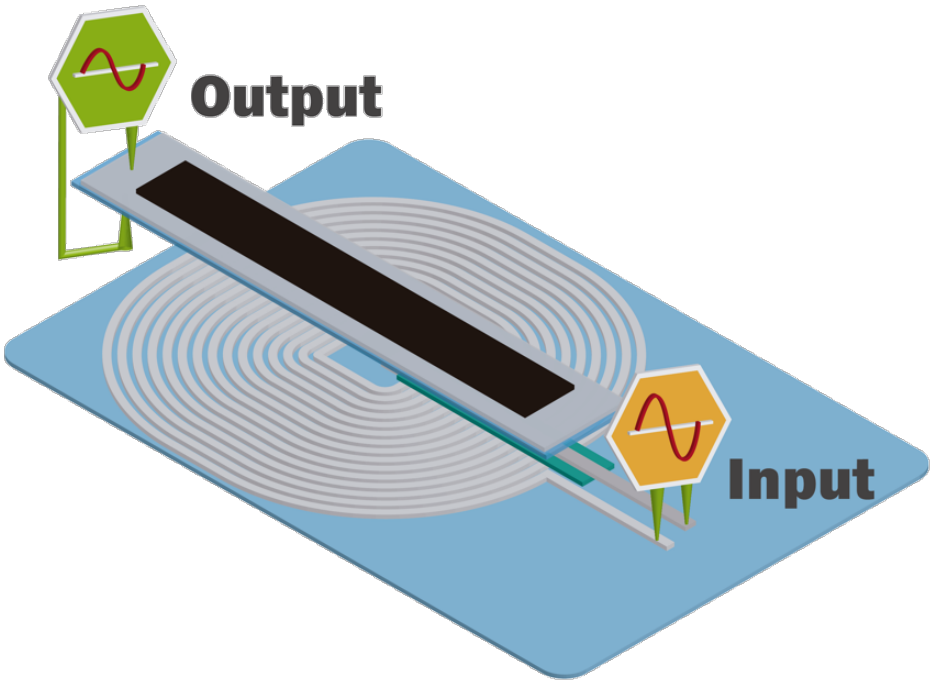

Chapter V – Magnetic Proximity Sensor Based on Magnetoelectric Composites and Printed Coils

Magnetic sensors are mandatory in a broad range of applications nowadays, being the increasing interest on such sensors mainly driven by the growing demand of materials required by Industry 4.0 and the Internet of Things concept. Optimized power consumption, reliability, flexibility, versatility, lightweight and low-temperature fabrication are some of the technological requirements in which the scientific community is focusing efforts. Aiming to positively respond to those challenges, this work reports magnetic proximity sensors based on ME PVDF/Metglas® composites and an excitation-printed coil. The proposed magnetic proximity sensor shows a maximum resonant ME coefficient (α) of 50.2 V cm^{-1} Oe^{-1}, an AC linear response (R^2 = 0.997) and a maximum voltage output of 362 mV, which suggests suitability for proximity-sensing applications in the areas of aerospace, automotive, positioning, machine safety, recreation and advertising panels, among others.

This chapter is based on the following scientific publication:

N. Pereira, **A. C. Lima**, V. Correia, N. Perinka, S. Lanceros-Méndez, and P. Martins, Magnetic proximity sensor based on magnetoelectric composites and printed coils, Materials, 13(7), 2020. DOI:10.3390/ma13071729

5.1 Introduction

Smart—or responsive—materials are defined as materials capable of changing their properties in a controlled and reproducible way, as a response to environmental changes and external stimuli such as stress, moisture, heat, pH, electric or magnetic fields [1, 2].

Since the beginning of the new millennium, strong efforts have been dedicated toward developing novel smart and multifunctional materials, and to integrate them into technological applications [1, 3].

Such efforts represent a multidisciplinary research field with contributions and implications in the areas of sensors and actuators, energy, mobility, interactivity and biomedical sciences, among others [4]. This interesting research scenario actively promotes the production, optimization and application of innovative materials with tailored or improved functionalities [4]. Those materials include hydrogels, covalent adaptive network materials [5], photomechanical materials [6], shape-memory alloys, electroactive and magnetoactive materials [7], self-cleaning and self-healing materials, among others [1].

Particularly interesting are magnetoactive smart materials [7, 8]. Magnetoactive materials have been used for more than two thousand years (202 BC–220 AD), initially for magnetic compasses [9] and nowadays as essential components for motors, generators and electronic devices [10]. Magnetoactive materials have become particularly optimized for the implementation of precision manufacturing tools, magnetic manipulation systems, memory devices, gyrators, filters, actuators and proximity sensors [11, 12].

Magnetoactive materials for proximity sensors are very popular, as they can be used for non-contact object detection beyond the normal limits of inductive sensors, offering very long sensing ranges in a small package and are able to detect objects through walls of non-ferrous metals, stainless steel, aluminum, plastic or wood [13, 14].

From the different types of magnetoactive materials that can be used for magnetoactive proximity sensors, magnetoelectric [15, 16] composites and related devices represent a growing field over the last decade, due to the magnetic to electric energy conversion capability [17], the magnetic control of polarization and the possibility of obtaining self-powered devices [18]. These ME composites have emerged as a solution to overcome the limitations of single-phase ME materials, namely, low-temperature

coupling and low-ME effect [19, 20], allowing innovative functionalities to develop ultra-fast, multifunctional and miniaturized devices [17, 21, 22].

In contrast to ME single-phase materials where the coupling occurs intrinsically, ME composite materials exhibit a ME response resulting from the mechanical coupling between a piezoelectric phase and a magnetostrictive phase [20, 23].

In this way, ME composites can be divided into two major groups, depending on the characteristics of the piezoelectric component: polymer-based ME materials and ceramic-based ME materials [24, 25].

Despite their (up to three orders or magnitude) lower ME-voltage response, polymer-based [26, 27] ME materials overcome three of the main limitations of piezoelectric-based ME materials: fragility, non-printability and high dielectric losses [28].

In polymer-based ME composite multiferroics, a non-magnetic piezoelectric, such as PVDF and its copolymer P(VDF-TrFE), is typically combined with a non-ferroelectric magnetic filler, such as $CoFe_2O_4$ in the case of nanocomposites [19] or Metglas® in the case of laminates [29], being the latter the ones in which the highest ME coefficient (1 kV cm^{-1} Oe^{-1}) has been reported [28].

Despite the large application potential in different areas, the typical operation of traditional polymer-based ME composites requires two applied magnetic fields, a DC (to drive the magnetostriction) and an external AC (to excite the response and enhance resonant excitation) [30] that complicates the design of devices. Thus, the development and integration of printed AC coils can represent a milestone in this research field [28].

In this way, this work reports on the development of a magnetic proximity sensor produced from a polymer-based ME laminate based on Metglas® and PVDF, combined with a printed magnetic coil (Figure V-1).

The selection of the Metglas®/PVDF composite is related to the fact that this combination provides the highest ME response and magnetic sensitivity among polymer-based ME materials [31].

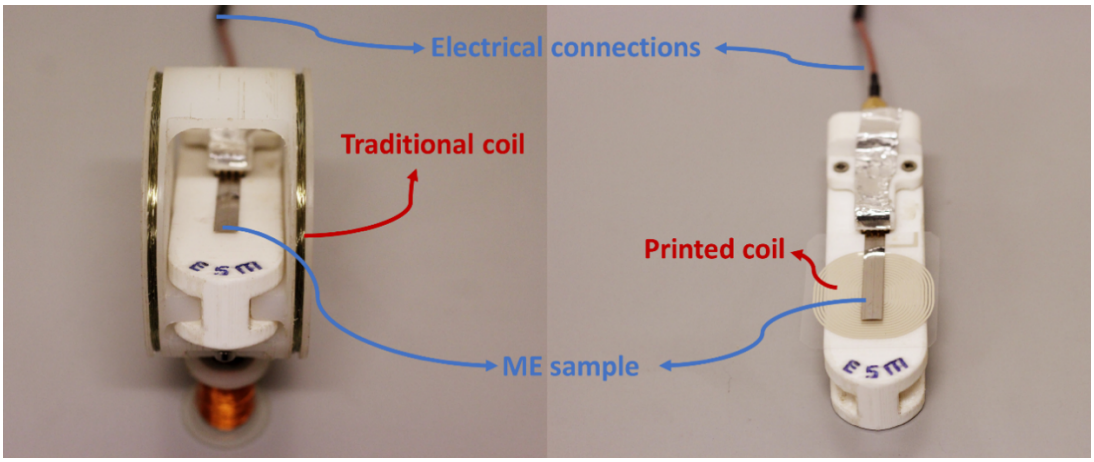

Figure V-1- *ME sample placed on a traditional coil (left) and on the top a printed coil (right).*

5.2 Experimental Section

Polymer-based ME composites were produced by direct bonding (M-Bond 600 epoxy—Vishay Precision Group, Malvern Pennsylvania, USA, under vacuum of a magnetostrictive alloy of Metglas® and a commercial β-PVDF film (Hampton, Virginia, USA), following the optimized conditions presented in [32]. The 2605SA1 Metglas® layer (30 mm × 2 mm × 25 μm, Hitachi Metals Europe GmbH, Düsseldorf, Germany) was magnetized along the length direction (λ = 25 ppm) and the PVDF layer (30 mm × 3 mm × 52 μm) was poled along the thickness direction (d_{33}= −33 pC N^{-1}).

The coils to be printed were first evaluated by a Finite Element Method Magnetics by an axisymmetric problem analysis, allowing to study the effect of geometry (thickness, spacing and number of turns) in the value of the generated AC magnetic field. The printed coils were then produced by screen-printing, using a semi-automatic screen-printer, DX-305D from Shenzhen Dstar (Shenzhen, China), with adjustable speed and with a polyester mesh of 100 wires per centimeter.

The printing process started by printing the silver layer with Metalon HPS-021L from Novacentrix (Austin, Texas, USA) into a polyethylene substrate and cured at 120 °C for 30 minutes on an electric Convection Oven (JP Selecta 2005165, (Barcelona, Spain). The non-conductive layer was printed with 118-12A/B119-44 solvent-resistant ink from Creative Materials (Ayer, Massachusetts, USA) and cured at 120 °C for 30 minutes.

The process was repeated for the last silver layer achieving an electric bridge from the middle contact.

Optical images of the coil were obtained on a 5M 300x USB Digital Mustech Microscope (Shenzhen, China) with 8 LEDs Brightness Adjustable Measurement Software (MicroCapture Pro.).

The characterization of the printed coil was carried out with a QuadTech 1920 Precision LCR Meter. The inductance (L) and impedance (Z) were obtained in the frequency range 1 kHz to 1 MHz.

The ME characterization of the composite was performed in a system composed of two Helmholtz coils in order to generate an HDC ranging from 0 to 43 Oe, via a DC input current (Keithley 2400, Cleveland, Ohio, USA), being the AC field generated in the printed coil produced with an AC current (Agilent 33220A Function/Arbitrary Waveform Generator, Santa Clara, California, USA). The ME voltage response was evaluated with a Rigol DS1074Z oscilloscope (Beijing, China).

The voltage ME coefficient (α_{33}) was calculated based on Equation I.1. To validate the use of the ME material (Figure V-1) as proximity magnetic sensor (ME composite + printed coil) its voltage response has been studied as a function of the distance to a commercial magnet (KJ Magnetics, Pipersville, PA, USA) and compared with the output value obtained on a Hall sensor (Hirst Magnetic Instruments gm08 Gaussmeter, Falmouth, UK).

5.3 Results and Discussion

The magnetic coil printing process was performed considering the results obtained through theoretical simulations (Figure V-2a). The coil details (width, spacing and turns) were optimized in order to ensure AC magnetic fields in the same order than the ones typically used in polymer-based ME materials (0.1 – 1 Oe) [31, 33].

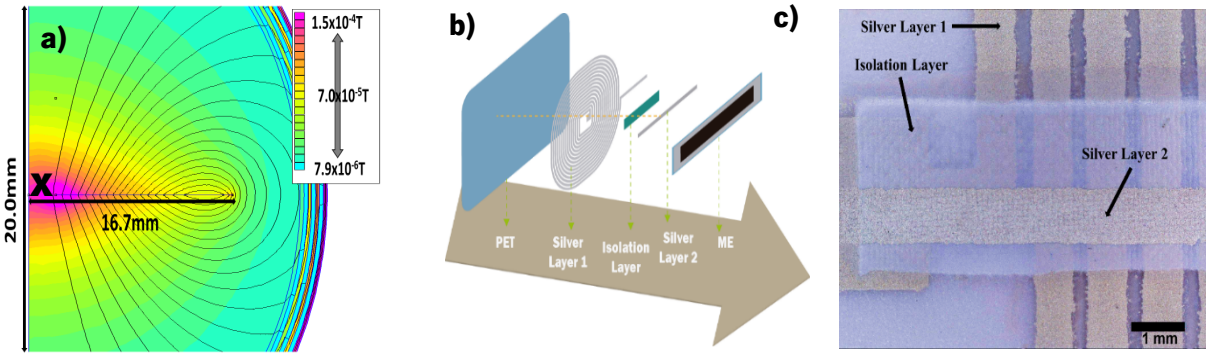

Figure V-2- a) *Theoretical simulation of the AC magnetic field (in T) generated for a printed coil with a width of 750 µm, 250 µm spacing, 15 turns and a current (I) = 0.02 A.* ***b)*** *Schematic representation of the printing process of the coils. c) Coil printing detail obtained with a digital microscope.*

The color map of Figure V-2a reveals that in the region in which the ME composite will be placed (**pink-red: X**) on a coil with 7 μm thick, 750 μm width, 250 μm lines spacing and 15 turns, AC magnetic fields will be generated in the 0 – 1.5 Oe range, by varying the electric current from 0 to 0.02 A.

After the printing of the different layers of the coil (PET, silver layer 1, isolation layer, silver layer 2 and ME layer: Figure V-2b), the macroscopic quality of the printed material was evaluated by optical images that revealed a printed coil with well-defined and compact lines with line width and spacing of ≈ 750 μm and ≈ 250 μm, respectively.

The printed coil's main features, including inductance and impedance as a function of frequency and H_{AC} generated as a function of the electric current, are presented in Figure V-3. Based on Equation V.1 and Equation V.2 [34]:

$$X_L = 2\pi f L \qquad \text{(Equation V.1)}$$

$$Z = \sqrt{R^2 + {X_L}^2} \qquad \text{(Equation V.2)}$$

where X_L is the inductive reactance, f the frequency, L the inductance of coil, Z the impedance and R the resistance, and being the inductance of the coil frequency independence and the X_L value much lower than R, the impedance value reported in Figure V-3a ≈ 80 Ω was determined by the ink resistivity (10 mΩ/sq - Novacentrix datasheet), line length (1.22 m, obtained from optical images) and printing process (mesh size and curing procedure).

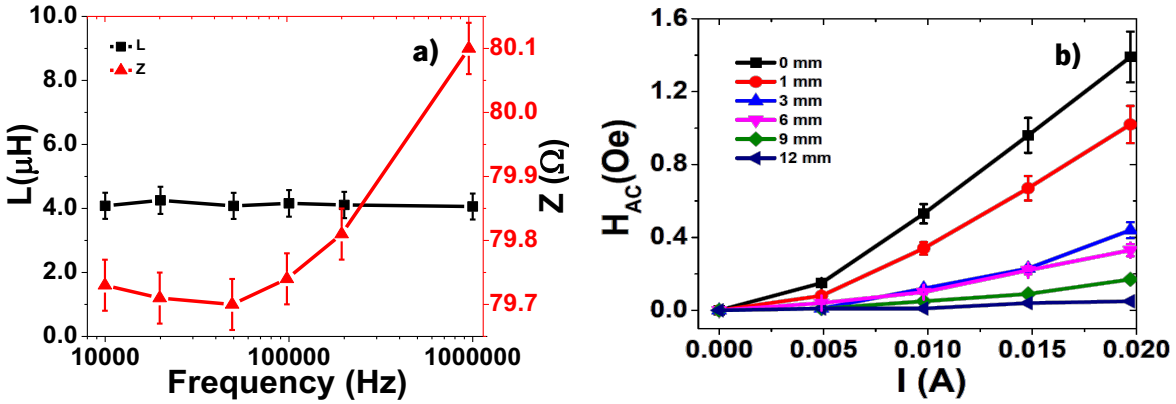

Figure V-3- a) *Inductance and impedance of the printed coil as a function of frequency.* ***b)*** *H_{AC} value as a function of the distance to the coil and current.*

Figure V-3b shows an increase in the value of H_{AC} value with increasing electric current (I) and decreasing distance to the coil as represented by Equation V.3:

$$H_{AC} = \frac{Na^2 I}{2(a^2 + z^2)^{3/2}} \qquad \text{(Equation V.3)}$$

where H_{AC} is the AC magnetic field generated by the coil, μ_0 the vacuum permeability, N the number of turns, *a* the radius of the coil in meters, I the electric current intensity in amperes and *z* the axial distance in meters from the center of the coil [35]. Based on the previous results, the ME characterization of the sensor was performed on the conditions that promote a higher coupling (higher magnetic AC field: I = 0.02 A and 0 mm distance to the coil).

For the AC ME characterization, the ME voltage response was studied as a function of the frequency (Figure V-4a) and H_{AC} magnitude (Figure V-4b).

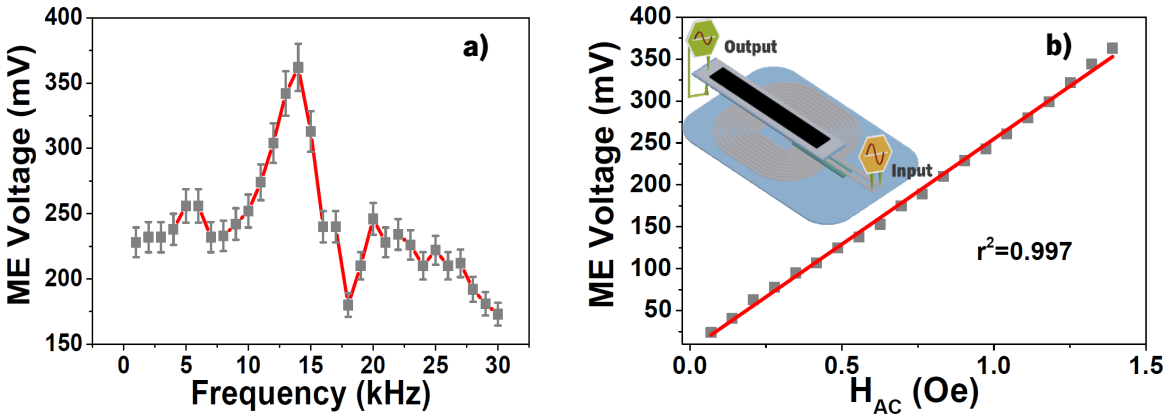

Figure V-4- *ME voltage response as a function of a) frequency and b) H_{AC} magnitude value generated by the printed coil.*

Figure V-4a shows that the ME voltage response strongly increased at ≈ 13.2 kHz, being reached a maximum voltage value of 362 mV. Figure V-4b reveals that the generated voltage increased almost linearly with increasing AC magnetic field up to 1.39 Oe when a maximum voltage of 365 mV was reached. Such high linearity (R^2 = 0.997) is suitable for the use of these ME composites not only for proximity sensors but also for AC sensing device applications such as digital compasses and earth's magnetic field sensors [29].

Before the ME composite being tested as a proximity sensor, its ME coupling (α) has been studied as a function of the DC magnetic field intensity (H_{DC}) (Figure V-5).

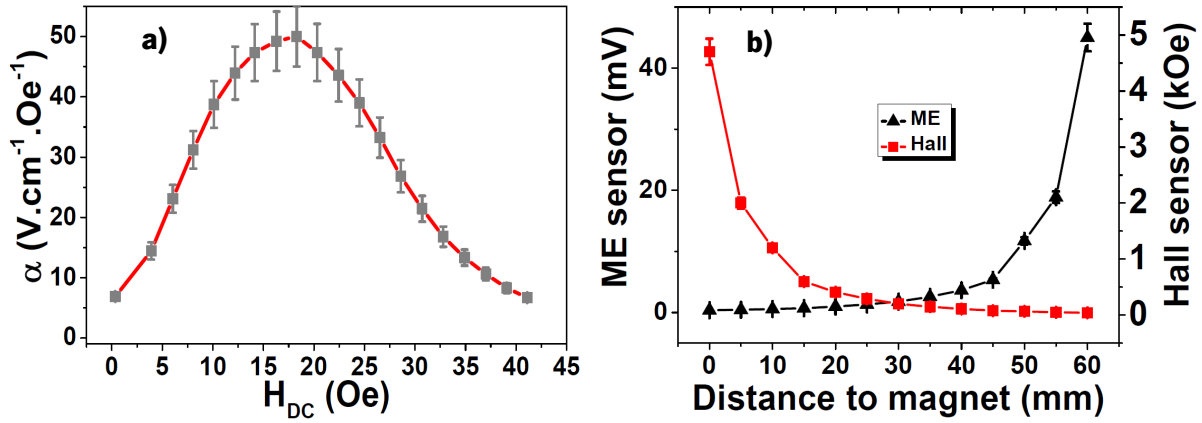

Figure V-5- a) *ME voltage coefficient (α) response as a function of the H_{DC}.* ***b)*** *ME sensor and Hall sensor response as a function of the distance to the magnet.*

Figure V-5a shows that the ME coefficient (α) increased with increasing applied DC magnetic field up to 18 Oe when a maximum α of 50.2 V cm^{-1} Oe^{-1} was reached. Such behavior is explained by the increase of the piezomagnetic coefficient until such optimum magnetostriction field was reached [32].

With further increase of the H_{DC}, a decrease of the ME coefficient was achieved, resulting from the saturation of the magnetostrictive effect.

To validate the use of the ME sensor as proximity magnetic sensor (Figure V-5b), its response has been studied as a function of the distance to a commercial magnet (KJ Magnetics) and compared with the one obtained on a Hall sensor (Hirst Magnetic Instruments gm08 Gaussmeter, Cornwall, UK).

As expected, the Hall sensor's response decreased with increasing distance to the magnet, being this decrease related with the decrease of the magnetic field. Once the ME sensor increased its response, with increasing H_{DC} for magnetic fields lower than 18 Oe, it was observed an increase in the ME sensor response with increasing distance to the permanent magnet. An obvious consequence of this comparison was that the sensitivity of the ME sensor increased with the distance to the magnet, while the Hall sensor sensitivity decreased in the same conditions.

The developed polymer-based ME proximity sensor, when compared with the three traditional types of proximity sensors [36] (resonant circuit method, bridge method and single-coil method) adds some competitive advantages such as being flexible, versatile, lightweight, low cost, able to conform to complicated shapes obtained from low-temperature fabrication process and foresee the future development of self-power proximity sensors [37].

5.4 Conclusions

A PVDF/Metglas®/printed coil proximity sensor device was presented showing suitable characteristics to be applied in sensing applications, particularly in multifunctional flexible devices, due to its good output AC linearity (R^2 = 0.997), high ME coefficient (50.2 V cm^{-1} Oe^{-1} at 13.2 kHz and 18 Oe DC field) and large voltage output (362 mV). Other applications such as magnetic transformers, magnetic tools for the automobile/aerospace industry and switches can be based on such ME composite.

5.5 References

1. Kim, H.C., Mun, S., Ko, H.U., Zhai, L., Kafy, A., Kim, J. Renewable smart materials. Smart Mater. Struct. 2016, 25, DOI: 10.1088/0964-1726/25/7/073001.

2. Bartkowiak, G., Dąbrowska, A., Greszta, A. Development of Smart Textile Materials with Shape Memory Alloys for Application in Protective Clothing. Materials 2020, 13(3): 689.DOI: https://doi.org/10.3390/ma13030689

3. Stadlober, B., Zirkl, M., Irimia-Vladu, M. Route towards sustainable smart sensors: Ferroelectric polyvinylidene fluoride-based materials and their integration in flexible electronics. Chem. Soc. Rev. 2019, 48, p. 1787–1825, DOI:10.1039/c8cs00928g.

4. Oliveira, J., Correia, V., Castro, H., Martins, P., Lanceros-Mendez, S. Polymer-based smart materials by printing technologies: Improving application and integration. Addit. Manuf. 2018, 21, p. 269–283, DOI: 10.1016/j.addma.2018.03.012.

5. Solouki Bonab, V., Karimkhani, V., Manas-Zloczower, I. Ultra-Fast Microwave Assisted Self-Healing of Covalent Adaptive Polyurethane Networks with Carbon Nanotubes. Macromol. Mater. Eng. 2019, 304, 1800405, DOI:10.1002/mame.201800405.

6. Yu, Q., Aguila, B., Gao, J., Xu, P., Chen, Q., Yan, J., Xing, D., Chen, Y., Cheng, P., Zhang, Z., et al. Photomechanical Organic Crystals as Smart Materials for Advanced Applications. Chem. A Eur. J. 2019, 25, p. 5611–5622, DOI:10.1002/chem.201805382.

7. Prem, N., Sindersberger, D., Monkman, G.J. Mini-Extruder for 3D Magnetoactive Polymer Printing. Adv. Mater. Sci. Eng. 2019, 2019, 8715718. DOI: 10.1155/2019/8715718.

8. Amirov, A., Baraban, I., Panina, L., Rodionova, V. Direct Magnetoelectric Effect in a Sandwich Structure of PZT and Magnetostrictive Amorphous Microwires. Materials 2020, 13(4), 916. DOI: https://doi.org/10.3390/ma13040916

9. Lowrie, W. Fundamentals of Geophysics; Cambridge University Press: London, UK, 2007.

10. Upadhyay, P. Magnetic Materials and Technologies Enabling an Even Brighter Future for Electrical Machines. In Proceedings of the 2018 IEEE International Magnetics Conference (INTERMAG), Singapore, 23–27 April 2018.

11. Vitol, E.A., Novosad, V., Rozhkova, E.A. Microfabricated magnetic structures for future medicine: From sensors to cell actuators. Nanomedicine 2012, 7, p. 1611–1624, DOIi:10.2217/nnm.12.133.

12. Shin, T.H., Kang, S., Park, S., Choi, J.S.; Kim, P.K.; Cheon, J. A magnetic resonance tuning sensor for the MRI detection of biological targets. Nat. Protoc. 2018, 13, p. 2664–2684, DOI:10.1038/s41596-018-0057-y.

13. Wu, F., Marechal, L., Vibhute, A., Foong, S., Soh, G.S., Wood, K.L. A compact magnetic directional proximity sensor for spherical robots. In Proceedings of the 2016 IEEE/ASME International Conference on Advanced Intelligent Mechatronics (AIM), Banff, AB, Canada, 12–15 July 2016; p. 1258–1264.

14. Paul, S., Chang, J., Rajan, A.; Mukhopadhyay, S. Design of linear magnetic position sensor used in permanent magnet linear machine with consideration of manufacturing tolerances. IEEE Sens. J. 2019, 19, p. 5239–5248, DOI:10.1109/JSEN.2019.2903292.

15. Mushtaq, F., Torlakcik, H., Vallmajo-Martin, Q., Siringil, E.C., Zhang, J., Röhrig, C., Shen, Y., Yu, Y., Chen, X.Z., Müller, R., et al. Magnetoelectric 3D scaffolds for enhanced bone cell proliferation. Appl. Mater. Today 2019, 16, p. 290–300, DOI: 10.1016/j.apmt.2019.06.004.

16. Venet, M., Santa-Rosa, W., da Silva, S.P., M'Peko, J.-C.; Ramos, P., Amorín, H., Algueró, M. Selection and Optimization of a K0.5Na0.5NbO3-Based Material for Environmentally-Friendly Magnetoelectric Composites. Materials 2020, 13, 731, DOI:10.3390/ma13030731.

17. Cheng, Y., Peng, B., Hu, Z., Zhou, Z., Liu, M. Recent development and status of magnetoelectric materials and devices. Phys. Lett. A 2018, 382, p. 3018–3025, DOI: 10.1016/j.physleta.2018.07.014.

18. Narita, F., Fox, M. A Review on Piezoelectric, Magnetostrictive, and Magnetoelectric Materials and Device Technologies for Energy Harvesting Applications. Adv. Eng. Mater. 2018, 20, 1700743, DOI:10.1002/adem.201700743.

19. Spaldin, N.A., Ramesh, R. Advances in magnetoelectric multiferroics. Nat. Mater. 2019, 18, p. 203–212, DOI:10.1038/s41563-018-0275-2.

20. Brito-Pereira, R., Ribeiro, C., Lanceros-Mendez, S., Martins, P. Magnetoelectric response on Terfenol-D/P (VDF-TrFE) two-phase composites. Compos. Part B Eng. 2017, 120, p. 97–102, DOI: 10.1016/j.compositesb.2017.03.055.

21. Hohenberger, S., Jochum, J.K., Van Bael, M.J., Temst, K., Patzig, C., Höche, T., Grundmann, M., Lorenz, M. Enhanced Magnetoelectric Coupling in BaTiO3-BiFeO3 Multilayers—An Interface Effect. Materials 2020, 13(1), 197.DOI: 10.3390/ma13010197

22. Tu, C., Chu, Z.Q., Spetzler, B., Hayes, P., Dong, C.Z., Liang, X.F., Chen, H.H., He, Y.F., Wei, Y.Y., Lisenkov, I., et al. Mechanical-resonance-enhanced thin-film magnetoelectric heterostructures for magnetometers, mechanical antennas, tunable RF inductors, and filters. Materials 2019, 12, 2259, DOI:10.3390/ma12142259.

23. Fetisov, Y., Chashin, D., Saveliev, D., Fetisov, L., Shamonin, M. Anisotropic Magnetoelectric Effect in a Planar Heterostructure Comprising Piezoelectric Ceramics and Magnetostrictive Fibrous Composite. Materials 2019, 12(19), 3228. DOI: https://doi.org/10.3390/ma12193228

24. Zong, Y., Zheng, T., Martins, P., Lanceros-Mendez, S., Yue, Z., Higgins, M.J. Cellulose-based magnetoelectric composites. Nat. Commun. 2017, 8, DOI:10.1038/s41467-017-00034-4.

25. Lu, C., Zhou, H., Yang, A.; Ou, Z.; Yu, F.; Gao, H. Nonlinear Magnetoelectric Response of $Fe_{73.5}Cu1Nb_3Si_{13.5}B_9$/Piezofiber Composite for a Pulsed Magnetic Field Sensor. Materials 2019, 12(18), 2866. DOI: https://doi.org/10.3390/ma12182866

26. Ye, S., Cheng, C., Chen, X., Chen, X., Shao, J., Zhang, J., Hu, H., Tian, H., Li, X., Ma, L., et al. High-performance piezoelectric nanogenerator based on microstructured P(VDF-TrFE)/BNNTs composite for energy harvesting and radiation protection in space. Nano Energy 2019, 60, p. 701–714, DOI: 10.1016/j.nanoen.2019.03.096.

27. Sanida, A., Stavropoulos, S.G., Speliotis, T., Psarras, G.C. Investigating the Effect of Zn Ferrite Nanoparticles on the Thermomechanical, Dielectric and Magnetic Properties of Polymer Nanocomposites. Materials 2019, 12 (18), 3015. DOI: https://doi.org/10.3390/ma12183015

28. Martins, P., Lanceros-Méndez, S. Polymer-based magnetoelectric materials: To be or not to be. Appl. Mater. Today 2019, 15, p. 558–561, DOI: 10.1016/j.apmt.2019.04.004.

29. Castro, N., Reis, S., Silva, M.P., Correia, V., Lanceros-Mendez, S.; Martins, P. Development of a contactless DC current sensor with high linearity and sensitivity based on the magnetoelectric effect. Smart Mater. Struct. 2018, 27, DOI:10.1088/1361-665X/aab969.

30. Fiebig, M. Revival of the magnetoelectric effect. J. Phys. D Appl. Phys. 2005, 38, p. 123-152, DOI:10.1088/0022-3727/38/8/R01.

31. Martins, P., Lanceros-Méndez, S. Polymer-based magnetoelectric materials. Adv. Funct. Mater. 2013, 23, p. 3371–3385, DOI:10.1002/adfm.201202780.

32. Lima, A.C., Pereira, N., Policia, R., Ribeiro, C., Correia, V., Lanceros-Mendez, S., Martins, P. All-printed multilayer materials with improved magnetoelectric response. J. Mater. Chem. C 2019, 7, p. 5394–5400, DOI:10.1039/c9tc01428d.

33. Levy, S.M. Section 12—Electrical Formulas and Calculations. In Construction Calculations Manual; Levy, S.M., Ed.; Butterworth-Heinemann: Boston, MA, USA, 2012; p. 635–671, DOI:10.1016/B978-0-12-382243-7.00014-0.

34. Samuel, J., Ling, J.S., Bill, M. University Physics; OpenStax: Houston, TX, USA, 2017; Volume 2.

35. Reis, S., Silva, M.P., Castro, N., Correia, V., Martins, P., Lasheras, A., Gutierrez, J., Barandiarán, J.M., Rocha, J.G., Lanceros-Mendez, S. Characterization of Metglas/poly (vinylidene fluoride)/Metglas magnetoelectric laminates for AC/DC magnetic sensor applications. Mater. Des. 2016, 92, p. 906–910, DOI: 10.1016/j.matdes.2015.12.086.

36. Lenz, J., Edelstein, A.S. Magnetic sensors and their applications. IEEE Sens. J. 2006, 6, p. 631–649, DOI:10.1109/JSEN.2006.874493.

37. Alnassar, M., Alfadhel, A., Ivanov, Y.P., Kosel, J. Magnetoelectric polymer nanocomposite for flexible electronics. J. Appl. Phys. 2015, 117, DOI:10.1063/1.4913943.

CHAPTER VI

CONCLUSIONS AND FUTURE WORK

This chapter presents the main conclusions of the work, devoted to the development of polymer-based magnetoactive printable composites for magnetic sensing. Further, some suggestions for future works are also provided.

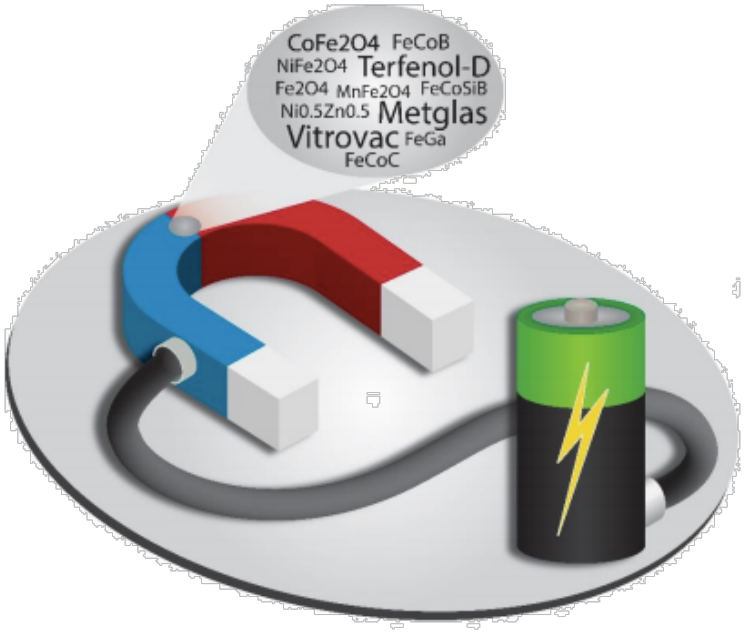

6.1 Conclusions

This work represents a relevant and original contribution to printable magnetoactive materials and printed electronics.

It was developed the first flexible and transparent ME composite composed of P(VDF-TrFE) and $Fe_{72.5}Si_{12.5}B_{15}$ microwires, exhibiting a maximum ME voltage response of 65 mV cm^{-1} Oe^{-1}, obtained at the critical longitudinal applied field of at 14500 A m^{-1} that equals the transverse anisotropy field at the external shell of the microwire. These properties allow to predict that such a maximum ME can be improved by the designed choice of the magnetostrictive character of the amorphous microwire, with the value of the internal mechanical stresses and with the use of a conductive ink with higher transparency. Transparent magnetic sensors, actuators, multifunctional touch displays, and transparent optical magnetic coatings are obvious advantages of the composite reported in this work.

Being the cost/efficiency ratio optimization of printing technologies, and their use in ME smart materials production a catalyst for the emergence of new device applications, this work presented the first fully printed ME composite. The APME was successfully printed with P(VDF-TrFE)/DMF as piezoelectric ink, PVDF-CFO/DMF as magnetic ink and silver ink as electrodes. The resulting composite exhibited a ferromagnetic behavior with 16 emu g^{-1} saturation magnetization, -26 pC N^{-1} piezoelectric response and a ME voltage coefficient of 164 mV cm^{-1} Oe^{-1} at a longitudinal resonance frequency of 16.2 kHz, the highest reported in the literature in this kind of composite. The additive manufacturing nature of the printing process results in improved usage of material and integration and, consequently, more efficient fabrication of the ME material for sensors and actuator applications.

With the aim of reduce of the ecological footprint in all types of sectors, being increasingly important the development of inks with alternative solvents (green solvents), is extremely important to reduce restrictions/concerns about waste disposal/treatment, safety, and handling of devices. In this way, it was demonstrated that $CoFe_2O_4$/P(VDF-TrFE) nanocomposites can be effectively prepared from solution using different environmental friendlier solvents: DMSO, DMPU and TEP with different dipolar moments. It was shown that the prepared composite films, with a maximum ME voltage coefficient of 35 mV cm^{-1} Oe^{-1} and a maximum sensitivity of 2.2 mV T^{-1}, are suitable for applications, highlighting the path for a new generation of more sustainable ME sensors.

Finally, being the development and integration of printed AC coils a milestone in this research field, it was presented PVDF/Metglas®/printed coil proximity sensor device, showing suitable characteristics to be applied in sensing applications, particularly in multifunctional flexible devices, due to its good output

AC linearity (R^2 = 0.997), high ME coefficient (50.2 V cm^{-1} Oe^{-1} at 13.2 kHz and 18 Oe DC field) and large voltage output (362 mV). Other applications like magnetic transformers, magnetic tools for the automobile/aerospace industry and switches can be based on such ME composite.

6.2 Future Work

In the present work, it has been demonstrated and optimized the formulation of different inks to print electronic components that can be integrated into a fully printed device. In this sense, some interesting studies can be carried out to further explore the development of new materials and technological approaches:

- The developed all printed ME sensor must be fully integrated in the IoT and 4.0 Industry 4.0;
- New piezomagnetic and piezoelectric materials need to be optimized for achieving higher magnetostrictive and piezoelectric coefficients;
- Decrease or even eliminate the external noise of ME sensors in order to improve sensitivity;
- Beyond the use of green solvents, explore the use of polymers from natural origin with piezoelectric properties, such as Keratin or Collagen, in case of ME applications;
- Explore "greener" synthesis processes of NP, for example biosynthesis processes;
- To print electronic components that can take advantage of printable magnetic materials, such as Inductors or Wireless Transfer Modules.
- To optimize ME inks for 4-state memories and communication applications.